The Interleukin 13 Receptor System: A Novel Pathomechanism Involved in Pulmonary Arterial Hypertension

Inaugural Dissertation
Submitted to the
Faculty of Medicine
in partial fulfillment of the requirements
for the PhD-Degree
of the Faculties of Veterinary Medicine and Medicine
of the Justus Liebig University Giessen

by
Hecker, Matthias

of
Kreuztal
Germany

Giessen 2008

From the Department of Medicine
Director: Prof. Dr. Werner Seeger
of the Faculty of Medicine of the Justus Liebig University Giessen

First Supervisor and Committee Member: Prof. Dr. Oliver Eickelberg

Second Supervisor and Committee Member: Prof. Dr. Susetta Finotto

Committee Members: Prof. Dr. Heinz-Jürgen Thiel

Priv.-Doz. Dr. Sandip Kanse

Date of Doctoral Defence: 11.05.2009

I declare that I have completed this dissertation single-handedly without the unauthorized help of a second party and only with the assistance acknowledged therein. I have appropriately acknowledged and referenced all text passages that are derived literally from or are based on the content of published of unpublished work of others, and all information that related to verbal communications. I have abided by the principles of good scientific conduct laid down in the charter of the Justus Liebig University of Giessen in carrying of the investigations described in the dissertation.

I. Table of contents

II. List of figures and tables

III. List of abbreviations

5-HT	5-Hydroxytryptamine
ANP	Atrial natriuretic peptide
AP-1	Activator protein 1
APS	Ammonium persulfate
BMPR	Bone morphogenic protein receptor
BNP	Brain natriuretic peptide
BSA	Bovine serum albumin
cAMP	Cyclic andenosine monophosphate
cDNA	Complementary deoxyribonucleic acid
CD	Cluster of differentiation
DAB	Diaminobenzidine
DAPI	4,6-diamidino-2-phenylindole
DNA	Deoxyribonucleic acid
dpm	disintegrations per minute
ECE	Endothelin-converting enzyme
ECM	Extracellular matrix
EDTA	Ethylenedinitrilo-N,N,N´,N´,-tetra acetate
ELISA	Enzyme linked immunosorbent assay
EMSA	Electrophoretic mobility shift assay
ET	Endothelin
FCS	Fetal calf serum
FITC	Fluorescein isothiocyanate
GFP	Green fluorescent protein
HRP	Horseradish peroxidase
IFN	Interferon
Ig	Immunoglobulin
IL	Interleukin
IPF	Idiopathic pulmonary fibrosis
IPAH	Idiopathic pulmonary arterial hypertension
LB	Luria Bertani
LCM	Laser-captured microdissection
LPS	Lipopolysaccharide
MAP	Mitogen-activated protein
MCT	Monocrotaline
MCTP	Monocrotaline pyrole

MDC	Macrophage-derived chemokines
MMP	Matrix metalloprotease
mRNA	Messenger ribonucleic acid
NOS	Nitric oxide synthetase
OVA	Ovalbumin
PAGE	Polyacrylamide gel electrophoresis
PAH	Pulmonary arterial hypertension
PAP	Pulmonary artery pressure
paSMC	Pulmonary artery smooth muscle cells
PBGD	Porphobilinogen deaminase
PBS	Phosphate-buffered saline
PCR	Polymerase chain reaction
PDE	Phosphodiesterase
PGI2	Prostaglandin I2
PH	Pulmonary hypertension
PI	Propidium iodide
psi	pound-force per square inch
qRT-PCR	Quantitative reverse transcriptase polymerase chain reaction
RNA	Ribonucleic acid
RT	Reverse transcriptase
RT-PCR	Reverse transcriptase polymerase chain reaction
SDS	Sodium dodecyl sulfate
SEM	Standard error of mean
SMA	Smooth muscle actin
SMC	Smooth muscle cell
STAT	Signal transducer and activator of transcription
TAE	Tris-acetate EDTA
TEMED	N,N,N´,N´ Tetramethylethylendiamine
Th	T-helper cell
TGF	Transforming growth factor
TNF	Tumor necrosis factor
T_{Reg}	Regulatory T-cells

1 Introduction

1.1 Pulmonary arterial hypertension

1.1.1 Characteristics of pulmonary arterial hypertension

Pulmonary arterial hypertension (PAH) is a rare (1-2 cases per million) and progressive disease characterized by increased pulmonary vascular resistance leading to diminished right heart function and finally a failure of an afterload-intolerant right ventricle [1]. By expert consensus, PAH is regarded as a mean pulmonary artery pressure (mPAP) greater than 25 mmHg (in healthy adults it does not exceed 12-16 mmHg) at rest or 30 mmHg (in healthy subjects the cardiac output increases, not the mPAP) during exercise in the setting of normal cardiac output and a normal pulmonary capillary wedge pressure [2-5]. Epidemiological studies show that most commonly, young and middle-aged women are afflicted with this fatal disease, which has a mean survival of two to three years after onset of first symptoms in untreated cases [2, 5-7]. The early symptoms of PAH are unspecific, mostly starting with exertional dyspnea due to an inability to increase pulmonary blood flow with exercise. In the progression of the disease, the right ventricular heart function is severely impaired resulting in exertional chest pain, syncope, and edema formation [3, 7-9].

The nomenclature and classification of pulmonary hypertension (PH) has been revised several times, the latest on the World Symposium 2003 [10]. The current classification distinguishes PH by pathogenesis, etiology and response to treatment [11].

1.1.2 Histopathological changes

The different forms of pulmonary hypertension exhibit structural changes that affect both the pulmonary vasculature and the right ventricle. This characteristic process of changes in pulmonary vascular structure, also referred to as vascular remodeling, includes all layers of the vessel wall, leading to significant changes in the structure, amount, phenotype and function of the cells located in the vessel wall, such as cellular hypertrophy, hyperplasia, and increased extracellular matrix deposition (ECM) (Figure 1.1) [2, 12]. During the development of the disease, the pulmonary arteries of PAH patients exhibit narrowing of the vessel lumen, which is caused by intimal proliferation and transdifferentiation of endothelial cells, media thickening (through the hypertrophy and hyperplasia of smooth muscle cells (SMC)) and remodeling of the adventitia, combined with fibroblast proliferation and deposition of ECM components, such as collagen and elastin, leading to a reduction in arterial dispensability [13-15]. Another characteristic hallmark of PAH is the formation of a so-called neointima, defined as a layer composed of ECM and myofibroblasts between the endothelium and the internal elastic lamina [14]. The process of remodeling also encompasses the distal extension of smooth muscle cells, leading to a muscularization of the peripheral, normally nonmuscular, pulmonary arteries due to the proliferation and differentiation of fibroblasts and pericytes [2, 15].

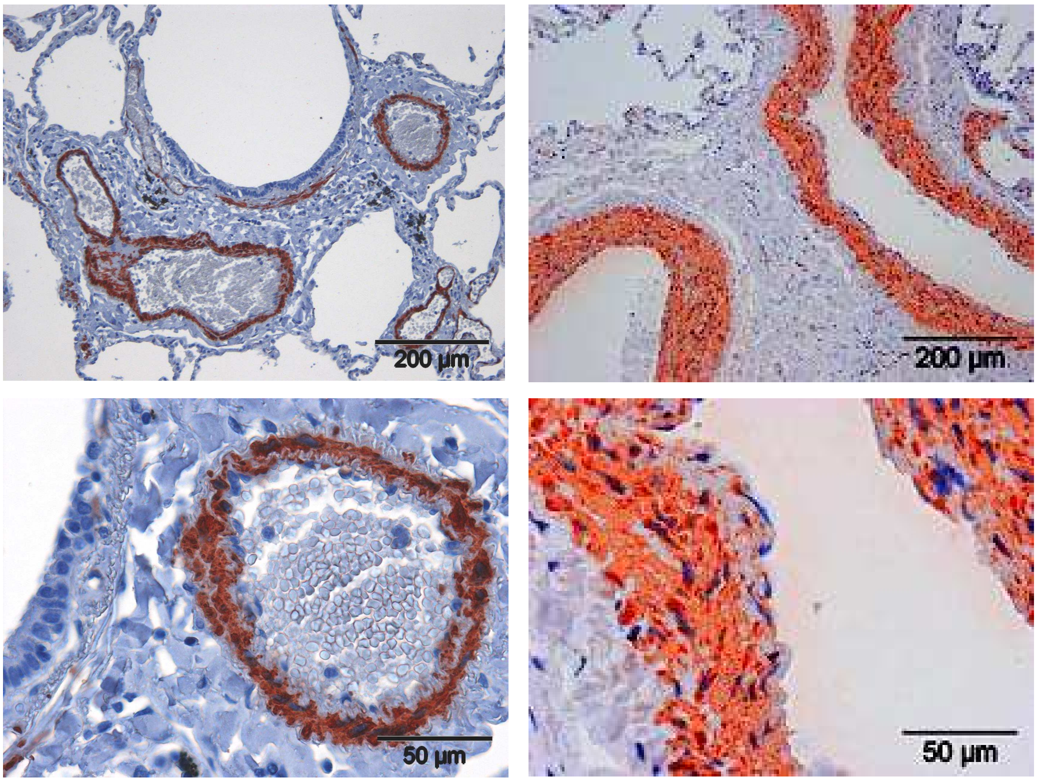

Figure 1.1 Histopathological changes in PAH
Pulmonary arterioles in a normal subject (left) and in patients with PAH (right) with significantly hypertrophic tunica media

A fascinating focal vascular structure, the plexiform lesion is another hallmark of PAH (Figure 1.2). In the literature, the prevalence of this lesion varies from 20% to 90%, depending on the form of pulmonary hypertension (PH), the sample size, and the rigor of the examination [2, 3, 16]. However, the cellular composition and pathogenesis of plexiform lesions is until now not fully understood. Ultrastuctural and three-dimensional analysis reveal that these lesions occur distal to obliterative intimal lesions and contain vascular channels comprising endothelial cells as well as smooth muscle cells, supporting the hypothesis of monoclonal cell proliferation and local angiogenesis, leading to an occlusion of small pulmonary arteries [3, 15, 17]. Plexiform lesions may also represent an angiogenetic response to local ischemia and hypoxia, or might be also caused by a transdifferentiation of endothelial cells into SMC [3, 15, 18, 19].

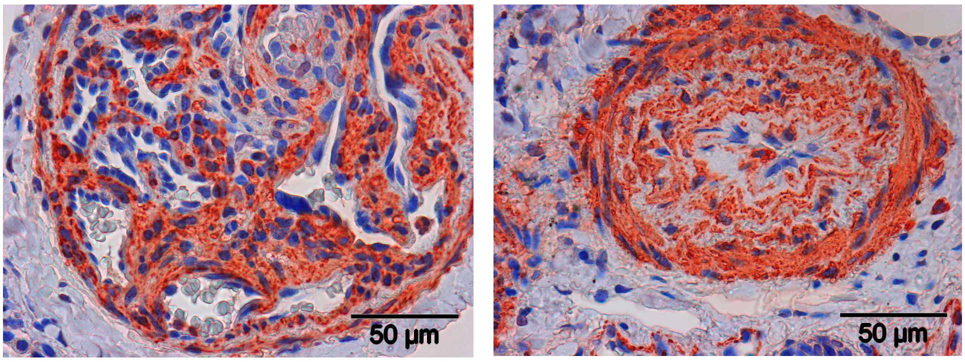

Figure 1.2 Histopathological changes in PAH
Plexiform lesion (left) and concentric lesion (right)

1.1.3 Pathogenesis and therapy of pulmonary hypertension

Despite our growing understanding of the pathobiology of PH, and the identification of various mediators and candidate genes playing a role in the progression of the disease the basic underlying mechanism and the linking of the different pathobiological observations is still poorly understood and thus under intense investigation. In the following some of the most important factors involved in the pathogenesis of pulmonary hypertension are briefly presented:

1.1.3.1 Prostacyclin/prostaglandin I2

Prostaglandin I2 (PGI2), a member of the prostacyclin family, is produced by endothelial cells and known as one of the most potent vasodilatators. In patients with PH an impaired balance between the local production of PGI2 and a reduced expression of PGI2 synthase has been described, leading to a significantly reduced expression of this potent vasodilatator in the case of PH [7, 13, 20]. PGI2 and its analogues have further been shown to inhibit smooth muscle cell proliferation and platelet aggregation [21]. The above mentioned effects of PGI2 are mediated by stimulation of adenylate cyclase and thus cAMP (cyclic andenosine monophosphate) production (Figure 1.3) [22]. Due to its beneficial effects on the pulmonary circulation, endothelial function and pulmonary vascular remodeling prostacyclin analogues like epoprostenol and iloprost belong to the basic therapies of pulmonary hypertension being administered either intravenously or by intermittent inhalation [2].

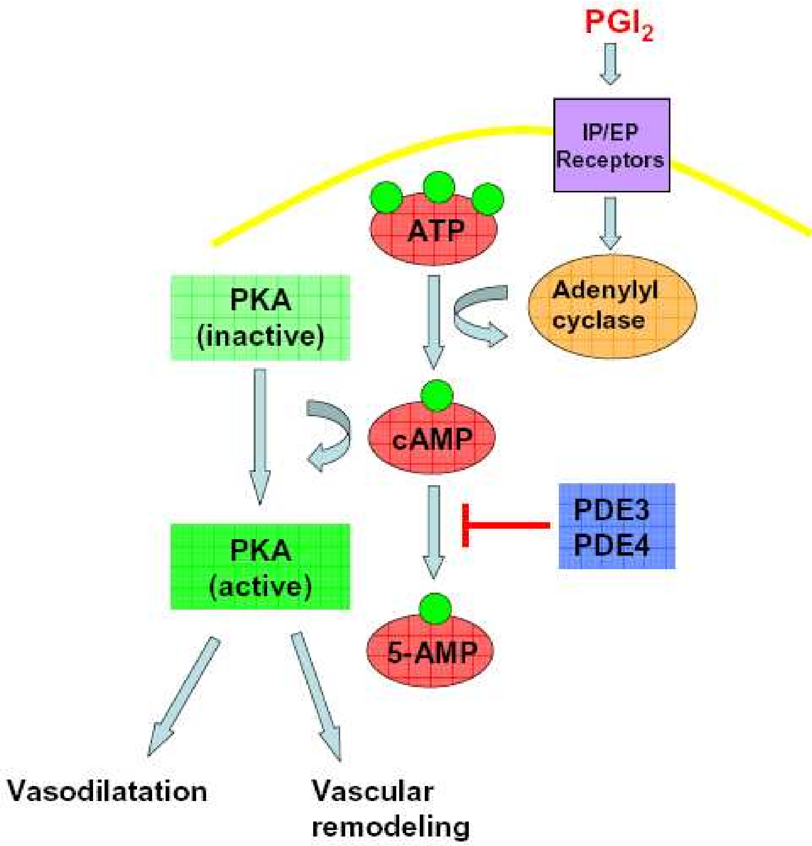

Figure 1.3 Regulation of pulmonary vascular tone and structure by cAMP

1.1.3.2 Endothelins

A second important group of molecules influencing the local vascular tone and regulating the balance between vasoconstrictors and vasodilatators are the endothelins (ET-1, -2 and -3) which are synthesized from large precursor molecules by endothelin-converting enzymes (ECE-1 and ECE-2) [13]. Endothelial and epithelial cells are thought to be the main source of ET-1, which is described of being one of the most potent vasoconstrictors and mitogens [23-25]. Endothelins exert their biological functions by binging to the two G-protein coupled receptors, ETA and ETB, which display marked regional differences in their distribution patterns (Figure 1.4) [26]. The ETA subtype is mainly expressed in the proximal pulmonary arteries mediating local vasoconstriction and proliferation, whereas

ETB receptors are thought to have a dual, partly antagonistic function, depending on their cellular localization [26, 27]. The ETB receptors expressed on vascular SMC in the distal resistance vessels are described to elevate pulmonary vascular resistance upon ET-1 binding, while ETB receptors located on the endothelium are thought to modulate the clearance to ET-1, inhibit ECE expression, and permit vasodilatation through NO and prostacyclin release [13, 28].

Several studies have demonstrated increased ET-1 levels in both lungs and plasma of patients with PH, suggesting that ET-1 might play a pivotal role in vascular remodeling and elevated pulmonary resistance observed in these patients [20, 29, 30]. The successful clinical use of combined ETA/ETB antagonists like bosentan as a novel therapeutic approach in PH treatment underlines the pathobiological relevance of the endothelin system in pulmonary hypertension.

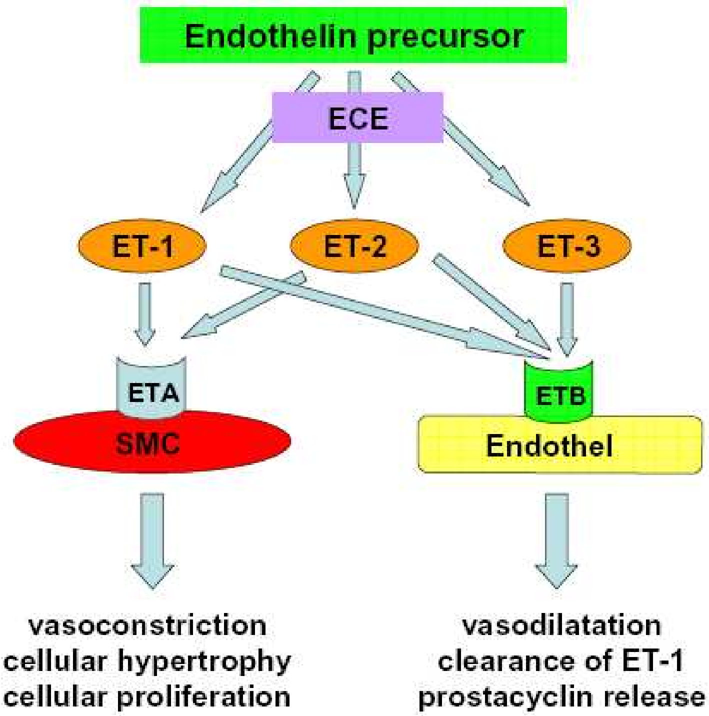

Figure 1.4 Schematic overview of the different endothelins, endothelin receptors and their biological effects

1.1.3.3 Nitric oxide

Nitric oxide (NO) is a potent vasodilatator of both pulmonary and systemic vessels which exerts a plethora of different functions like antiplatelet activity, inhibition of vascular growth and migration [11]. The NO is synthesized in the endothelium from the amino acid

L-arginine by the action of NO synthetase (NOS) which can be classified into three different isoforms (endothelial (eNOS), inducible and neuronal), all expressed in the lung [13]. So far, there are conflicting data about the adverse or protective role of NO in the development of PH. Several authors describe a decreased eNOS immunostaining in lungs from PAH patients, whereas Mason and colleagues observe high expression levels of eNOS in plexiform lesions in PH [31-33].

In spite of the still ongoing discussion about the role of NO and NOS in the pathogenesis of PAH, short-term beneficial effects of inhaled NO on oxygen consumption and pulmonary hemodynamics have been reported [34]. Nevertheless there is still a limited experience with long-term therapy of inhaled NO requiring further clinical exploration [2]. Apart from therapeutic administration, acute responsiveness to NO during cardiac catheterization seems to predict the subset of patients who might be responsive to oral Ca^{2+}-channel blockers.

1.1.3.4 K^+ Channels

Nine families of voltage-gated potassium (Kv) (Kv1 to 9) channels, each with many members (for example, Kv1.1 through Kv1.6) have been identified so far, and several might be involved in mediating hypoxic pulmonary hypertension [2]. Hypoxia inhibits Kv channels in the pulmonary artery smooth muscle cells (paSMC), opening voltage-gated calcium channels, raising cytosolic Ca^{2+} and thus initiating constriction (Figure 1.5) [2, 13]. Whereas acute hypoxia inhibits Kv function, chronic hypoxia reduces the expression of these channels in SMC [35]. Several studies demonstrated a down-regulation of Kv1.5 and Kv2.1 channels in paSMC in patients with PAH, and in rats with chronic hypoxia-induced PH [35, 36]. This downregulation is associated with inhibition of K^+ current, membrane depolarization, elevation of cytosolic Ca^{2+} and thus, vasoconstriction [35]. This theory is supported by the finding that the Kv2.1 channel activity is inhibited by the appetite-suppressing drug dexfenfluramine, use of which has been associated with the development of pulmonary arterial hypertension [37, 38].

Modulation of Kv channel function may have therapeutic potential. Several oral treatments such as the metabolic modulator dichloroacetate and sildenafil might be able to increase expression and function of Kv2.1 and thus be useful in the treatment of pulmonary hypertension [39].

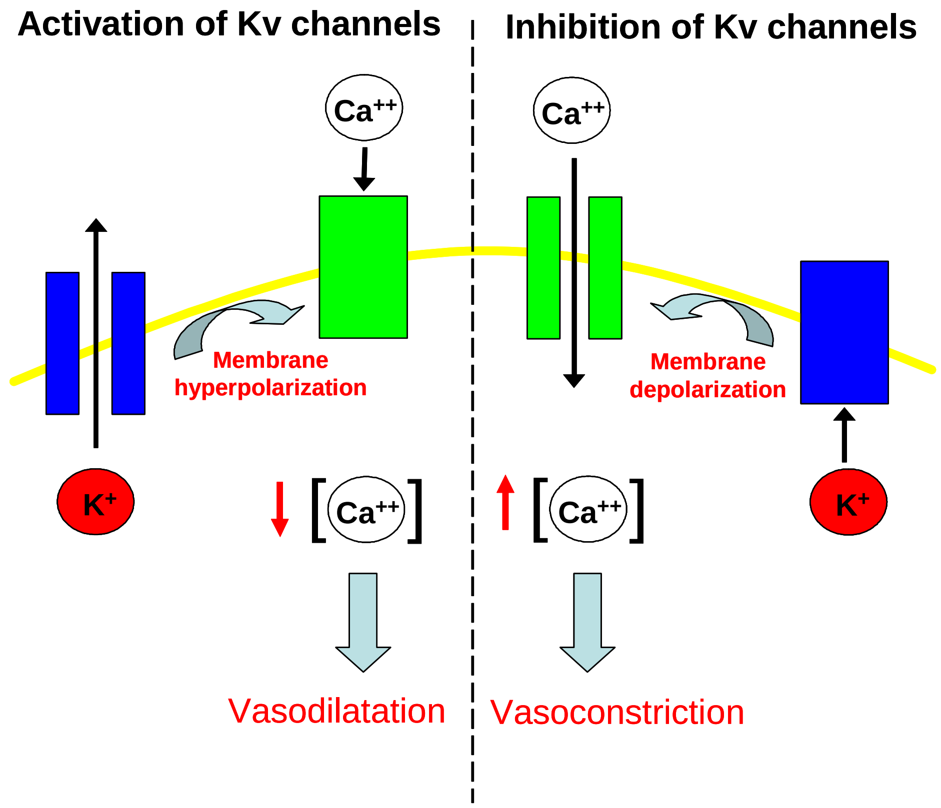

Figure 1.5 Role of Kv channels in the regulation of pulmonary vascular tone (adapted from [13])

1.1.3.5 Serotonin (5-hydroxytryptamine)

Investigations on 5-hydroxytryptamine (5-HT) in the control of the pulmonary circulation have clearly demonstrated a strong vasoconstrictive, mediated via 5-HT_{1B} receptors, and mitogenic effect. By activation of NADPH oxidase, the formation of reactive oxygen species (ROS) and the stimulation of mitogen-activated protein (MAP) kinases, 5-HT is involved in SMC hyperplasia and hypertrophy [13].

The initial rationale to investigate a possible association between 5-HT and PH was raised by the observation in the 1960s that persons taking anorectic agents like aminorex and defenfluramine have a significantly higher risk of developing pulmonary hypertension than did control subjects [2, 40]. These appetite suppressants are known to increase local and circulating 5-HT levels and also act as serotonin transporter substrates, interfering in intracellular signaling [2].

Apart from the above-mentioned association with anorectic drugs, other observations support a potential role for 5-HT in the pathogenesis of PH: Compared with control subjects, patients with PAH have decreased platelet 5-HT and increased plasma 5-HT concentrations [41, 42]. Furthermore, paSMC from patients with pulmonary hypertension grow faster than those from healthy persons when stimulated with 5-HT [43].

1.1.3.6 Natriuretic peptides

The family of natriuretic peptides consists of three major members, atrial or A-type (ANP), brain or B-type (BNP) and C-type (CNP), interacting with three receptor isotypes (NPR-A, NPR-B and NPR-C) [44]. Several studies have indicated that both ANP and BNP act as vasodilators in the pulmonary circulation, whereas CNP has only weak vasodilatory effects [13]. Both ANP and BNP exert this effect through binding to the receptor subtype NPR-A, which is guanylate cyclase-linked and thus increases the concentration of the potent vasodilator cGMP [45]. The effects of cGMP are abolished by phosphodisterases (PDE) which convert cGMP to 5-GMP [46].

The development of potent and selective PDE inhibitors, such as sildenafil, has revolutionized the therapeutic concepts for pulmonary hypertension. Several reports clearly indicate that sildenafil reduces pulmonary artery pressure in humans and is for this reason a basic component of modern PH therapy [13].

1.1.3.7 BMPR2 and Alk/endoglin mutations

At least 6 % of all cases of PH have a known family background of the disease. Genome-wide screens and linkage studies in families with multiple affected members suffering from pulmonary hypertension provided evidence for a linkage of PAH with markers on chromosome 2q31-32 [2, 47-49]. Fine-mapping and detailed linkage analysis of this interval led to the identification of mutations in the BMPR2 (bone morphogenic protein receptor 2) gene [47]. These mutations are mainly described to act as loss-of-function mutations (frame shift, nonsense mutation or splice-site variants), exaggerating the susceptibility of vascular smooth muscle cells to proliferate. Detailed genetic analysis demonstrated that heterozygous mutants have been found in approximately 60% of patients with a family history and 26% of sporadic cases of PH [49, 50].

1.2 Interleukin 13 and its receptors

1.2.1 T helper cell type 1 and 2 immune response

As illustrated in figure 1.7 native CD4+ T helper cells (Th0) can, depending on the environment of the cell, differentiate into at least two different subsets of Th cells (Th1 and Th2) which are classified on the basis of the cytokines produced [51]. The key to polarization into a Th1 phenotype is the exposure of Th0 cells to interleukin (IL) -12. Activated Th1 cells then induce a cell-mediated immune response mediated mainly by the secretion of interferon-γ (IFN- γ) [52, 53]. This pro-inflammatory chemokine stimulates phagocytosis, the up-regulation of MHC class I and II molecules on a variety of cells, thereby stimulating antigen presentation on macrophages and also initiates the oxidative burst - all together powerful weapons against intracellular pathogens [54, 55].
The induction of a Th2 cell differentiation occurs in the presence of IL-4. These differentiated Th2 cells produce a variety of anti-inflammatory cytokines, including IL-4, IL-6, IL-10 and IL-13 [53, 56]. With the help of these mediators, a humoral immune response, directed against extracellular pathogens, is promoted. Furthermore, a Th2-dominated immune response activates B cell proliferation, antibody production, and a class-switching from IgG to IgE, implicating allergic and atopic reactions, as well as airway inflammation as observed in asthma and reactive airway disease [56, 57].
In addition to their stimulatory effects, Th1 and Th2 cells cross-regulate each other. Secretion of INF- γ by Th1 cells directly suppresses IL-4 secretion and thus inhibits the development of Th2 cells, whereas IL-4 and IL-10 block the ability of Th0 cells to polarize into Th1 cells [57].

1.2.2 Interleukin-13

The cytokine Interleukin-13 (IL-13) is regarded as one of the key mediators of the T-helper cell type 2 immune response, as mentioned above. This cytokine was first cloned in the mouse in 1989 by differential hybridization of cDNA libraries of activated Th1 and Th2 cells, whereas its human homologue was cloned in 1993 [58]. It is a 132 amino-acid non-glycosylated protein with a molecular mass of 12 kD [58]. The human IL-13 gene has been mapped on chromosome 5q31 in close proximity to the IL-4 gene which is positioned in the same orientation, suggesting a common ancestral origin [58, 59]. IL-4 and IL-13 polypeptides share approximately only 25% amino acid homology, but the major α-helical regions that are responsible for their activity are highly homologous [60].

High levels of IL-13 are produced by Th2 cells after activation. Interestingly, significant levels of IL-13 can be detected early after T-cell activation and ongoing IL-13 production can still be observed 72 hours after T-cell activation whereas IL-4 levels disappear already after 12 hours [60]. For this reason, IL-13 appears as an abundant cytokine produced early and for prolonged time by activated T-cells. In contrast to IL-4, IL-13 is furthermore produced by CD45RA+ T-cells and dendritic cells (DC), whose regulatory function on these cells remains to be investigated [61].

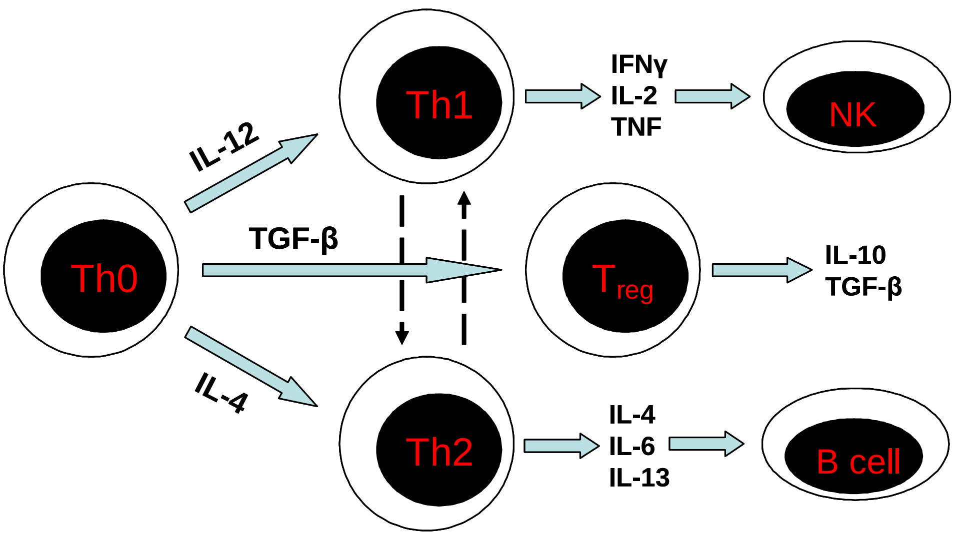

Figure 1.6 The polarization and differentiation of Th0 cells into Th1 and Th2 responses
Solid lines indicate stimulatory pathways, and dotted lines indicate inhibitory pathways.

1.2.2.1 Biological activities of IL-13

The IL-13 shares many, but not all biologic activities with IL-4. As classical key members of the Th2 system, both play an important role in the coordination of the humoral immune response. But unlike IL-4, which is know as a dominant mediator of Th2 cell differentiation, proliferation, and activity, IL-13 appears to have only minimal effects on T-cell function, and thus Th2 cell differentiation [62]. The reason for this phenomenon is a lack of IL-13Rα1 surface expression, required for IL-13 signaling, on human T cells which is consistent with the notion that activated T cells failed to bind detectable levels of radiolabeled IL-13 [58, 62]. Although IL-13 failed to have direct effects on T cells it amplifies a Th2 response by stimulating the release of macrophage-derived chemokines (MDC) binding on CCR4 and CCR3 receptors expressed on Th2 cells [63]. In addition, IL-13 supports Th2 polarization by downregulation of IL-12 in monocytes, which is known to direct Th1 development [58].

In spite of its inability to exert biological effects directly on T cells, many studies indicate that IL-13 mainly contributes to the induction of the humoral immune response through its direct activities on B cells. Binding of IL-13 to IL-13R complexes on B cells, together with CD40L-CD40 contact-mediated signals, stimulate B cell proliferation and survival [64]. Furthermore, IL-13 enhances the production of IgM, IgG, IgA and is essentially required for Ig class switching to IgG4 and IgE. This IL-13-induced IgE synthesis is initiated by germline ε transcription – a fact that outlines the importance of IL-13 as an inducer of allergic and atopic responses [65, 66].

The IL-13 cytokine has dual effects on the monocyte/macrophage system: IL-13 prolongs monocyte survival *in vitro* and enhances the expression of a variety of adhesion molecules on human monocytes, such as CD 11b/c, CD18 and CD29, probably promoting increased extravasation, mobility and trafficking of these cells (Figure 1.7) [58, 67]. Alternatively, IL-13 also enhances the antigen presentation capabilities of monocytes by increasing the expression of class II MHC antigens, CD80 and C86 – ligands for CD28 on T cells resulting in an elevated capacity to stimulate allergen-specific T cells [67].

In addition to these immunomodulatory properties IL-13 can be considered as an important anti-inflammatory cytokine as it can dampen a Th1-cell driven immune response by inhibiting the transcription of IL-12 which is necessary for Th1-cell differentiation [64]. The anti-inflammatory activities of IL-13 are further exemplified by its capacity to effectively down-regulate the production of pro-inflammatory cytokines (IL-1α, IL-6 and TNF-α) and chemokines (IL-8, MIP-1β and MCP-3) [68]. These data are supported by *in vivo* experiments in which mice with LPS-induced lethal endotoxemia could be rescued by application of IL-13 [58].

In addition to its ability to induce IgE synthesis and thus contribution to allergic-inflammatory processes, IL-13 induces VCAM-1 expression on endothelial cells resulting in the adhesion and subsequent extravasation of eosinophils, monocytes, and T cells to sites of allergic inflammation [58].

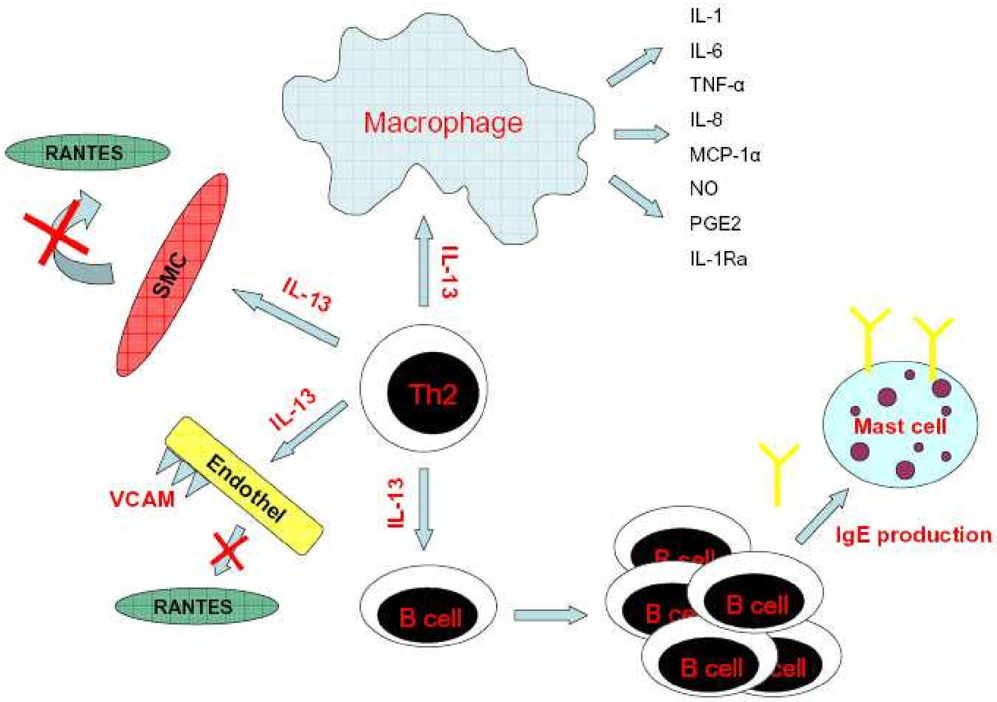

Figure 1.7 Schematic representation of some major activities of IL-13 on allergic and inflammatory processes
Stimulation of allergen specific Th2 cells by allergen-derived peptides presented by antigen-presenting cells in the context of class II MHC molecules results in production of IL-13, which induces IL-13 signaling. Together with CD40L-CD40 contact-mediated signals, B-cells are induced to proliferate and to switch into IgE-producing cells. Binding of IL-13 to IL-13R on activated macrophages induces an anti-inflammatory state of these cells, resulting in the downregulation of proinflammatory cytokine, chemokines, NO, superoxide, and PGE-2 production. In addition, IL-13 inhibits production of RANTES (Regulated on Activation, Normal T Expressed and Secreted), which is a potent eosinophil attractant, on the other hand, IL-3 induces VCAM-1 (vascular cell adhesion molecule 1) expression on endothelial cells, which promotes adhesion and extravasation of eosinophils, monocytes and T-cells to sites of allergic inflammation (adapted from [58])

1.2.3 IL-13 receptor complexes

The overlapping biological functions of IL-4 and IL-13 and studies using antibodies directed against IL-4Rα chain (IL-4R) inhibiting the biological activities of both cytokines indicate that the IL-4R and IL-13R complexes share the IL-4Rα chain as an essential component for signal transduction (Figure 1.8) [64]. The classical IL-4R complex consists of the 140 kD IL-4Rα chain which binds IL-4 with a relatively high affinity, and the 70 kD common γ-chain (γc), the later also being shared by the receptors for IL-2, IL-7, IL-9 and IL-15. The IL-13 exerts its biological functions through binding to the IL-13R complex which bears, as mentioned above, the IL-4Rα chain as an essential component [58, 63, 64, 69]. It is combined with the so-called IL-13Rα1, a 427 amino acid protein binding specifically IL-13 with a low affinity (approximately 4 nM kD). The IL-13Rα1 is expressed on naïve and memory B cells, monocytes and non-hematopoietic tissues, especially heart, liver and skeletal muscle. Besides this receptor, a second IL-13-binding protein, designated IL-13Rα2, has been identified. The IL-13Rα2 is a 380 amino acid protein, which binds IL-13 with high affinity (Kd 50 pM) in the absence of the IL-4Rα chain [58]. The human IL-13Rα1 and IL-13Rα2 chains share 27% homology – the respective genes encoding these receptors are both located on the X chromosome [58, 63]. While IL-13Rα2 alone binds IL-13 with high affinity and lacks a significant intracellular component it, appeared for a long time to act as a non-signaling decoy receptor [70].

As both IL-4R and IL-13R complexes share the signal transducing IL-4Rα chain, binding of IL-4 or IL-13 to the respective complex results in comparable signaling pathways. Upon ligand binding, Jak1 and Tyk2 kinases are activated and induce tyrosine phosphorylation of the IL-4Rα chain that allows recruitment of STAT6, a transcription factor that exists in a latent non-phosphorylated form in the cytoplasm [71, 72]. The Jak1 phosphorylates tyrosine residue 641 of STAT6, leading to a homodimerization, nuclear translocation of STAT6 and finally the activation of IL-13- and IL-4-responsive genes in various cell types expressing IL-13R and IL-4R complexes [71, 73].

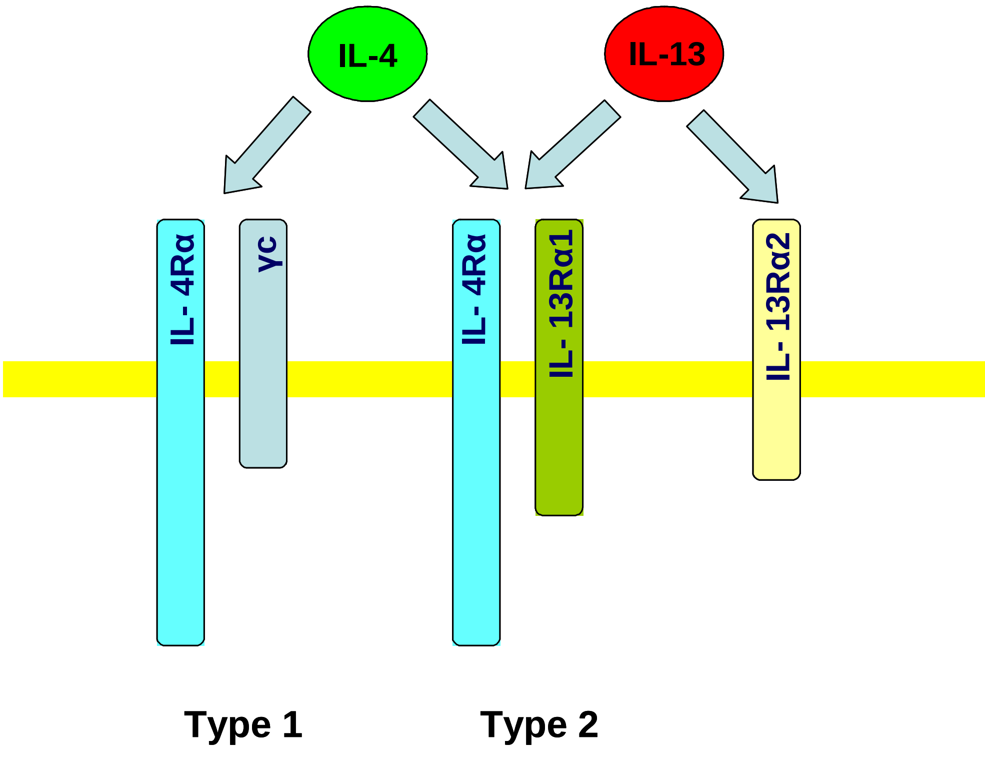

Figure 1.8 Schematic overview of IL-4 and IL-13 receptor complexes
The IL-4 interacts with the IL-14Rα binding protein in combination with either common γ-chain (γc) (type 1 complex) or IL-13Rα1 (type 2 complex). IL-13 can only functionally signal by binding to IL-4 type 2 receptor complex. The IL-13Rα2 is thought to act as a non-signaling decoy receptor.

1.2.4 Pathobiological relevance of IL-13 and its receptors

Interleukin-13 acts as a key molecule on several immunological and biological processes. The list of important effector functions of IL-13 continues to grow – including the resistance to most gastrointestinal nematodes, the mediation of allergic asthma, eosinophilic inflammation and airway hyperresponsiveness or the regulation ECM deposition. The functions, diseases and regulations of the IL-13 system or its receptors are briefly introduced, below.

1.2.4.1 Resistance to gastrointestinal nematodes and helminth expulsion

Helminth infections are in many parts of the world endemic, and nematode diseases account for more than 60 million cases per year [74]. Helminth parasites induce a strong Th2 immune response which is of major importance for the expulsion and eradication of the worms. Especially in *Nippostrongylus brasiliensis* infections, IL-13 clearly plays a superior role to IL-4 concerning host immunity and resistance [64]. Evidence for this observation arose from infection studies using IL-4Rα-deficient, STAT6- and IL-13-deficient mouse strains [64, 75-77]. In contrast to IL-4-deficient mice or wild-type controls which could expel the worms early after infection, these mutant mice were unable to do so [64]. Furthermore, studies conducted with soluble IL-13 antagonists or IL-13-deficient mice confirmed the unique and non-redundant role of IL-13 in worm eradication [64, 78, 79]. As illustrated in Figure 1.9, the Th2 induced worm expulsion is achieved by induction of gut muscle hypercontractibility and increased mucus/intestinal fluid secretion by goblet cells, facilitating the expulsion of parasites by a “weep and sweep” mechanism.

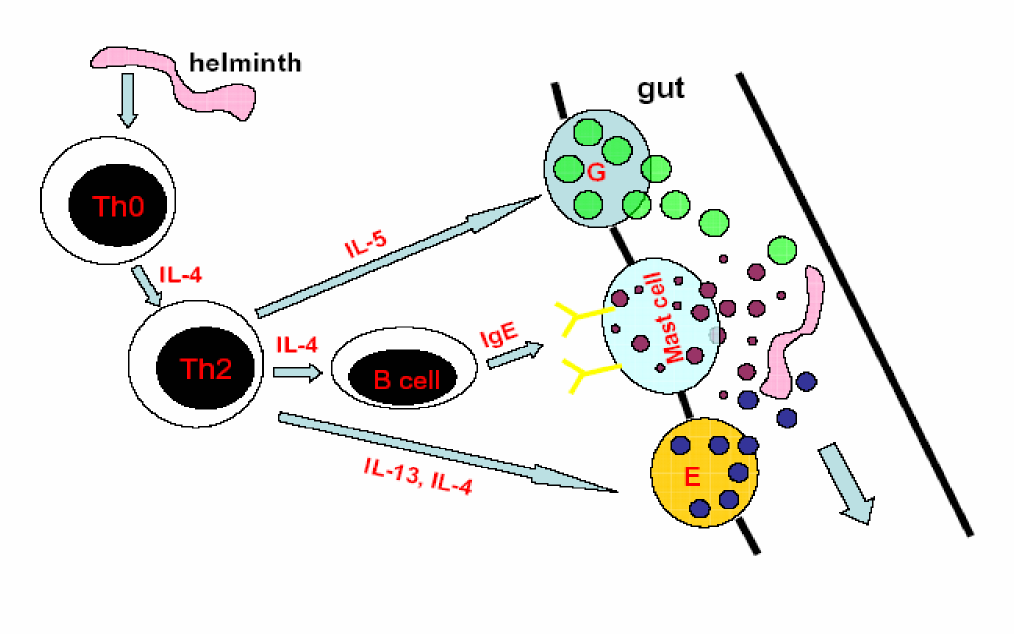

Figure 1.9 Proposed helminth model
Role of Th2 cells, effector cells and cytokine network in helminth-induced tissue injury and worm expulsion. Th0=naïve T helper cell, E=eosinophil, G=goblet cell (adapted from [64])

1.2.4.2 Allergic asthma and airway hyperresponsiveness

Allergic asthma is a wild-spread disorder characterized by allergic inflammation associated with elevated IgE levels, inducing mast cell activation/degranulation, eosinophilia, airway remodeling and reversible airway obstruction (Figure 1.10) [64]. Many studies have indicated an association between the pathology of asthma and a Th2-dominated phenotype [64]. The role of IL-4 in particular has been thoroughly investigated, indicating a clear involvement in the pathogenesis of the disease. Allergic patients exhibit elevated mRNA and protein levels, compared to controls [80, 81]. *In vivo* blockage of IL-4 or its receptors in ovalbumin (OVA)-challenged mice causes reduced airway hyperresponsiveness, inflammation and IgE production, demonstrating an important role for IL-4 [82-84].

Interleuin-13 can be also regarded as a key factor in the asthmatic phenotype. Elevated serum levels of IL-13 are significantly associated with allergic asthma [85]. In a genetic approach, endogenous IL-13 was neutralized by a soluble IL-13Rα2 Fc fusion protein in OVA-challenged wild-type mice, resulting in an attenuated asthma phenotype in these mice [86]. Moreover, administration of recombinant IL-13 was sufficient to induce an asthmatic phenotype in non-immunized wild-type mice, indicating significant involvement of Th2 cytokines, namely IL-4 and IL-13, in the pathology of asthmatic diseases, suggesting promising targets for anti-asthma therapy [64, 87].

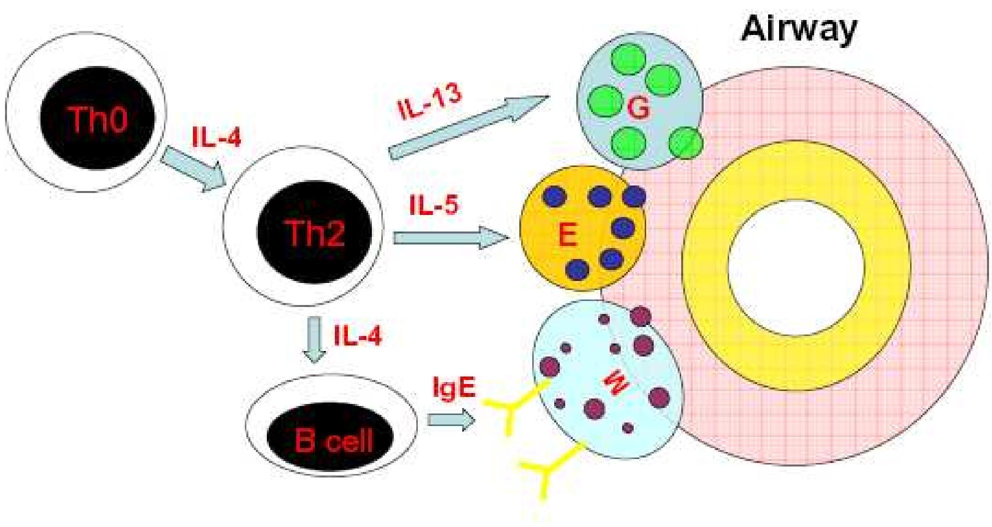

Figure 1.10 Proposed allergic asthma model
Role of Th2 cells, effector cells and cytokine network in the pathogenicity of asthma. Th0=naïve T helper cell, E=eosinophil, G=goblet cell, M=mast cell (adapted from [64, 87])

1.2.4.3 Tissue remodeling and fibrosis

Fibroproliferative disorders including interstitial lung disease or liver cirrhosis are one of the major causes of morbidity and mortality worldwide, also playing a critical role in the pathogenesis of several different chronic diseases [88]. A great deal of research provides proof that fibrogenesis is intimately linked with Th2 cytokine production. Each of the main Th2 cytokines, IL-4 and IL-13, has a distinct role in the regulation of tissue remodeling and fibrosis (Figure 1.11) [89].

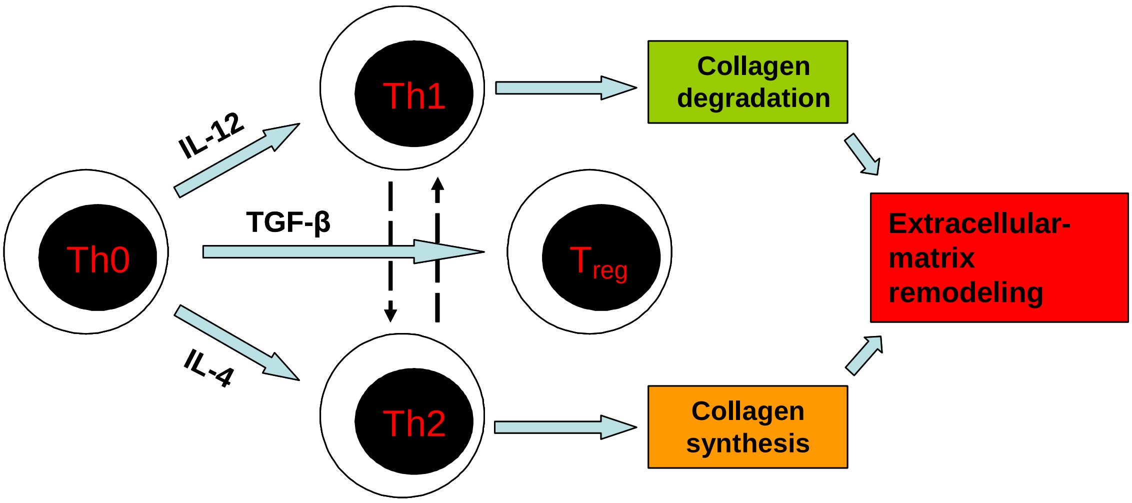

Figure 1.11 Opposing roles for Th1 and Th2 cytokines in fibrosis
The Th1 cell cytokine IFN-γ directly suppresses collagen synthesis by fibroblasts by regulation of the balance of matrix metalloproteinase (MMP) and tissue inhibitor of matrix metalloproteinase (TIMP) expression. IFN-γ and/or IL-12 might also indirectly inhibit fibrosis by reducing pro-fibrotic cytokine expression by Th2 cells. The main Th2 cytokines enhance collagen deposition by various mechanisms (adapted from [89]).

One of the most common experimental models used to study fibrosis is schistosomiasis in mice, which leads to egg-induced liver fibrosis [89]. In this model, the administration of neutralizing antibodies specific for IL-4 was associated with a consistent reduction of hepatic collagen deposition [90]. In line with these findings, inhibitors of IL-4 were able to reduce the development of dermal fibrosis. Apart from IL-4, IL-13 was also identified as a dominant mediator of tissue remodeling [91, 92]. The IL-13 can stimulate collagen deposition by fibroblasts *in vitro*, and *in vivo* blocking studies revealed a unique and non-redundant role for IL-13 in murine schistosomiasis [93, 94]. Overexpression of IL-13 in the lungs of transgenic mice induced significant subepithelial airway fibrosis, whereas administration of neutralizing IL-13-specific antibodies markedly reduced collagen deposition in murine lungs challenged with bleomycin [95, 96].

As indicated in figure 1.12, IL-13 promotes collagen deposition, and thus fibrosis, by three distinct but possibly overlapping mechanisms. The IL-13, produced by activated CD4 cells could stimulate the production of latent transforming growth factor-β (TGF-β) by macrophages, which then functions as a stimulus for fibroblast activation (Figure 1.12 A) [97, 98]. As fibroblasts express IL-13 receptors, IL-13 might also directly activate the collagen-producing machinery in fibroblasts (Figure 1.12 B) [94, 99, 100]. The IL-13 can alternatively promote the up-regulation of arginase activity, and thus increase the concentrations of L-ornithine, L-proline and polyamine which have the ability to induce collagen production and cell proliferation (Figure 1.12 C) [101].

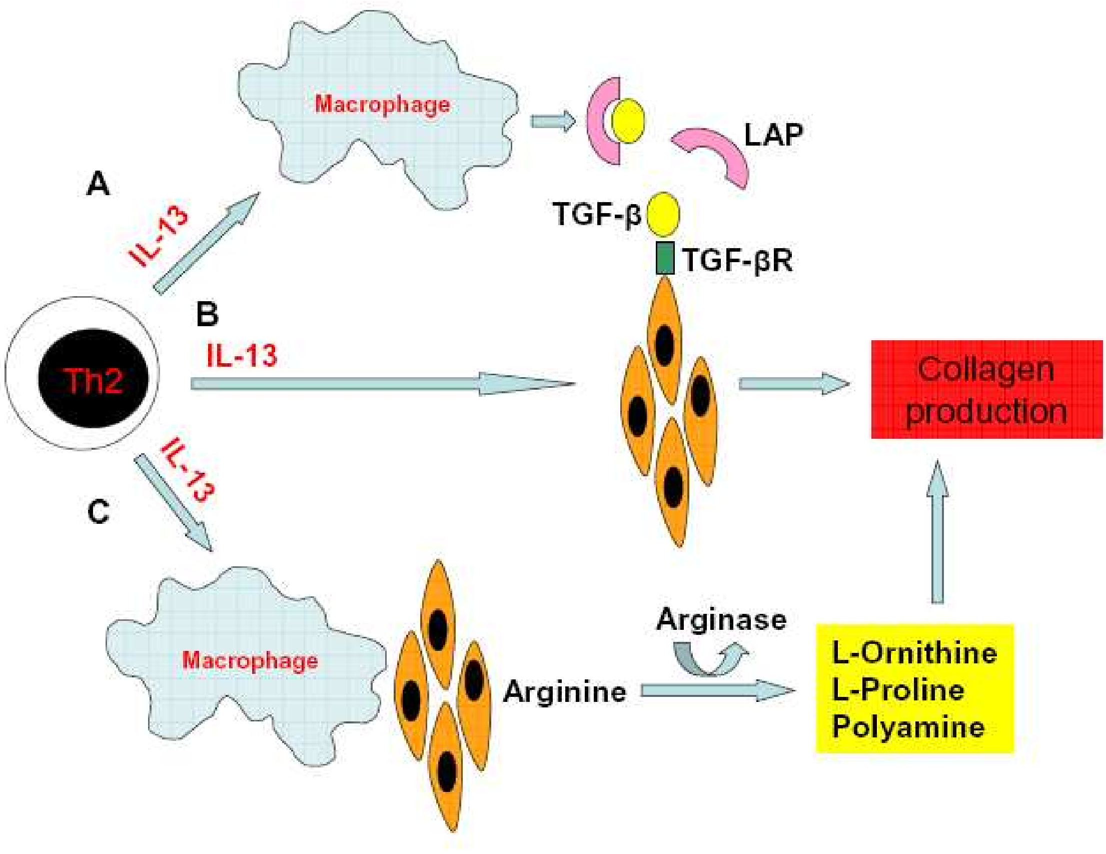

Figure 1.12 IL-13 promotes collagen production by three mechanisms
A) Activated CD4+ Th2 cells produce IL-13 which stimulates the production of latent TGF-β by macrophages. After latency-associated protein (LAP) is cleaved, TGF-β is converted to its active form and is free to bind and activate TGF-β receptors (TGF-βRs) expressed on fibroblasts and thus initiate collagen production. B) As also fibroblasts by itself express IL-13R isotypes, IL-13 might also directly activate the collagen-producing machinery in fibroblasts. C) IL-13 is also able to up-regulate arginase activity in macrophages/fibroblasts, leading to increased L-ornithine, L-proline and polyamine concentrations promoting fibroblast proliferation and collagen deposition. (adapted from [89])

1.3 Aims of the Study

Interleukin-13 has recently been implicated in the pathogenesis of tissue remodeling and fibrosis due to its potent effects on ECM deposition and cell proliferation. We therefore hypothesize that IL-13 can regulate the growth of paSMC and that this regulation is altered in IPAH. To test this hypothesis we intend to analyze IL-13R expression in IPAH patients and two animal models of pulmonary hypertension. To assess the biological effects of IL-13 on paSMC, the key cells in the pathogenesis of PAH, we aimed to investigate cell proliferation, cell cycle analysis and signaling pathways, in response to IL-13 stimulation.

2 Materials and Methods

2.1 Materials

2.1.1 Equipment

Cell Culture Incubator; Cytoperm2		Heraeus, Germany
Chroma SPIN-1000 DEPC-H_2O Columns		Biosciences, Clontech, USA
Developing machine; X Omat 2000		Kodak; USA
Electrophoresis chambers		Bio-Rad, USA
Fluorescence microscope; LEICA AS MDW		Leica, Germany
Freezer -20 ℃		Bosch, Germany
Freezer -40 ℃		Kryotec, Germany
Freezer -80 ℃		Heraeus, Germany
Fridge +4 ℃		Bosch, Germany
Mini spin centrifuge		Eppendorf, Germany
Multifuge centrifuge, 3 s-R		Heraeus, Germany
Light microscope; LEICA DMIL		Leica, Germany
PCR thermocycler		MJ Research, USA
Pipetboy		Eppendorf, Germany
Pipetmans: P10, P20, P100, P200, P1000		Gilson, France
Power Supply; Power PAC 300		Bio-Rad, USA
PVDF membranes		GE Osmotics, USA
Western blot chambers:	Mini Trans-Blot	Bio-Rad, USA
	Mini-Protean 3 Cell	Bio-Rad, USA
Vortex machine		Eppendorf, Germany
Film cassette		Sigma-Aldrich, Germany
Filter Tip FT: 10, 20, 100, 200, 1000		Greiner Bio-One, Germany
Filter units 0.22 µm syringe-driven		Millipore, USA
Glass bottles: 250, 500, 1000 ml		Fisher, Germany
Gel bloting paper 70 × 100 mm		Bioscience, Germany
Olympus BX51 microscope		Olympus, Japan
Petri dish with vents		Greiner Bio-One, Germany
Pipette tip: 200, 1000 µl,		Sarstedt, Germany
Pipette tip 10 µl		Gilson, USA
Radiographic film X-Omat LS		Sigma-Aldrich, Germany
Serological pipette: 5, 10, 25, 50 ml		Falcon, USA
Test tubes: 15, 50 ml		Greiner Bio-One, Germany
Tissue culture chamber slides		BD Falcon, USA
Tissue culture dish 100 mm		Greiner Bio-One, Germany
Tissue culture flask 250 ml		Greiner Bio-One, Germany
Tissue culture plates: 6, 24, 48 well		Greiner Bio-One, Germany
Trans blot transfer medium (0.2 µm)		Bio-Rad, USA

2.1.2 Chemicals and reagents

Acetic acid	Merck, Germany
Acrylamide solution, Rotiphorese Gel 30	Roth, Germany
Agarose	Invitrogen, UK
Ammonium persulfate (APS)	Promega, Germany

Ammonium sulfate	Sigma-Aldrich, Germany
Ampicillin sodium	Sigma-Aldrich, Germany
Annexin apoptosis detection kit	BD Bioscience, USA
Basic nucleofactor kit	Amaxa, Germany
Bradford reagent	Bio-Rad, USA
Bromophenol blue	Sigma-Aldrich, Germany
Calcium chloride	Sigma-Aldrich, Germany
Complete (Inhibitor cocktail)	Roche, Germany
D-(+)-Glucose	Sigma-Aldrich, Germany
D-MEM medium	Gibco BRL, Germany
RPMI 1640 medium	Gibco BRL, Germany
Difco yeast nitrogen base without amino acids	Biosciences, Clontech, USA
Dimethyl sulfoxide (DMSO)	Sigma-Aldrich, Germany
ECL plus	Amersham, Sweden
Endothelin-1 ELISA	R&D Systems, USA
Ethidium bromide	Roth, Germany
Ethylendinitrilo-*N, N, N´, N´,* -tetra-acetic acid (EDTA)	Promega, USA
Dublecco' s phosphate buffered saline 10 × (PBS)	Laboratories, Austria
Ethanol absolute	Riedel-de Haen, Germany
Foetal bovine serum (FBS)	Gibco BRL, Germany
Gel extraction kit	Qiagen, Germany
Glass beads	Sigma-Aldrich, Germany
β-glycerophosphate	Sigma-Aldrich, Germany
Glycine	Roth, Germany
Glycerol	Merck, Germany
2-(-4-2-hydroxyethyl)-piperazinyl-1-ethansulfonate (HEPES)	Sigma-Aldrich, Germany
Histostain-SP Kit	Zymed, USA
Hoechst 33342	Molecular probes, USA
[^{3}H]-thymidine	GE Healthcare, UK
IL-4, recombinant	R&D Systems, USA
IL-13, recombinant	R&D Systems, USA
IL-13 ELISA	R&D Systems, USA
Igepal CA-630	Sigma-Aldrich, Germany
Lipofectamine	Invitrogen, UK
Lithium acetate	Sigma-Aldrich, Germany
Luria–bertani medium	Invitrogen, UK
MiniElute Gel Extraction Kit	Qiagen, Germany
Magnesium chloride	Sigma-Aldrich, Germany
Magnesium sulfate	Sigma-Aldrich, Germany
β-mercaptoethanol	Sigma-Aldrich, Germany
Methanol	Fluka, Germany
pcDNA3.1	Invitrogen, USA
pGEM-T Easy Vector System Kit	Promega, Germany
Phosphate-buffered saline (PBS)	PAA, USA
Platinum Taq DNA polymerase	Invitrogen, Germany
Polyethylene glycol 6000	Merck, Germany
Potassium acetate	Sigma-Aldrich, Germany
Potassium chloride	Merck, Germany
Potassium phosphate	Sigma-Aldrich, Germany
Precision Plus Protein™ Standards	Bio-Rad, USA
2-Propanol	Merck, Germany
Pure Yield Plasmid Midiprep System	Promega, Germany
Restriction endonucleases	Promega, Germany
RNase inhibitor	Promega, Germany

RNeasy midi Kit	Qiagen, Germany
Rnase H$^-$ reverse transcriptase	Promega, Germany
Select agar	Invitrogen, UK
Sodium acetate	Sigma-Aldrich, Germany
Sodium chloride	Merck, Germany
Sodium dodecyl sulfate (SDS)	Promega, USA
Sodium phosphate	Sigma-Aldrich, Germany
Sodium sulfate	Merck, Germany
Taq DNA polymerase	Invitrogen, Germany
T4 DNA ligase	Promega, Germany
TEMED	Invitrogen, Germany
Tween 20	Sigma-Aldrich, Germany
Tris	Roth, Germany
Triton X-100	Promega, USA
Trypsin/EDTA	Gibco BRL, Germany
QIAprep spin miniprep kit	Qiagen, Germany
Xylene	Merck, Germany

2.1.3 Antibodies

STAT-Sampler Kit	Cell Signaling, USA
HRP-conjugated secondary antibodies	Pierce, USA
Anti-IL-13 antibody	R&D Systems, USA
Anti-IL-13Rα1 antibody	R&D Systems, USA
Anti-IL-13Rα2 antibody	R&D Systems, USA
Anti-IL-4R antibody	Santa Cruz, USA
Anti-SMA antibody	Santa Cruz, USA
FITC-conjugated IgG	Zymed, USA
Anti-Alexa Fluor 647	Molecular Probes, USA

2.2 Methods

2.2.1 Polymerase chain reaction

The Polymerase chain reaction (PCR) is a molecular biological technique for enzymatic amplification of specific regions of the DNA strand. To perform a PCR, several basic components are required:

- DNA template (containing the DNA fragment to be amplified)
- A pair of primers (flanking the beginning and end of the region to be amplified)
- DNA polymerase (catalyses the *in vitro* DNA amplification)
- Deoxynucleotidetriphosphates, which are incorporated into the new DNA strand by the polymerase
- Reaction buffer and magnesium to generate an optimal environment for DNA polymerase

This reaction mix is transferred to a thermal cycler, which performs the PCR process, consisting of a series of 20 to 40 repeating cycles. In principal, each PCR cycle consists of three steps:

- Denaturation (by heating double-stranded DNA to 95 °C two separated single strands are generated)
- Annealing (primers attach to the respective single DNA strands)
- Elongation (at a temperature of 72 °C the DNA poly merase amplifies the specific primer-flanked DNA region by adding complementary nucleotides)

After each PCR cycle, one new copy of the primer-flanked DNA fragment is generated; by repeating this process 30 to 40 times, one can achieve a 10^6-10^7 fold amplification. At the end, the PCR product can be separated due to its size by agarose gel electrophoresis and visualized by the use of intercalating dyes like ethidium bromide.

2.2.1.1 Quantitative reverse-transcriptase PCR

This PCR method allows the simultaneous amplification and quantification of a specific DNA fragment. In principal, it follows the basic pattern of a conventional PCR (2.2.1) but this technique quantifies the amount of amplified PCR-products after each cycle ("real-time"). In addition to the basic components, the reaction mix of a qRT-PCR contains a fluorescent dye (for example, SYBR Green) that intercalates with double-stranded DNA.

During the PCR reaction the DNA-binding dye now intercalates with the newly synthesized double-stranded DNA, resulting in an increase in fluorescence intensity which is measured at the end of each cycle thus allowing to quantify the initial DNA concentration by using a housekeeping gene, whose expression levels remain constant in most cells or tissues, or external standard samples with known concentration.
Briefly, 2 µl cDNA were places into 23 µl reaction volume containing SYBR Green PCR mix and sequence-specific oligonucleotide primers. All real-time reactions were carried on a ABI 7700 Sequence Detection System, and analysis were performed with the accompanying software.

2.2.1.2 Reverse-transcription PCR (RT-PCR)

Reverse transcription polymerase chain reaction (RT-PCR) is an enzymatic reaction carried out by reverse transcriptase (RT), which synthesizes complementary DNA (cDNA) using mRNA as a template. In order to perform such a RT-PCR, 50-500 ng of total RNA was added to 1 µl of oligo-$(dT)_{15}$ (100 µg/ml) primers in a appropriate reaction tube and heated at 70 ℃ for 5 min. After cooling on ice, th e following RT reaction reagents were added:

Components:	Volume:	Final concentration:
5 × RT buffer ($MgCl_2$ free)	4 µl	1 ×
25 mM $MgCl_2$	4.8 µl	6 mM
10 mM dNTP mix	1 µl	0.5 mM
RNAsin inhibitor (1 U/µl)	1 µl	1.0 U
Reverse transcriptase (1 U/µl)	1 µl	1.0 U
RNAse free water	to 20 µl	not applicable

To complete the RT amplification, this reaction mix was incubated at 25 ℃ for 5 min, followed by incubation at 42 ℃ for 1 h.

2.2.2 RNA Isolation

In order to isolate RNA from lung tissue and cultured cells, we performed RNA isolation with the RNeasy mini kit (QIAGEN, Germany) according to the manufacturer's instructions.

2.2.3 Cloning of PCR products

2.2.3.1 PCR product purification

To design a pair of primers for subcloning a DNA fragment into a vector, the DNA template was analyzed for the appropriate restriction sites using the program DNA Star (DNAStar, Madison, USA). The DNA fragment was amplified using PCR, analyzed and separated by agarose gel electrophoresis, excised and gel-purified using a commercially-available gel extraction kit according to the manufacturer's instructions.

2.2.3.2 Ligation of PCR products into pGEM-T Easy vector

Both the purified PCR product and the pGEM-T Easy vector were ligated using the following ligation mix:

Components:	Volume:
2 × rapid ligation buffer	5 µl
pGEM-T Easy vector (50 ng)	1 µl
Purified PCR product	dependent on DNA concentration
T4 DNA ligase	1 µl
Autoclaved, deionized water	to 10 µl

This reaction mix was incubated overnight at 4 °C.

2.2.3.3 Transformation and propagation of plasmids

After ligation, the plasmids were transformed into competent *E. coli* DH5α for further amplification. For this purpose, 1 µg plasmid DNA was added to 50 µl of competent bacteria and the samples were incubated on ice for 30 min. After the incubation, cells were heat-shocked for 1 min in a 42 °C water bath. Eight hundred µl of LB medium (1% bacto tryptone, 0.5% bacto yeast extract, 1% NaCl, adjusted to pH 7.0 and sterilized for 20 min at 120°C, 15 psi) was added and bacteria wer e shaken for 1 h at 37 °C, 250 rpm. After centrifugation (room temperature, 5 min, 3000 x g) 800 µl of the supernatant was discarded, the bacterial pellet was resuspended in the medium left and then plated on LB plates (LB medium plus 1.5% agar) containing appropriate antibiotics. The plates were then incubated at 37 °C overnight. The following da y, individual bacterial colonies were picked from the plate, inoculated into LB medium containing the appropriate antibiotics and shaken overnight at 37 ℃, 250 rpm. Afterwards, plasmids were isolated using a Qiagen plasmid isolation kit.

2.2.3.4 Subcloning in expression vectors

To subclone a PCR fragment cloned into pGEM-T Easy into a mammalian expression vector, both empty expression vector and the pGEM-T Easy plasmid containing the PCR product of interest were digested with the same restriction enzymes for 1-3 h at 37 ℃, separated by agarose gel electrophorsis and gel-purified. The purified PCR product and the purified vector were then ligated at a ratio 3:1, adding T4 DNA ligase and incubating at 30 min at room temperature. The following steps are performed as described in the previous chapter (2.2.3.3). All constructs used were verified by sequencing.

2.2.4 Western blot

2.2.4.1 Cell lysis and protein extraction

In order to isolate proteins from cells grown on cell culture plates, confluent monolayers of cells were washed twice with ice-cold phosphate buffered saline (PBS), lysis buffer was applied directly onto the cell culture plate, and cells were detached by scraping, were transferred to a microcentrifuge tube, and were incubated for 30 min on ice, for complete lysis. After centrifugation for 15 min, the supernatant was mixed with 2 x SDS buffer, boiled, and proteins were resolved by SDS-PAGE.

<u>Lysis buffer:</u>
20 mM Tris-HCl, pH 7.5
150 mM NaCl
1 mM EDTA
1mM EGTA
1% Triton X-100
2.5 mM sodium pyrophosphate
1 mM β-glycerophosphate
1 mM sodium vanadate
Proteases inhibitor cocktail

<u>2 × SDS buffer:</u>

125 mM Tris-HCl, pH 6.8

20% (v/v) glycerol

4% (w/v) SDS

10% (v/v) β-mercaptoethanol

0.025% (w/v) bromophenol blue

2.2.4.2 SDS polyacrylamide gel electrophoresis

The denaturating SDS polyacrylamide gel electrophoresis (SDS-PAGE) was used to separate proteins electrophoretically according to their molecular weight. Separation gels with 5-12.5 % of acrylamid, covered with a 6 % stacking gel, were used. Before loading samples were denaturated with 2 x SDS buffer for 5 min at 95 ºC. The electrophoresis was performed using the SDS-PAGE running buffer and constant voltage of 120 V.

<u>Stacking gel:</u>

5% acrylamide/bisacrylamide

125 mM Tris-HCl, pH 6.8

0.1% (w/v) SDS

0.1% (w/v) APS

0.1% (v/v) TEMED

<u>Separating gel:</u>

8-12% acrylamide/bisacrylamide

375 mM Tris-HCl, pH 8.8

0.1% (w/v) SDS

0.1% (w/v) APS

0.1% (v/v) TEMED

<u>SDS-PAGE running buffer:</u>

25 mM Tris-HCl, pH 8.3

250 mM glycine

0.1% (w/v) SDS

2.2.4.3 Protein blotting and detection

Proteins were denatured in SDS sample buffer containing 5% β-mercaptoethanol, resolved by SDS-PAGE and transferred to 0.25 µm pure nitrocellulose membranes. The protein transfer was performed for 60 min with constant voltage of 100 V. After transfer, membranes were blocked with blocking buffer for 1 h at room temperature. Immunoblotting was performed with the appropriate primary antibodies diluted in blocking buffer at 4 ºC overnight. After washing 3 x TBST for 10 min membranes were incubated with a horseradish peroxidase (HRP)-coupled secondary antibody for 1 h at room temperature. After washing (5x), proteins were detected by incubating the membrane with the enhanced chemiluminescent immunoblotting system for 5 min at room temperature. Protein bands were visualized by applying a X-ray film for 10 s – 15 min depending on the strength of the signal.

Transfer buffer, pH 7.4:
24 mM Tris base
193 mM glycine
10% (v/v) methanol

Blocking buffer:
5% (w/v) non-fat dry milk in PBS, containing 0.01% (v/v) Tween 20

TBST buffer:
20 mM Tris, pH7.4
15 mM NaCl
0.05% (v/v) Tween 20

2.2.5 Proliferation assay

To assess the effects of IL-13 on SMC proliferation, a [^{3}H]-thymidine incorporation assay was performed, which monitors DNA synthesis. For this, cells were seeded into 48-well plates. Cells were pulsed with 0.6 µCi of [^{3}H]-thymidine for 4-8 h and washed ice-cold PBS. Subsequently, samples were solubilized in 0.5 M NaOH and incubated overnight at 4 ℃. The following day the content of each well wa s then transferred into scintillation fluid and incorporated radioactivity counted in a scintillation counter.

2.2.6 Apoptosis assay

Cells were cultured in six-well culture dishes and treated as indicated. Following trypsinization, cells were centrifuged (1200 x g, 7 min), resuspended in cell culture medium, and incubated with Hoechst 33342 nuclear dye according to the manufacturer's instructions. Necrotic cells were excluded by propidium iodide (PI) staining. The cell suspension was transferred to a glass slide and individual cells were analyzed by fluorescence microscopy by counting.

2.2.7 Flow cytometric cell cycle analysis

For the analysis of cell cycle distribution, control and IL-13-treated cells were harvested by trypsinization, fixed overnight with 75% methanol at -20 °C, washed in PBS, and incubated with 100 µg/ml RNase and stained with 10 µg/ml PI for 1 h at 37 °C. Samples were analyzed for DNA content using a high-speed cell sorter. Gates based on forward and side scatter were set to eliminate cellular debris and cell clusters. Data were computer-analyzed with commercially-available software (Multicycle; Phoenix Flow Systems, San Diego, CA).

2.2.8 Flow cytometry

Cells were harvested by trypsinization and fixed by incubation with 1% paraformaldehyde for 15 min at 4 °C, washed once in PBS before resuspending in 1% BSA in PBS. Staining of the IL-13Rα2 was performed for 1 h at 4 °C with anti-human IL-13Rα2 antibody (dilution: 1:20), washed and then incubated with rabbit anti-goat-Alexa Fluor 647 secondary antibody (dilution: 1:500) for 30 min. Positively-stained cells were gated using a secondary antibody control samples incubated in the absence of the anti-IL-13Rα2 antibody. Data were collected using a FACSCanto flow cytometer and analyzed by the WinMDI 2.8 software package (Scripps Institut, La Jolla, CA). A minimum of 10000 cells was analyzed per sample. Gates based on forward and side scatter were set to eliminate cellular debris and cell clusters.

2.2.9 Immunofluorescence

Pulmonary artery smooth muscle cells were seeded onto eight-well chamber slides at 10 x 10^3 per well and treated as indicated. Cells were then washed with cold PBS and fixed with ice-cold methanol for 10 min at -20 ℃. After washing twice with PBS slides were incubated in blocking buffer (5% (v/v) FCS in 1 x PBS) for 1 h at room temperature, followed by an overnight incubation with the primary antibodies at 4 ℃, as depicted. After washing, incubation with FITC-labeled secondary antibodies, cells were washed 5x with PBS, the plastic border of the slide was removed and slides were covered with mounting medium and a cover slide. Nuclei were visualized by 4,6-diamidino-2-phenylindole (DAPI) staining and individual cells analyzed by deconvolution fluorescence microscopy using the Leica AS-MDW.

2.2.10 Immunohistochemistry

To localize and assess the expression of particular proteins in human lung sections, immunohistochemical analysis was performed using a standardized avidin/biotin detection system (Histostain-SP Kit). At first, formalin-fixed paraffin-embedded tissue sections (3 µm thickness) were incubated overnight at 48 ℃ and deparaffinized in xylene. After rehydration using a stepwise decreasing gradient of ethanol concentrations (100 % to 70 %), and quenching of endogenous peroxidase activity with 1% (v/v) H_2O_2, slides were blocked with serum blocking solution for 1 h at room temperature and incubated with the relevant primary antibody at the desired concentration overnight at 4 ℃. The following day, slides were incubated with biotinylated secondary antibody for 10 min at room temperature and subsequently 100 µl of a substrate chromogen mixture was added to each section. Slides were developed for 5 min with diaminobenzidine (DAB) and counterstained with Mayers hematoxylin. Finally, sections were coverslipped in glycerol and evaluated using an Olympus BX51 microscope.

2.2.11 Laser-captured microdissection

The technique of laser-captured microdissection (LCM) was used to isolate pulmonary arteries from lung sections. For this purpose, cryo-sections from lung tissue were mounted on uncoated glass slides. After hemalaun staining, the sections were immersed in 70% and 96% ethanol and stored in 100 % ethanol until use. Pulmonary arteries were selected and microdissected under optical control using the Laser Microbeam System (P.A.L.M, Germany). Afterwards, vessels were isolated using a sterile 30 G needle. Needles with adherent material were transferred into a reaction tube containing RNA lysis buffer.

2.2.12 Agarose gel electrophoresis

DNA fragments of vectors were separated on 1% or 1.5% agarose gels according to their size. For preparation of the gels and the running buffer 1x TAE buffer was used. Agarose was mixed with TAE buffer and melted in a microwave. Before pouring the gel 10 µg/ml of ethidium bromide was added to visualize the DNA.

Before loading the sample on the gel 6 times concentrated loading buffer was added. Gels were run at 100 Volt for 20 minutes. The isolation of DNA fragments from the gel was done with the help of the Qiagen gel extraction kit according to the manual.

1 × TAE buffer:
40 mM Tris-acetate, pH 8.0
1 mM EDTA; pH 8.0

6 × loading buffer:
0.025% (w/v) bromophenol blue
40% (w/v) sucrose

2.2.13 Cell culture of pulmonary artery smooth muscle cells

2.2.13.1 Isolation of pulmonary artery smooth muscle cells

Primary smooth muscle cells (SMC) were isolated from human pulmonary arteries from healthy transplant donors by carefully preparing <1 mm³ pieces without adventitial tissue as assessed by microscopic control. The pieces of tissue were placed into cell culture dishes filled with 500 µl of smooth muscle cell growth medium supplemented with growth factors and cultured at 37 °C, 95% air-5% CO_2. Pulmonary artery smooth muscle cells (paSMC) were characterized by typical morphological appearance in phase-contrast microscopy and indirect immunofluorescent antibody staining for smooth muscle-specific isoform of α-actin. Experiments were performed with cells in passage 3-8.

2.2.13.2 Cell culture of pulmonary artery smooth muscle cells

Pulmonary artery smooth muscle cells were cultured in cell culture plates in smooth muscle cell growth medium supplemented with 5 % fetal bovine serum (FBS), epidermal growth factor (0.5 µg/l), basic fibroblast growth factor (2 µg/l) and insulin (5 mg/l) and maintained under 5 % CO_2 at 37 °C in a humidified atmosphere. To split the cells, confluent cell culture plates were washed once with PBS and incubated with trypsin-EDTA solution for 5-10 min. The detached cells were then diluted with cell culture medium containing FBS in ratios from 1:5 to 1:10 and transferred into a new cell culture plate [102]. Pulmonary artery smooth muscle cells exhibited typical spindle-shaped morphology throughout culture, and stained positive for smooth muscle-specific α-actin. For all experiments reported, only passages four to eight were used. Quiescence, when indicated, was achieved by serum withdrawal for 24 h [102].

PBS (phosphate-buffered saline):
0.08% (m/v) NaCl
0.02% (m/v) KCl
0.115% (m/v) $Na_2HPO4 \cdot 2H_2O$
0.02% (m/v) $KH_2PO4 \cdot 2H_2O$
pH 7.4 adjusted with NaOH; sterilized for 20 min at 121 ℃, 15 psi

Trypsin-EDTA solution:
0.25% (m/v) trypsin
1.23 g/l EDTA

2.2.13.3 Cell culture under hypoxic conditions

To study the effect hypoxia in paSMC, cells were seeded onto culture dishes and supplemented with cell culture medium during time of adherence (20-24 h) as described above. To simulate hypoxic conditions cells were placed into a chamber equibrilated with a water-saturated gas mixture of 1% O_2, 5% CO_2, and 94% N_2 at 37℃ for a 24 h period. Control cells were cultured in water-saturated room air supplemented with 5% CO_2 at 37℃.

2.2.14 Enzyme linked immunosorbant assay

In order to determine both IL-13 and endothelin-1 protein concentrations in serum and cell culture supernatants, an enzyme linked immunosorbant assay (ELISA) systems from R&D systems was used according to the manufacturer’s instructions.

2.2.15 Transfection of pulmonary artery smooth muscle cells

Transient transfection of plasmids is a technique to transfer DNA into eukaryotic cells. This method is transient, as the transfected DNA is not integrated into the host genome.
For transfection of paSMC the Nucleofactor technology from Amaxa Biosystems has been used. This assay is based on the principle of a unique combination of electrical parameters and cell-type specific solutions that transport DNA directly into the nucleus. Under optimal conditions a transfection efficiency in primary smooth muscle cells of 60% – 90% can be achieved. In addition, paSMC transfected with this method are viable and continue to retain the paSMC phenotype. The transfection was performed according to the protocol from the Basic Nucleofector Kit (Amaxa Biosystems, Gaithersburg, MD, USA).

2.2.16 Microarray experiments

Microarray experiments were performed in collaboration with Dr. Jochen Wilhelm (Institut for Pathology). In brief, paSMC were isolated and cultured for 24 h. Cells were stimulated with IL-13 (10 ng/ml) for 2 and 6 h.
The RNA was purified using the RNeasy Mini Kit (Qiagen, Hilden, Germany) following the kit instructions. The RNA quality was assessed by capillary electrophoresis using the Bioanalyzer 2100 (Agilent Technologies, Palo Alto, CA). Purified total RNA was amplified and Cy-labeled using the dual-color LIRAK kit (Agilent) following the kit instructions. Per reaction, 1 µg of total RNA was used. The samples were labeled with either Cy3 or Cy5 to match a balanced dye-swap design. The Cy3- and Cy5-labeled aRNA were hybridized overnight to a 44K 60mer oligonucleotide spotted microarray slides (Human Whole Genome 44K; Agilent Technologies). Hybridization and subsequent washing and drying of the slides was performed following the Agilent hybridization protocol.
The dried slides were scanned using the GenePix 4100A scanner (Axon Instruments, Downingtown, PA). Image analysis was performed with GenePix Pro 5.0 software, and calculated values for all spots were saved as GenePix results files. Stored data were evaluated using the R software (R Foundation for statistical computing, 2007) and the limma package from BioConductor [103]. The spots were weighted for subsequent analyses according to the spot intensity, homogeneity, and saturation. The spot intensities were corrected for the local background using the method of Edwards [104] with an offset of 64 to stabilize the variance of low-intensity spots. The M/A data were LOESS normalized [105] before averaging. Genes were ranked for differential expression using a moderated t-statistic [106]. Pathway analyses were performed using Pathway-Express from the Onto-Tools [107].

2.2.17 Animal models of pulmonary hypertension

2.2.17.1 The monocrotaline rat model of pulmonary hypertension

Monocrotaline (MCT) is a pyrrolizidine alkaloid, which after single administration in rats, causes pathologic alterations in the lung and heart comparable to what is observed in human PAH. After administration, MCT is first activated by the liver to the electrophile monocrotaline pyrole (MCTP), which has characteristics of a bifunctional cross-linking agent, and has a half-life of~3 s in aqueous environments at neutral pH.

Stabilization of MCTP by red blood cells facilitates its subsequent transport to the lung, where it induces endothelial injury by covalent reactions with cytosolic and cytoskeletal proteins.

To induce pulmonary arterial hypertension adult male Sprague-Dawley rats received a single intraperitoneal injection of MCT (60 mg/kg). Monocrotaline was dissolved in 0.5 N HCl, and the pH was adjusted to 7.4 with 0.5 N NaOH. Control rats received an equal volume of isotonic saline. Hemodynamic measurements and lung extraction were performed as described [108, 109]. All experiments performed in this thesis dealing with the MCT-treated animals were performed in collaboration with the group of Prof. Schermuly (University of Giessen Lung Center).

2.2.17.2 The hypoxia-induced pulmonary hypertension model

During early period of hypoxic exposure, pulmonary vascular resistance is increased due to hypoxic vasoconstriction, whereas chronic hypoxic treatment elevates vascular resistance by causing structural changes in pulmonary vasculature.

For the experiments male Balb/c mice were exposed to normobaric hypoxia (FiO_2 = 0.1) in a ventilated chamber. Mice exposed to normobaric normoxia were kept in similar chambers at a FiO_2 of 0.21. After seven and 21 days, animals were intraperitoneally anesthetized, a mid-sternal thoracotomy was performed, and the lungs were flushed through catheter in the pulmonary artery with an equilibrated Krebs Henseleit buffer (125 mM/l NaCl, 4.3 mM/l KCl, 1.1 mM/l KH_2PO_4, 2.4 mM/L $CaCl_2$, 1.3 mM/l $MgCl_2$, and 13.32 mM/l glucose) at a pressure of 20 cm H_2O at room temperature [110, 111]. During perfusion of the lungs the buffer was allowed to drain freely from the catheter in the left ventricle. Once the effluent was clear of bubbles, 800 µl prewarmed TissueTek was installed into the airways. After ligation of the trachea, the lungs were excised and immediately frozen in liquid nitrogen [111]. Preparation of the hypoxic animals was continuously performed in the hypoxic environment. All experiments performed in this thesis dealing with the hypoxia-treated animals were performed in collaboration with the group of Prof. Weissmann (University of Giessen Lung Center).

3 Results

3.1 Interleukin-13 receptor gene expression

In our initial experiments the gene expression IL-13 receptor isotypes IL-4Rα, IL-13Rα1 and IL-13Rα2 was analyzed by profiling a human multiple tissue panel. As shown in Figure 3.1, IL-4Rα and Il-13Rα1 genes were consistently expressed in all tissues investigated, while mRNA levels of IL-13Rα2 varied significantly amongst tissues. The L-13Rα2 mRNA levels were highest in the lung, liver, brain, kidney, and thymus.

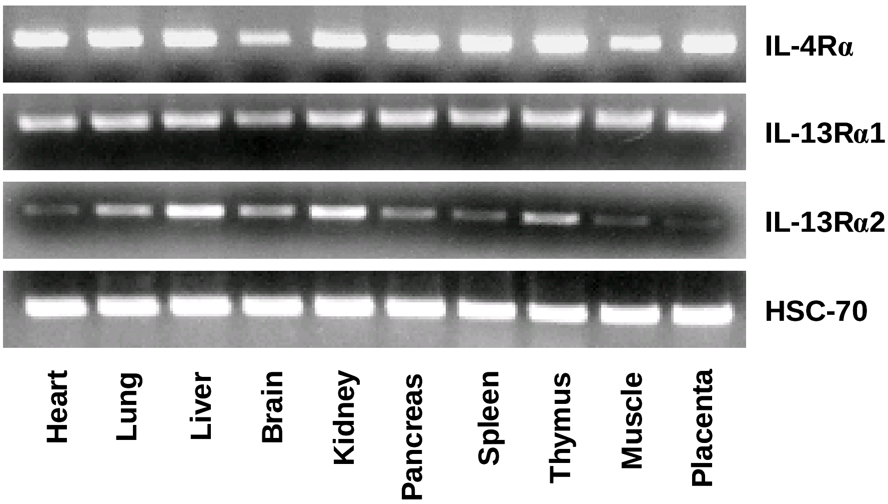

Figure 3.1 Gene expression of IL-13R isotypes in multiple tissues
Expression analysis of IL-4Rα, IL-13Rα1 and IL-13Rα2 was performed by RT-PCR of a multiple tissue RNA panel (in average 3 different donors pooled). Heat shock cognate (HSC)-70 served as a housekeeping gene.

As all IL-13 receptor isotypes were highly expressed in lung tissues, the relative expression levels of the IL-13 receptor isotypes were analyzed in whole lung homogenates, as well as in isolated paSMC. We observed that IL-13Rα2 was highly enriched in paSMC (as indicated by a ΔCt value of 4.39+/-0.4 in paSMC, compared with -4.72+/-1.2 in lung homogenates) as depicted in Figure 3.2. In contrast, the relative expression of IL-4Rα and IL-13Rα1 mRNA was similar in these samples. The enrichment of IL-13Rα2 mRNA in paSMC was confirmed at the protein level by immunostaining of human lungs, demonstrating an intense staining of IL-13Rα2 in vascular smooth muscle cell (Figure 3.3.).

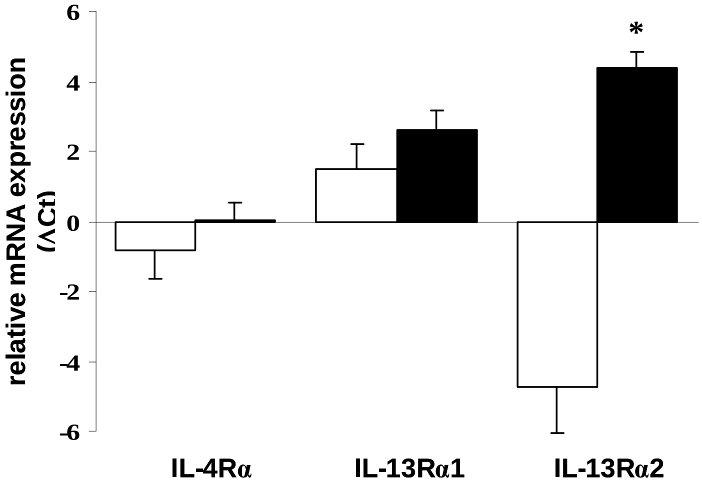

Figure 3.2 Expression patterns of IL-13R isotypes in the lung
Quantitative RT-PCR analysis of IL-13R receptor isotypes comparing mRNA isolated from lung homogenates (n=4, white bars) and primary isolated of paSMC (n=4, black bars). PBGD was used as an internal control. Values represent mean +/- SEM; *, p<0.05

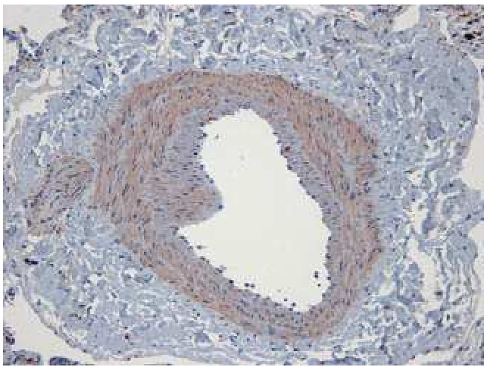

Figure 3.3 Localization of IL-13Rα2 in the lung
A representative picture of IL-13Rα2 protein localization in the normal human lung analysed by immunohistochemistry

3.2 IL-13 receptor expression in IPAH

The high expression of IL-13Rα2 in paSMC *in vivo* and *in vitro* prompted us to investigate whether this receptor system may play a role in vascular remodeling of the pulmonary arteries, a key feature of pulmonary hypertension. To elucidate a potential association between IL-13R isotypes and PAH, we thus analyzed IL-13R gene expression by RT-PCR, comparing mRNA samples derived from six control donors and six lungs from patients with idiopathic pulmonary arterial hypertension (IPAH). Using semi-quantitative RT-PCR, we were able to observe a significant up-regulation of IL-13Rα2 mRNA expression in lungs of IPAH patients compared with donors (Figure 3.4). In contrast, the mRNA expression of IL-4Rα, IL-13Rα1 and the housekeeping gene porphobilinogen deaminase (PBGD) which was employed as a loading control, remained unchanged (Figure 3.4).

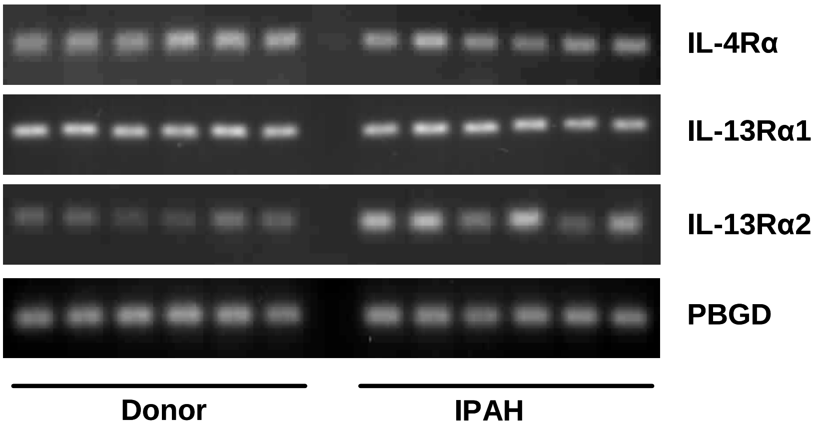

Figure 3.4 Analysis of IL-13 receptor isotype expression in IPAH
Semiquantitative RT-PCR was performed using RNA from fresh frozen lung tissues derived from healthy controls (n=6, donor lungs) or IPAH patients (n=6). PBGD served as a loading control.

The above described up-regulation of IL-13Rα2 in samples derived from patients with IPAH could also be confirmed by quantitative RT-PCR (Figure 3.5).

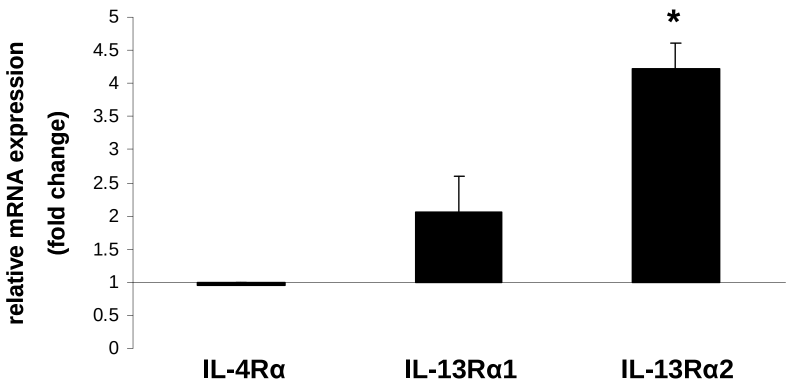

Figure 3.5 Quantitative analysis of IL-13R expression in IPAH
Quantitative RT-PCR of IL-13 receptor expression was performed using RNA from fresh frozen lung tissues derived from healthy controls (n=6) or IPAH patients (n=6). PBGD was used as an internal control. Values represent mean +/- SEM; *, p<0.01.

To assess whether this increased expression of IL-13Rα2 indeed occurred in paSMC *in vivo*, we performed laser-captured microdissection (LCM) analysis of small pulmonary arteries from donor and IPAH lungs (Figure 3.6). Quantitative RT-PCR of microdissected pulmonary arteries demonstrated an up-regulation of IL-13Rα2 mRNA (ΔCt of -1.69+/-0.3 and -0.12+/-0.9 for donor and IPAH, respectively) (Figure 3.7).

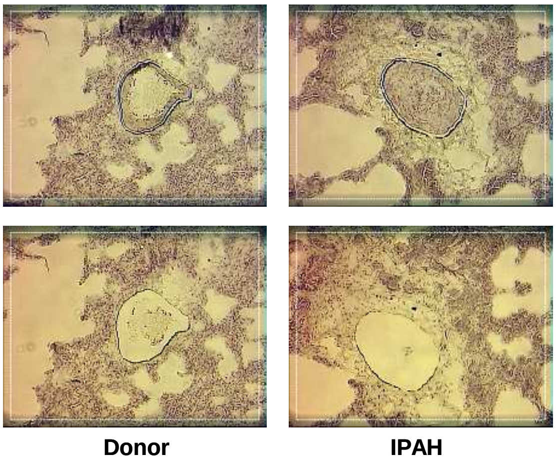

Figure 3.6 ***In vivo* expression of IL-13Rα2 analysed by LCM**
Laser-captured microdissection (LCM) of pulmonary arteries derived from healthy controls and IPAH patients (n=4 for each) was performed and pre- and post-dissection photos depicted in the upper and lower row, respectively.

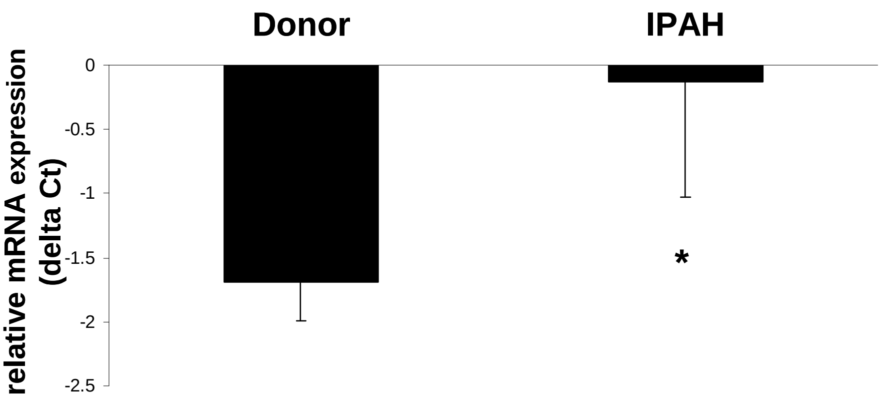

Figure 3.7 Quantitative analysis of IL-13Rα2 in microdissected arteries
Quantitative RT-PCR analysis of IL-13Rα2 gene expression was performed with mRNA from LCM-retrieved pulmonary arteries derived from donor or IPAH patients, as indicated (n=3). Values represent mean +/- SD; *, $p<0.05$.

3.3 IL-13 receptor localization in IPAH patients

We next sought to analyze the localization of IL-13 receptor isotypes, as well as IL-13, using immunohistochemistry of sections derived from donor and IPAH lungs. As depicted in Figure 3.8, IL-4Rα showed weak staining in the border between media and adventitia in pulmonary arteries, while IL-13Rα1 was primarily localized in bronchial epithelium, interstitial fibroblasts, and vascular smooth muscle cells. No differences in IL-4Rα and IL-13Rα1 localization were noted comparing donor with IPAH lungs.

IL-13Rα2 was predominantly localized in vascular smooth muscle cells (VSMC), and to a lesser extent, in the bronchial epithelium in donor lungs. In IPAH lungs, IL-13Rα2 staining in pulmonary vessels was more intense, but remained primarily localized to

VSMC. Interleukin-13 ligand was clearly localized in pulmonary arteries and displayed a stronger staining in VSMC of donors compared with IPAH lungs.

As depicted in Figure 3.9, intense expression of both IL-13Rα2 and its ligand IL-13 was also observed in concentric and plexiform lesions of IPAH sections, the histological hallmarks of IPAH.

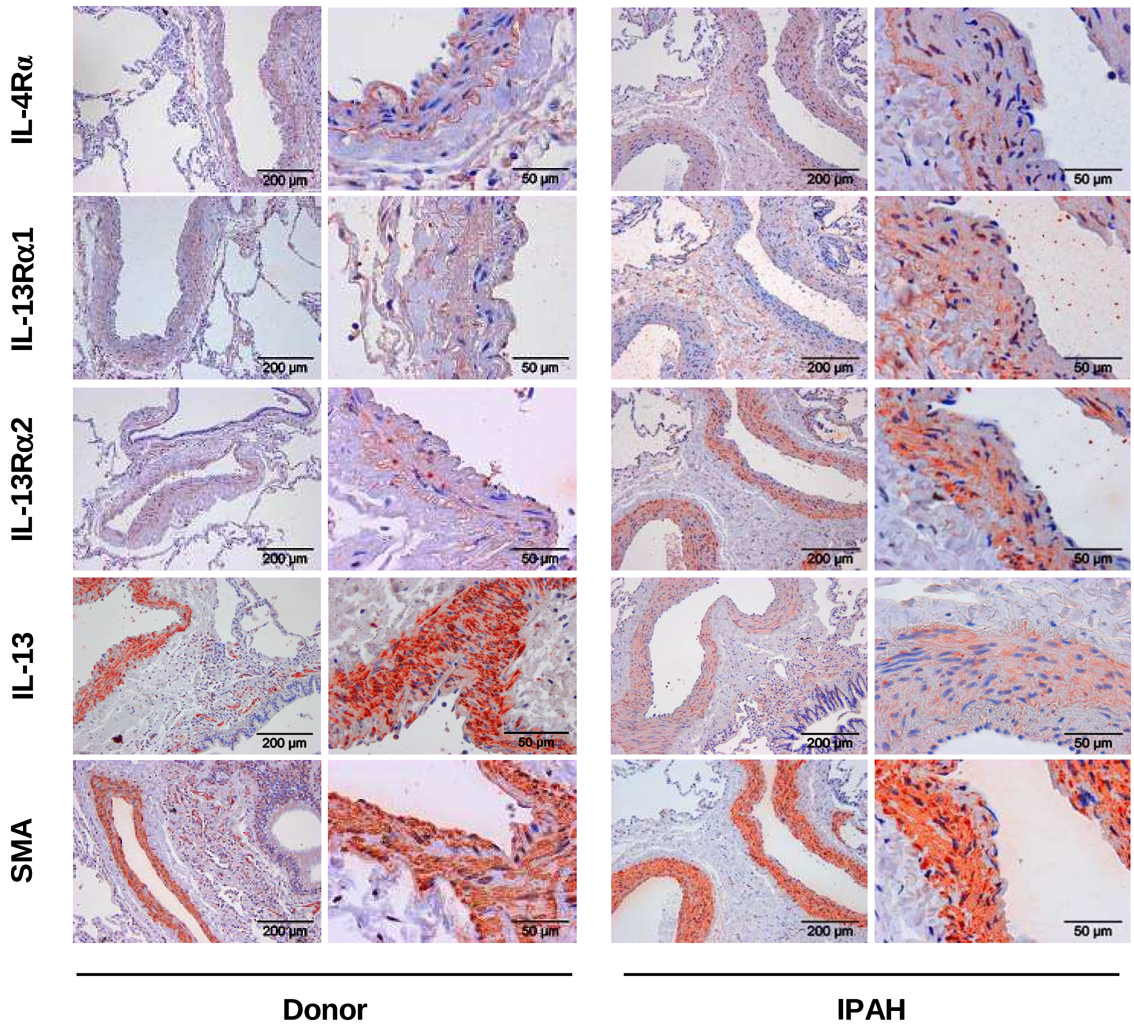

Figure 3.8 Immunohistochemical localization of IL-13 receptors
Paraffin-embedded specimens from healthy donors (left columns) and IPAH patients (right columns) were stained for IL-4Rα, IL-13Rα1, IL-13Rα2, IL-13, and smooth muscle actin (SMA). All immunostaining photographs are representative for at least five different donors and IPAH patients.

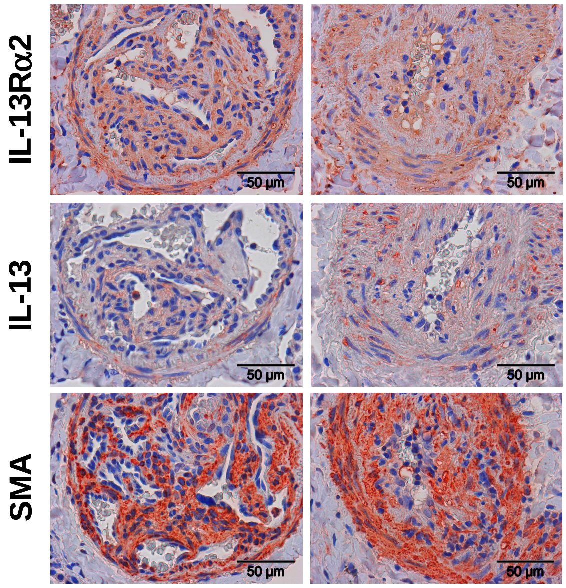

Figure 3.9 IL-13Rα2 and IL-13 expression in IPAH lesions
Section of lungs from IPAH patients demonstrating plexiform and concentric lesions on the left and right column, respectively were stained for IL-13Rα2, IL-13, and SMA, as depicted.

3.4 IL-13 receptor expression in experimental pulmonary hypertension

To gain further insight into the disease relevance of the IL-13 system and whether similar changes of IL-13 receptor expression occurred during pathogenesis of PAH, we investigated two animal models of PH, the mouse model of hypoxia-induced PH, and the rat model of monocrotaline-induced PH.

For RT-PCR analysis of IL-13R isotype expression, mRNA was extracted from lung homogenates obtained from mice subjected to chronic hypoxia for 1 or 3 weeks, respectively (Table 3.1).

	Normoxia	Hypoxia (7 days)	Hypoxia (21 days)
Hematocrit (%)	43 ± 0	53.6 ± 0.6	56.6 ± 1.2
RV/LV+IVS	0.34 ± 0.02	0.45 ± 0.01	0.44 ± 0.02

Table 3.1 Hypoxic parameters from mice subjected to chronic hypoxia

In line with the observations from the humans, we could detect a significant up-regulation of IL-13Rα2 mRNA gene expression in lungs from mice exposed to one and three weeks of hypoxia compared to control animals, whereas, as expected, IL-4Rα and IL-13Rα1 levels remained unchanged (Figure 3.10). These findings could be confirmed by quantitative RT-PCR (Figure 3.11).

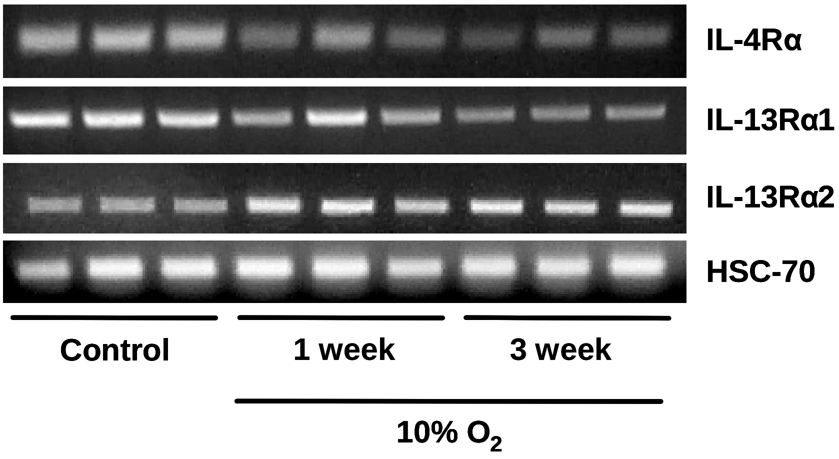

Figure 3.10 IL-13R expression in hypoxia-induced pulmonary hypertension
Mice were exposed to normobaric hypoxia (10% O2) for one or three weeks, lung RNA isolated and semi-quantitative RT-PCR performed for IL-13 receptor isotypes, as indicated

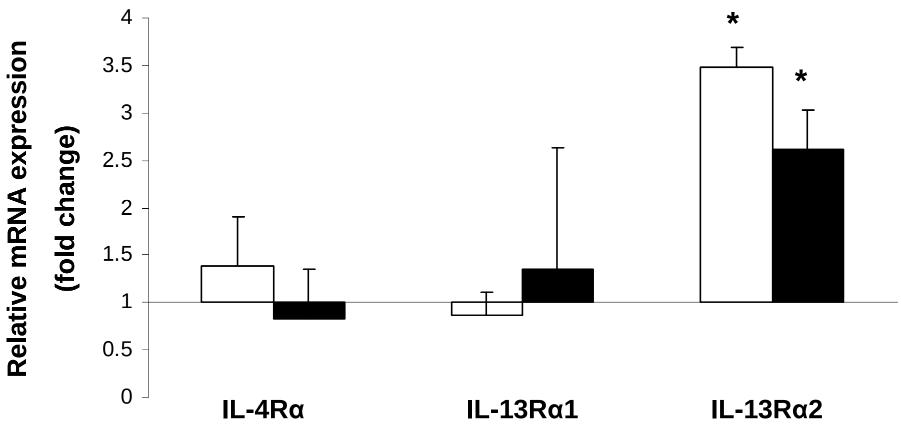

Figure 3.11 Quantitative analysis of IL-13R expression in hypoxia-induced pulmonary hypertension
Quantitative RT-PCR analysis was performed using the RNA samples described in Figure 3.10. Results are depicted as relative mRNA levels after one week (white bars) or three weeks (black bars) of hypoxia compared with normoxia. Values represent the mean +/- SD; *, p<0.05.

Next we switched to the above mentioned second animal model of experimental pulmonary hypertension, namely the rat model of monocrotaline-induced PH. As expected, we were also able to detect an up-regulation of IL-13Rα2 gene expression in this model in lungs of MCT-treated rats compared to control animals, 2 weeks after MCT injection (Figure 3.12).

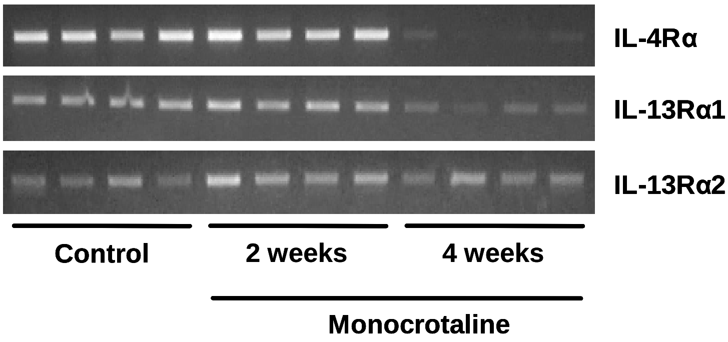

Figure 3.12 IL-13R expression in monocrotaline-induced pulmonary hypertension
Lungs were harvested two or four weeks after MCT administration, inducing pulmonary hypertension. Lung RNA was isolated from lung homogenates and semi-quantitative RT-PCR was performed for IL-13 receptor isotypes, as indicated.

Finally, the effects of hypoxia on IL-13Rα2 surface expression was assessed in cell culture conditions. For this purpose, freshly isolated human paSMC were subjected to hypoxia (1% of oxygen) for 24 h. Cell-surface expression of IL-13Rα2 was significantly increased in paSMC exposed to hypoxia, as assessed by flow cytometry, indicating functional contribution of IL-13Rα2 to disease pathogenesis. (Figure 3.13)

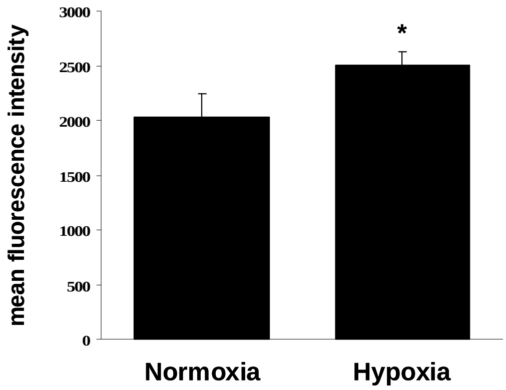

Figure 3.13 IL-13Rα2 expression in paSMC exposed to hypoxia
Human primary pulmonary artery smooth muscle cells were subjected to hypoxia (1% O2) for 24 hours and IL-13Rα2 surface expression was analysed by flow cytometry (n=3). Values represent the mean +/- SEM; *, p<0.05.

3.5 Effect of IL-13 on paSMC growth and apoptosis

As IL-13Rα2 is predominantly expressed in paSMC, we next sought to elucidate its function by first investigating the biological effect of IL-13 treatment of primary cultures of freshly isolated paSMC. As depicted in Figure 3.14, IL-13 causes a significant, dose-dependent decrease in the proliferation of paSMC, as assessed by direct counting of cell numbers (37+/-3.4 x 10^3 versus 52+/-2.1 x 10^3 cells of IL-13-treated and control cells, respectively).

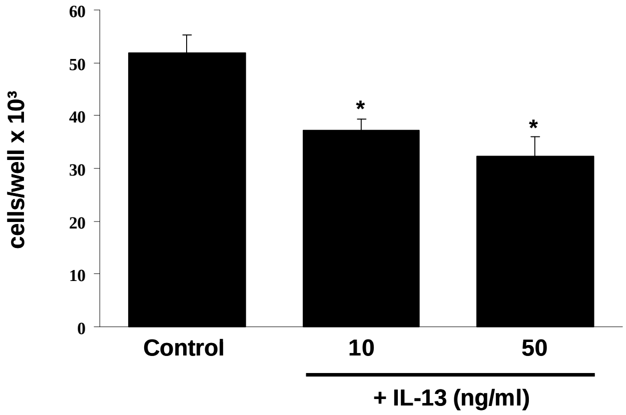

Figure 3.14 Effect of IL-13 on paSMC proliferation I
Primary paSMC were treated with the indicated concentrations of IL-13 and cell counting was performed after 48 h. Values represent the mean +/- SEM; *, p<0.001 versus untreated controls.

To confirm and quantify this effect, a [^{3}H]-thymidine incorporation assay was performed, further demonstrating a significant anti-proliferative effect of IL-13, which was elicited at concentrations as low as 1 ng/ml. The maximal anti-proliferative effect of IL-13 was observed at concentration of 10 ng/ml, a dose which was thus used for further experiments (Figure 3.15).

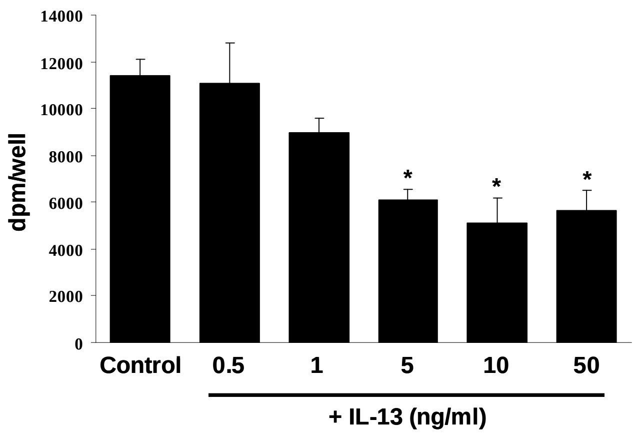

Figure 3.15 Effect of IL-13 on paSMC proliferation II
Primary paSMC were treated with the indicated concentrations of IL-13 and thymidine incorporation was performed after 48 hours. dpm, disintegrations per minute. Values represent the mean +/- SEM; *, p<0.001 versus untreated controls.

Interestingly, Interleukin-4 (IL-4), a ligand that can also bind to IL-13 receptor isotypes, also elicited a strong anti-proliferative effect on paSMC which was further augmented by co-stimulation with IL-13 (Figure 3.16).

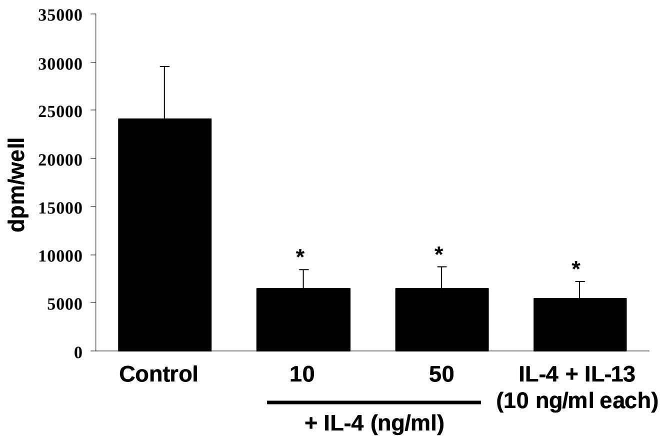

Figure 3.16 Effect of IL-4 on paSMC proliferation
Cells were treated with IL-4 and/or IL-13 at various concentration of IL-13 and thymidine incorporation was performed after 48 h. Values represent the mean +/- SEM. dpm, disintegrations per minute; *, $p<0.001$

To exclude that the observed anti-proliferative effect of IL-13 on paSMC was due to apoptosis, a Hoechst 33342 apoptosis assay was performed indicating that this growth-inhibitory effect was not due to induction of apoptosis, since IL-13 treatment did not induce apoptosis of paSMC, compared with untreated cells (3.0+-0.6% versus 2.3+-1.1% apoptotic cells, respectively). In contrast, staurosporine, which was used as a positive control, caused a significant increase in the percentage of apoptotic cells (Figure 3.17)

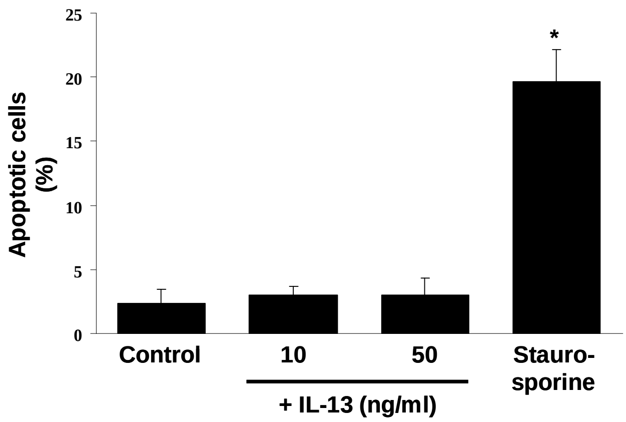

Figure 3.17 Effect of IL-13 on apoptosis in paSMC
Primary paSMC were incubated for 24 h with IL-13 at the indicated concentrations and stained with Hoechst 33342 to detect apoptotic cells. Staurosporine-treated cells served as a positive control for apoptosis. Values represent the mean +/- SEM; *, $p<0.001$

To further elucidate the mechanism of the growth-inhibitory effect induced by IL-13, we next analyzed cell cycle distribution using flow cytometric analysis (Figure 3.18). Synchronized paSMC exhibited an expected cell cycle arrest in the G_0/G_1 phase (90%, 5.6%, and 4.4% for G_0/G_1 , S, and G_2/M phase, respectively). Serum stimulation increased the S and G_2/M population to 13.8% and 30.3%, respectively. As depicted in Figure 3.18, the S phase entry was completely blocked by IL-13 treatment at 10 ng/ml, while the population of cells in G_2/M phase decreased by 50%. This indicated that IL-13 induced a G_0/G_1 phase arrest in paSMC, results that were also obtained with IL-13 at 50 ng/ml and IL-4 (data not shown).

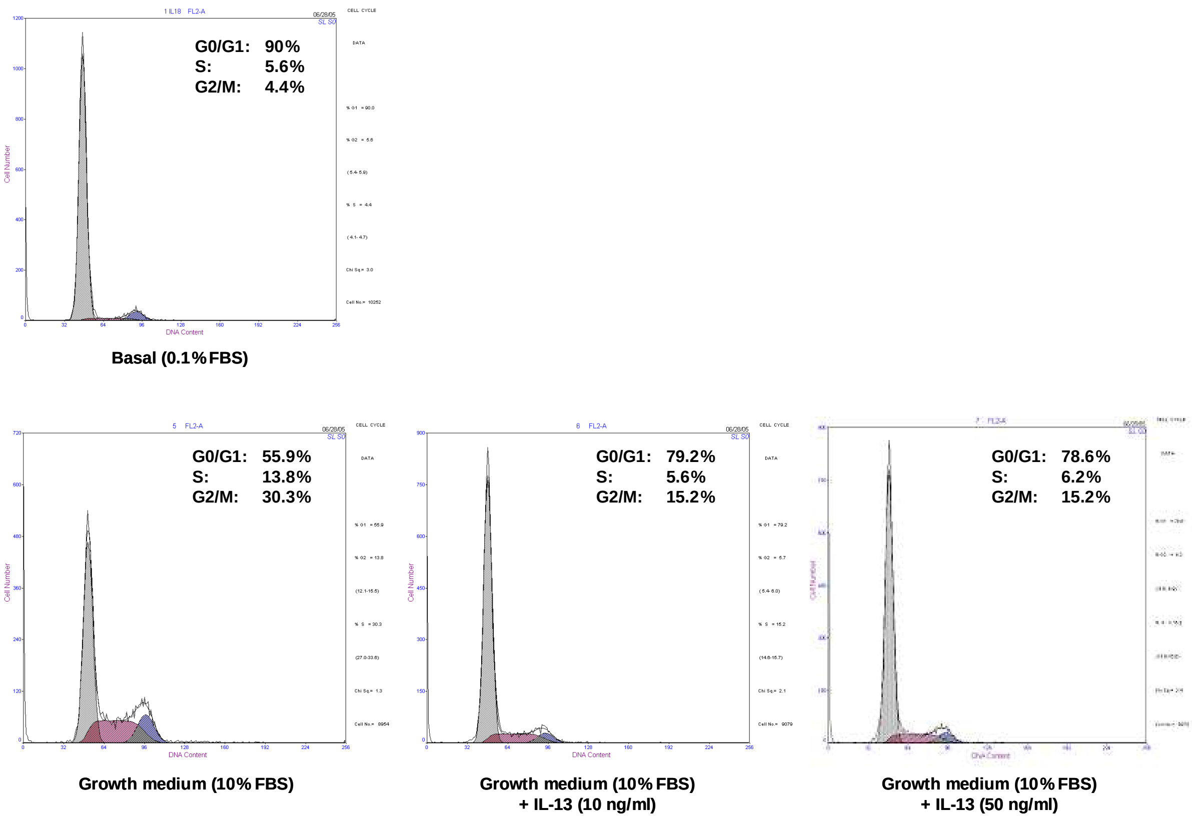

Figure 3.18 Effect of IL-13 on paSMC cell cycle progression
Synchronized paSMC were treated as indicated and harvested after 24 h, fixed, stained, and analyzed for DNA content by flow cytometry. The distribution and percentage of cells in Go/G1 phase (grey), S phase (pink) and G2/M phase (blue) are indicated, and all plots are representative for at least 3 independent experiments.

3.6 IL-13 serum levels in IPAH

In the following, we sought to investigate whether IPAH is correlated with altered serum levels of IL-13. For this purpose, sera of 10 IPAH patients and 10 sex- and age-matched healthy subjects were measured by ELISA and compared. In both groups we could not detect significant serum levels IL-13 and thus no difference between IPAH and controls.

3.7 IL-13-induced signaling in paSMC

To elucidate IL-13 signaling in paSMC, IL-13-treated cells were analyzed for the activation of STAT molecules at various time-points by western blot. As depicted in Figure 3.19, IL-13 induced phosphorylation of STAT6 as early as 15 minutes after stimulation. This effect was IL-13 specific, as interferon (IFN)-γ did not elicit STAT6 phosphorylation in paSMC. The STAT3 phosphorylation at Ser727, but not at Tyr705, was also induced by IL-13 after 30 min. In contrast, IL-13 did not induce STAT1, 2, 4, or 5 phosphorylation, and did not affect total STAT1, 3, or 6 protein levels in paSMC.
To confirm these results, immunofluorescence analysis, stimulating paSMC with IL-13 at a concentration of 10 ng/ml for 30 min, was performed. As expected, this assay demonstrated phosphorylation and nuclear translocation of both STAT3 and STAT6 in response to IL-13 (Figure 3.20).

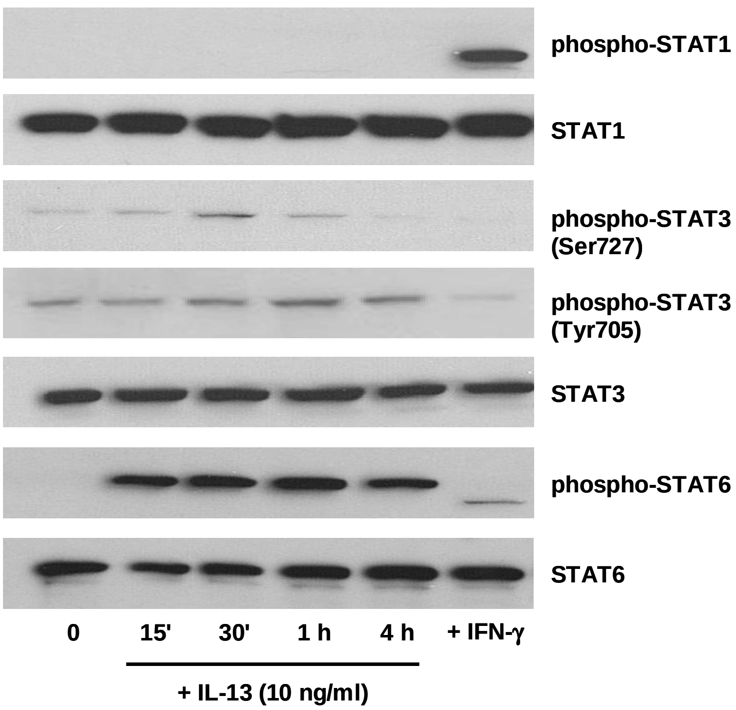

Figure 3.19 Effect of IL-13 on STAT phosphorylation in paSMC
Cells were treated with IL-13 (10 ng/ml) for indicated times, lysed, and protein extracts prepared. Phosphorylated and total STAT proteins were detected by SDS-PAGE, followed by western blot analysis.

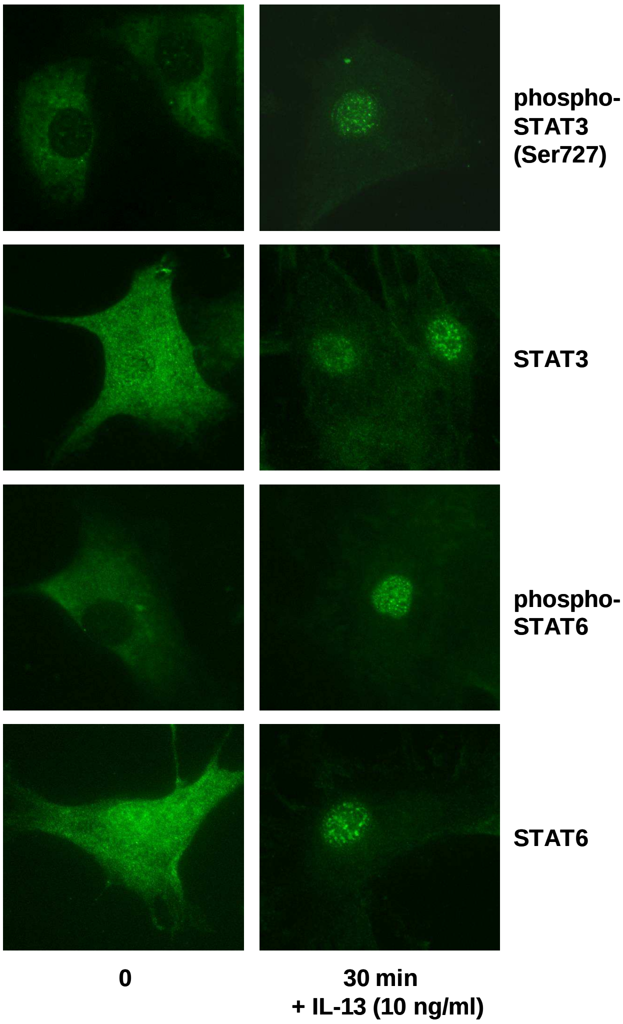

Figure 3.20 Effect of IL-13 on STAT phosphorylation and translocation in paSMC
Cells were seeded onto chamber slides and treated with IL-13 (10 ng/ml) for 30 min. Immunofluorescence analysis was performed using primary antibodies directed against phospho-STAT3, total STAT3, phospho-STAT6, total STAT6, as indicated.

3.8 Effect of IL-13Rα2 overexpression on paSMC

To investigate whether ectopic overexpression of IL-13Rα2 would mimic the effects observed with paSMC from patients or animal models of PAH, where we were able to demonstrate an up-regulation of IL-13Rα2, full-length IL-13Rα2 cDNA was cloned into the expression plasmid pcDNA3.1 and transfected into primary paSMC by electroporation. The efficiency of transfection by electroporation was analyzed with the help of a transfected GFP plasmid and subsequent flow cytometric analysis. After establishment of optimal transfection conditions we were able to achieve transfection efficiencies of up to 85% (Figure 3.21).

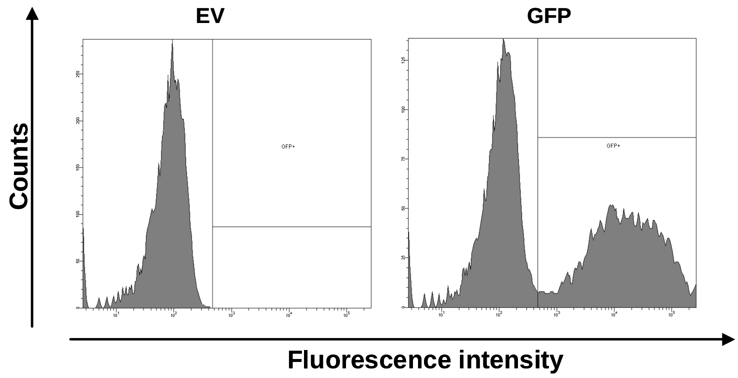

Figure 3.21 Analysis of transfection efficiency on GFP-transfected paSMC
Pulmonary artery smooth muscle cells were transfected with empty vector and GFP constructs by electroporation and GFP expression analyzed by flow cytometry

As depicted in Figure 3.22, [³H]-thymidine incorporation demonstrated that the growth-inhibitory effect of IL-13 on cells transfected with an empty vector (EV) was significantly attenuated in cells transfected with IL-13Rα2 cDNA.

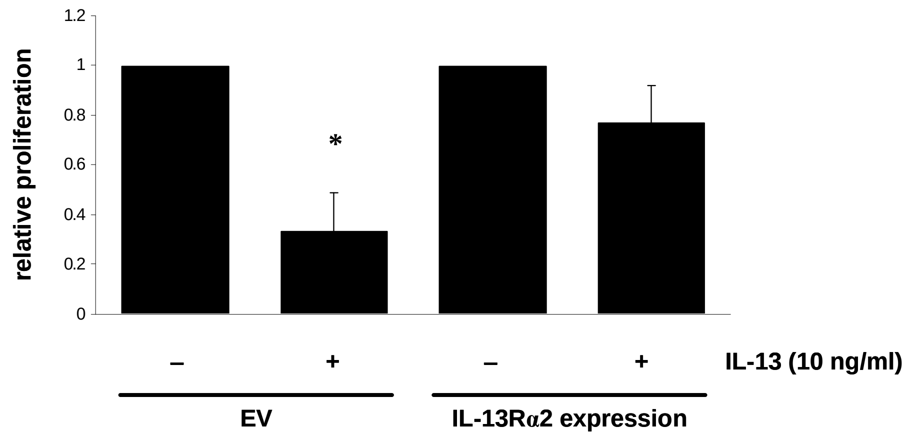

Figure 3.22 Effect of IL-13Rα2 overexpression on paSMC proliferation
Cells were transfected with IL-13Rα2 expression plasmid or empty control vector (EV), and stimulated with IL-13 (10 ng/ml) for 24 h. Cell proliferation was analyzed by thymidine incorporation. Values represent the mean +/- SEM; *, $p<0.05$

Furthermore, overexpression of IL-13Rα2 led to a less rapid and intense phosphorylation of STAT3 and STAT6 upon IL-13 stimulation compared with paSMC transfected with empty vector (Figure 3.23).

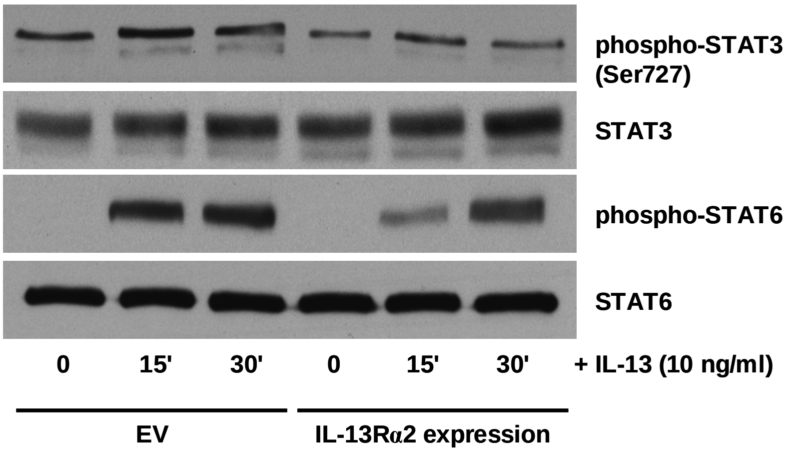

Figure 3.23 Effect of IL-13Rα2 overexpression on paSMC signaling
Empty vector (EV)- and IL-13Rα2-transfected paSMC were treated with 10 ng/ml of IL-13, and phosphorylated and total STAT proteins were detected by Western Blot analysis.

3.9 Analysis of IL-13 induced genes by DNA microarray

In order to elucidate possible transcriptional mechanisms of how IL-13 might exert its growth-inhibitory effect on paSMC and thus to analyze IL-13 regulated genes in these cells we decided to perform DNA microarray experiments. For this purpose, paSMC were stimulated with IL-13 (10 ng/ml) for 2 and 6 h, mRNA was subsequently extracted and a microarray analysis performed.

In total, 164 genes were regulated after 2 h (106 genes were up-, and 58 genes were down-regulated), 415 genes after 6 h (206 genes were up-, und 209 genes were down-regulated) of IL-13 stimulation (Figure 3.24).

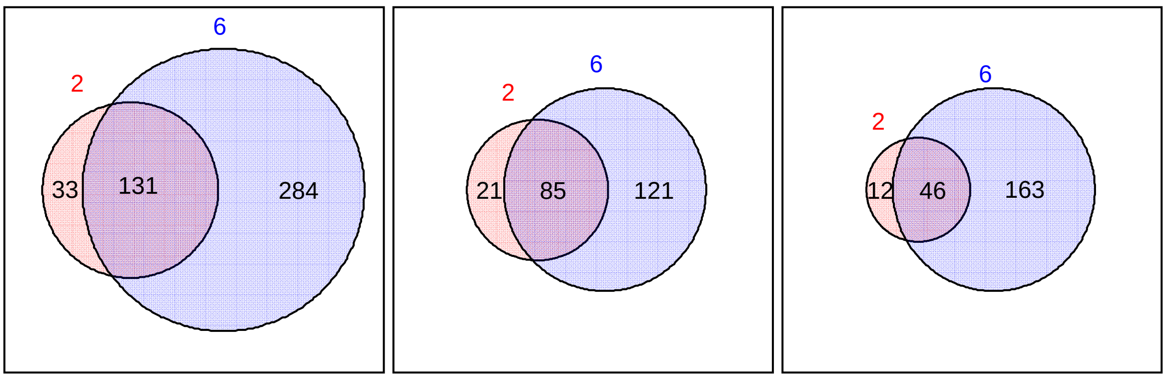

Figure 3.24 Genes regulated after IL-13 stimulation
Number of genes regulated after 2 h (red circle) and 6 h (blue circle) of IL-13 stimulation. Left box: Number of up- and down-regulated genes. Middle box: Only up-regulated genes. Right box: Only down-regulated genes.

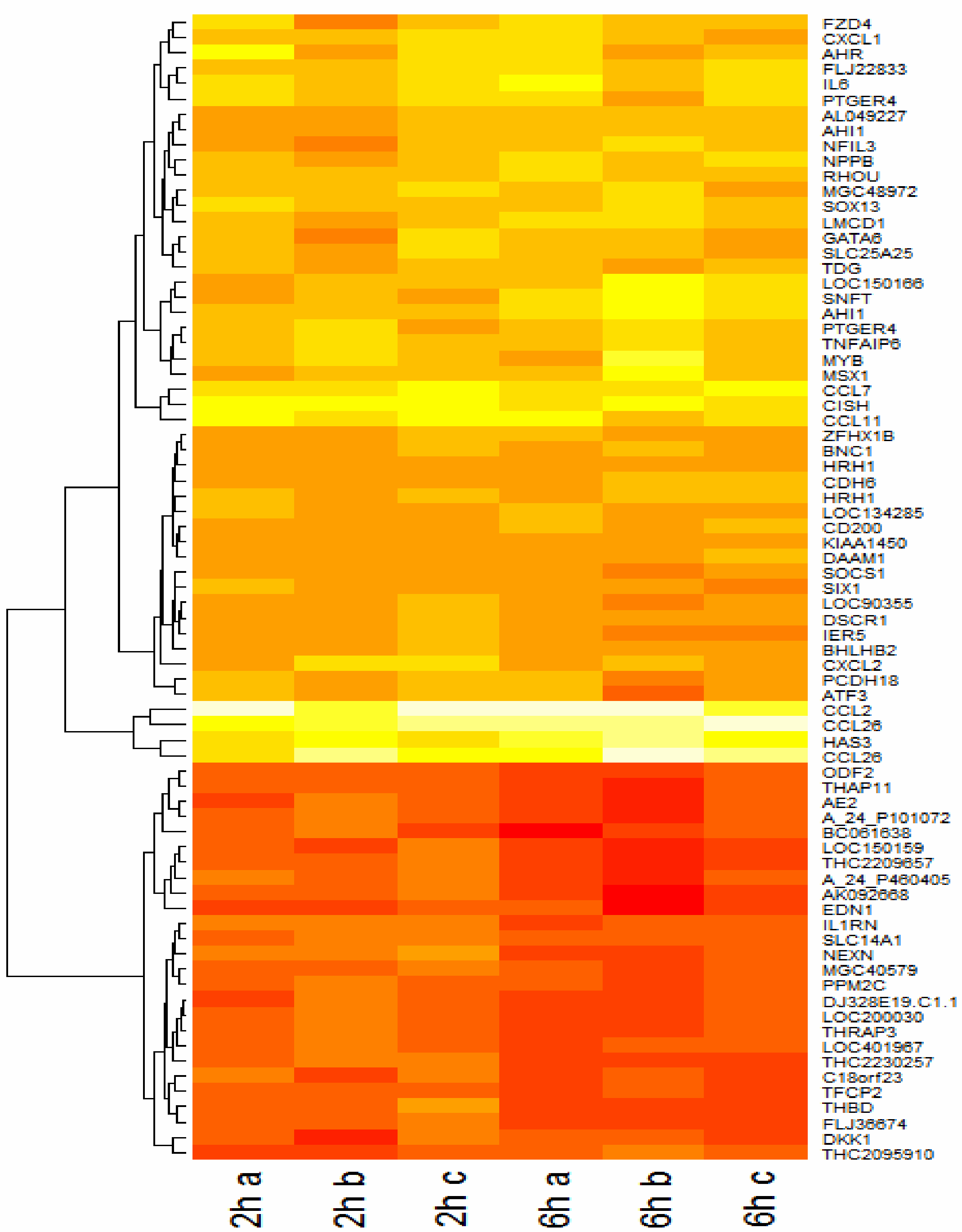

Figure 3.25 Heat Map analysis of IL-13 regulated genes
Visualization of the microarray results by heat map analysis. Rows represent the 50 most regulated genes, columns the respective experiments. Red: downregulation, yellow: intermediate regulation, white: up-regulation. A dendrogram is depicted on the left.

To further investigate IL-13 regulated genes and visualize the generated data heatmap analysis was performed (Figure 3.25). This method is a graphical way of displaying expression levels of genes (50) across a number of experiments (n=3, a-c). Furthermore, the expression data is analyzed by hierarchical clustering (dendrogram at the right).

3.9.1 IL-13 regulated genes after 2 h of stimulation

Table 3.2 lists the 10 most regulated genes 2 h after IL-13 stimulation (the entire list of all genes regulated can be found in the Appendix):

Up-regulation:

Accession	Gene	coeff.	A mean
NM_002982	chemokine (C-C motif) ligand 2 (CCL2)	3.844	10.529
NM_006072	chemokine (C-C motif) ligand 26 (CCL26)	2.643	8.523
NM_002986	chemokine (C-C motif) ligand 11 (CCL11)	1.914	8.503
NM_013324	cytokine inducible SH2-containing protein (CISH)	1.844	7.550
NM_006273	chemokine (C-C motif) ligand 7 (CCL7)	1.624	8.248
NM_005329	hyaluronan synthase 3 (HAS3)	1.491	7.681
NM_001621	aryl hydrocarbon receptor (AHR)	1.467	9.383
NM_001511	chemokine (C-X-C motif) ligand 1 (melanoma growth stimulating activity alpha (CXCL1)	1.420	9.950
NM_000958	prostaglandin E receptor 4 (subtype EP4) (PTGER4)	1.403	8.106
NM_000600	interleukin 6 (interferon beta 2) (IL6)	1.374	9.071

Down-regulation:

NM_183372	hypothetical protein LOC200030	-0.502	10.058
NM_030932	diaphanous homolog 3 (Drosophila) (DIAPH3)	-0.527	7.788
NM_139173	CG10806-like (LOC150159)	-0.535	7.804
NM_002729	hematopoietically expressed homeobox (HHEX)	-0.604	7.685
NM_153437	outer dense fiber of sperm tails 2 (ODF2)	-0.620	9.268
CR620977	cDNA clone CS0CAP004YK15 of Thymus of Homo sapiens (human)	-0.634	8.531
NM_145161	mitogen-activated protein kinase kinase 5 (MAP2K5)	-0.649	8.217
THC2095910	truncated DNA architectural factor HMGA2 (Homo sapiens)	-0.813	7.764
NM_001955	endothelin 1 (EDN1)	-0.854	7.764
NM_019070	DEAD (Asp-Glu-Ala-Asp) box polypeptide 49 (DDX49)	-0.883	8.544

Table 3.2 Most regulated genes 2 h after IL-13 stimulation

3.9.2 IL-13 regulated genes after 6 h of stimulation

Table 3.3 lists the 10 most regulated genes 6 h after IL-13 stimulation (the entire list of all genes regulated can be found in the Appendix):

Up-regulation:

Accession	Description	coeff	A. mean
NM_002982	chemokine (C-C motif) ligand 2 (CCL2)	4.044	10.529
NM_006072	chemokine (C-C motif) ligand 26 (CCL26)	3.399	8.523
NM_005329	hyaluronan synthase 3 (HAS3) transcript variant 1	2.353	7.681
NM_006273	chemokine (C-C motif) ligand 7 (CCL7)	1.918	8.248
NM_017651	Abelson helper integration site (AHI1)	1.761	8.315
NM_000600	interleukin 6 (interferon beta 2) (IL6)	1.746	9.071
NM_002986	chemokine (C-C motif) ligand 11 (CCL11)	1.639	8.503
AK056836	cDNA FLJ32274 fis	1.636	7.890
NM_022837	hypothetical protein FLJ22833	1.596	9.767
NM_013324	cytokine inducible SH2-containing protein (CISH) transcript variant 1	1.561	7.550

Down-regulation:

NM_153437	outer dense fiber of sperm tails 2 (ODF2) variant 2	-1.156	9.268
NM_139173	CG10806-like (LOC150159)	-1.201	7.804
AK095678	cDNA FLJ38359 fis	-1.235	11.474
NM_001901	connective tissue growth factor (CTGF)	-1.238	12.069
NM_020457	THAP domain containing 11 (THAP11)	-1.245	8.692
NM_001955	endothelin 1 (EDN1)	-1.247	7.764
NM_032264	hypothetical protein AE2 (AE2)	-1.247	9.513
BC061638	cDNA clone IMAGE:5547707	-1.315	8.751
NM_181690	v-akt murine thymoma viral oncogene homolog 3 (AKT3)	-1.390	8.415
AK092668	cDNA FLJ35349 fis	-1.475	7.994

Table 3.3 Most regulated genes 6 h after IL-13 stimulation

3.9.3 Classification of genes according to biological processes

In the following, we grouped IL-13 regulated genes according to their biological processes. At first, regulated genes were divided due to their molecular function. Both after 2 h and 6 h of IL-13 stimulation, most induced genes were involved in DNA-dependent regulation of transcription, followed by genes responsible for signal transduction and inflammatory responses (Figure 3.26).

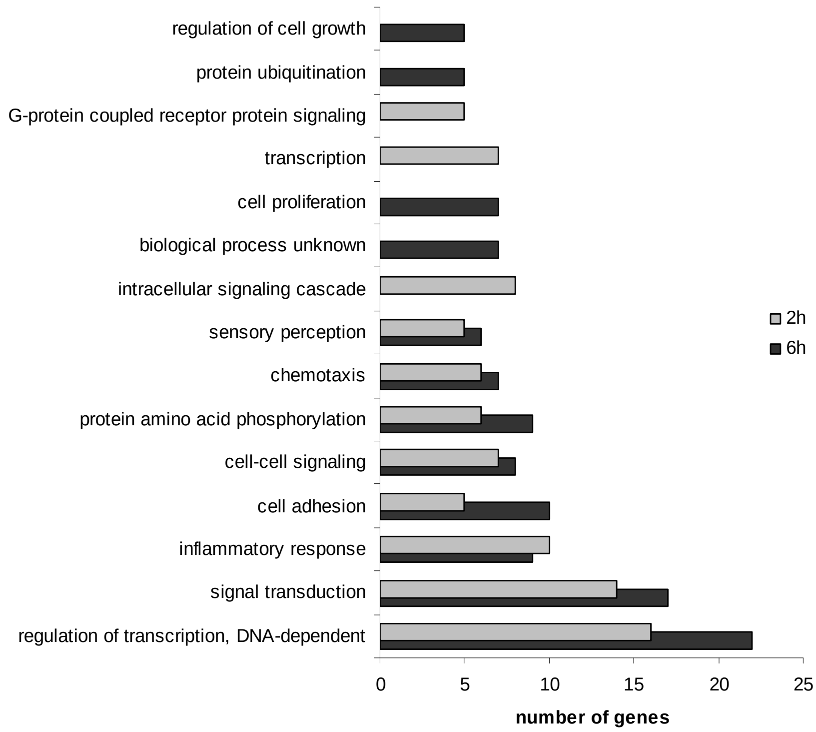

Figure 3.26 Cluster analysis of IL-13 regulated biological processes

Regarding cluster analysis of IL-13 regulated genes involved in signaling pathways, most genes are connected to cytokine-cytokine receptor interaction, followed by genes involved in JAK-STAT signaling and MAPK signaling pathways (Figure 3.27).

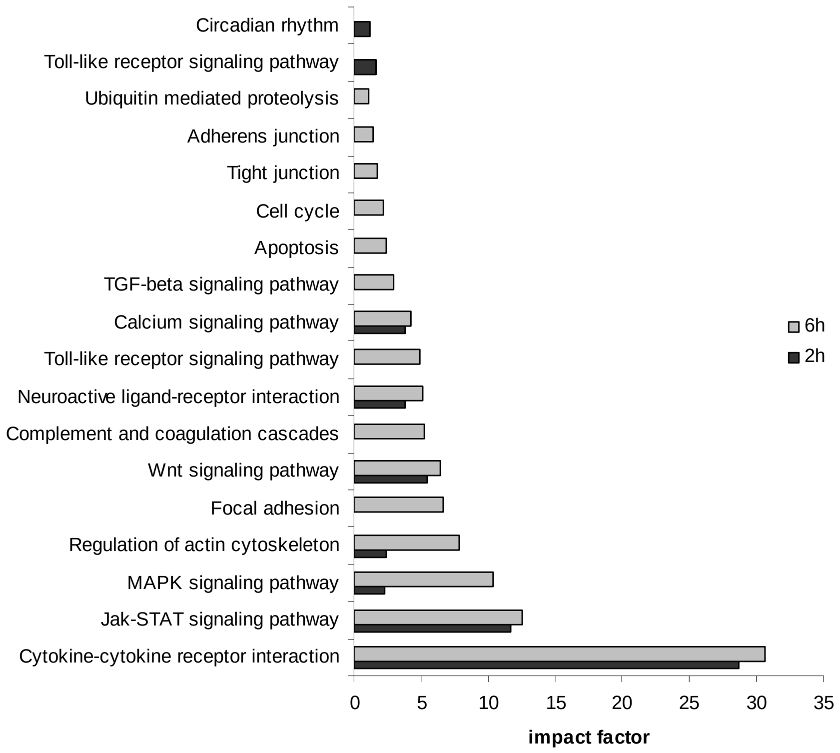

Figure 3.27 Cluster analysis of IL-13 regulated signaling pathways

3.10 IL-13 induces down-regulation of endothlin-1

For further analysis we chose endothlin-1, a potent vasoconstrictor, which was interestingly significantly down-regulated after both, 2 and 6 h of IL-13 stimulation. First we assessed endothelin-1 mRNA expression after IL-13 stimulation at several time points. We could observe an almost complete down-regulation of endothelin-1 expression even 24 h after stimulation (Figure 3.28). No mRNA of endothelin-2 and endothelin-3 was detected in paSMC after IL-13 stimulation (data not shown).

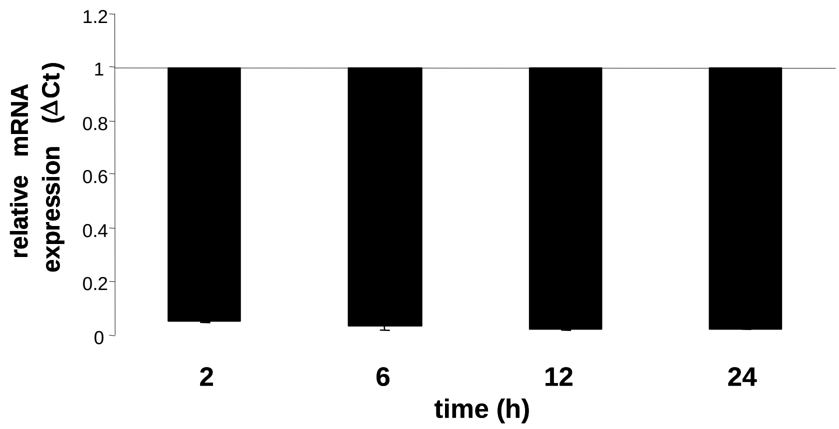

Figure 3.28 IL-13 induced down-regulation of endothelin-1 mRNA expression
paSMC were stimulated with IL-13 for the indicated time points. Endothelin-1 expression was subsequently analyzed by quantitative RT-PCR.

To confirm these data at the protein level, endothelin-1 concentrations were measured in the cell culture supernatant of paSMC stimulated with IL-13. As expected, endothelin-1 levels significantly decreased 6 h after stimulation, an effect which could be observed even after 48 h.

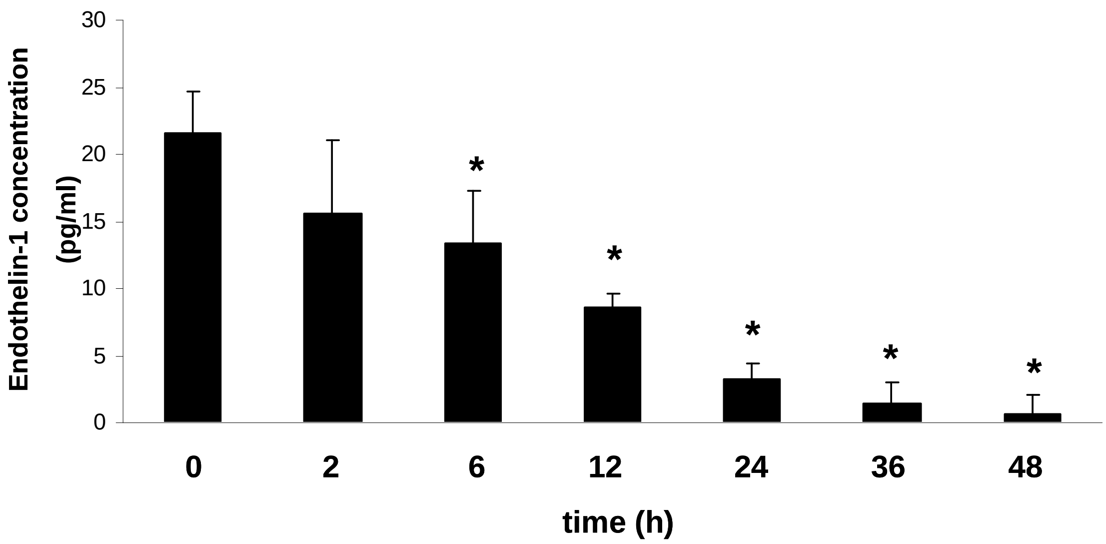

Figure 3.29 IL-13 induced down-regulation of endothelin-1 protein levels
The paSMC were stimulated with IL-13 for the indicated time points, cell culture supernatant was collected and subjected to ELISA to determine endothelin-1 concentration. Values represent the mean +/- SEM; *, $p<0.05$.

4 Discussion

Increased proliferation of paSMC is an essential feature of the vascular remodeling process in PAH. Several mediators which control paSMC growth have been described that also exhibited alterations in expression and/or function in PAH, such bone morphogenetic proteins, transforming growth factors, serotonin, angiopoietins, vascular endothelial growth factor, or platelet-derived growth factor (as described in the introduction section) [43, 112-117].

In the current study, we report the unexpected and novel finding that IL-13, along with its receptor isotypes IL-4Rα, IL-13Rα1, and IL-13Rα2 present an entirely novel and potent regulatory system for paSMC proliferation.

The novel findings reported in this study can be summarized as follows:

a) The IL-13Rα2 isotype is highly expressed in paSMC
b) IL-13Rα2, but not IL-13Rα1 or IL-4Rα expression is significantly increased in lung homogenates and paSMC of IPAH patients, as well as in two animal models of pulmonary hypertension
c) IL-13 concentrations in sera from PAH patients were not different compared with age-matched controls
d) IL-13 acts as a potent anti-proliferative, but not pro-apoptotic, factor for paSMC
e) IL-13 stimulates the phosphorylation and nuclear translocation of STAT3 and STAT6
f) Ectopic overexpression of IL-13Rα2 in primary paSMC attenuates the anti-proliferative effect exerted by IL-13, and diminishes IL-13-induced STAT3 and STAT6 phosphorylation
g) IL-13 induces the downregulation of endothelin-1 expression, both at the mRNA and protein level

These results suggest that the expansion of and enhanced ECM deposition by paSMC in PAH result from an inherent abnormality of the paSMC itself. While baseline IL-13 concentrations in the vascular wall may be responsible for maintaining paSMC quiescence, increased expression of the IL-13Rα2 isoform will lead to a loss of the anti-proliferative effect normally exerted by IL-13, even in the absence of changes in serum IL-13 levels. Indeed, IL-13 concentrations in sera from PAH patients were not different compared with age-matched controls, indicating that the cell's response is primarily dictated by the IL-13 receptor expression profile in the presence of unchanged ligand levels. As IL-13Rα2 is significantly up-regulated in PAH it might play a pivotal role in triggering and regulating vascular smooth muscle cell proliferation or remodeling. In the following, the influence and association of IL-13Rα2 on several disease processes, especially tissue fibrosis, will be discusses in detail.

4.1 IL-13Rα2

As already described in the Introduction, IL-13Rα2 belongs to the IL-13R family and is able to bind IL-13 with a 100-fold higher affinity than IL-13Rα1 [70, 118, 119]. Several studies show that IL-13Rα2 is expressed in various tissues – the corresponding transcripts have been identified in spleen, liver, lung, thymus and kidney, an observation which we could reproduce in this study [120-123]. In addition, the existence of a soluble IL-13Rα2 in the urine and serum of mice has been described [121, 124].

Large pools of IL-13Rα2 are also present intracellularly in cultured monocytes, respiratory epithelial cells, primary respiratory epithelium, and primary human monocytes [125, 126]. This intracellular pool can be rapidly mobilized to the cell surface upon treatment with IFN-γ [127]. As IL-13Rα2 binds IL-13 rapidly and with a very high affinity it plays thus a dominant role in the regulation of IL-13 levels and biological effects [118, 121]. The IL-13Rα2 itself is highly regulated *in vivo* and *in vitro*. Several studies demonstrated that IL-4, IL-10 and IFN-γ are potent regulators of the expression and production of IL-13Rα2 [119, 127, 128]. Furthermore, its ligand, IL-13, is also able to effectively increase IL-13Rα2 expression of mRNA and protein level as shown in various cell types [119, 128-131].

The generation of IL-13Rα2 -/- knockout mice in 2003 has initiated a plethora of important experiments investigating the biological and functional relevance of IL-13Rα2 [132]. These animals are viable, fertile, and display no overt abnormalities in appearance, weight, or behavior. Furthermore, histology, serum chemistry, and hematology do not reveal any obvious pathological changes [132]. Interestingly, the absence of IL-13Rα2 in these animals correlates with a complete loss of serum IL-13, whereas the levels of IL-13 in tissue are significantly increased, suggesting that in wild-type animals serum IL-13Rα2 may bind and neutralize serum IL-13 temporarily and thus extend IL-13 half-life [128, 132].

Moreover, IL13Rα2-deficient mice displayed enhanced serum IgE, IgG2, and IgA level, confirming and supporting studies showing increased levels of the above mentioned immunoglobulins after IL-13 administration [132]. IL-13Rα2 -/- mice exhibit in addition increased levels of macrophage progenitors and decreased tissue macrophage NO and IL-12 production [128]. The decreased responsiveness of immune cells to LPS (lipopolysaccharide) in IL-13Rα2 -/- animals, as shown by decreased expression of IL-12, underlines to protective role of IL-13 in the scenario of LPS-induced shock [132].

4.2 IL-13Rα2: Decoy or signaling receptor?

According to literature, IL-13Rα2 was for a very long time believed to act exclusively as a non-signaling decoy receptor after IL-13 binding. Several facts and observations supported this dogma:

- IL-13Rα2 has, compared to the other IL-13Rα isotypes, an extremely short cytoplasmatic tail, only consisting of 17 amino acids in the human subject [132, 133]
- Sequence analysis of this short cytoplasmatic tail indicated the absence of Box-1 or Box-2 signaling motifs [72, 127]
- The cytoplasmatic region of murine IL-13Rα2 does not posses any further signaling motif or Janus kinase/signal transducer and activator of transcription (STAT) binding sequence [121, 132]
- High IL-13 binding affinity [70]

Surprisingly, Fichtner-Feigl and colleagues recently published a study showing possible signaling properties of IL-13Rα2 upon IL-13 stimulation [134]. In this study, the authors investigated the underlying mechanism for IL-13 induced TGF-β secretion in macrophages in the context of tissue fibrosis and autoimmune diseases [134]. They found out that IL-13 activates the TGFB1 promoter and thus promotes the expression of TGF-β. Interestingly, IL-13Rα2 seems to be essential for this TGFB1 promoter activation: MonoMac6 (MM6) cells, originally not expressing IL-13Rα2, could be only induced to activate TGFB1 promoter after transfection with a plasmid encoding IL-13Rα2, indicating that IL-13Rα2 acts in fact as signaling receptor necessary for such a TGFB1 promoter activation [134]. Further analysis revealed that full-length IL-13Rα2 molecule is essential for this activation, as IL-13Rα2 lacking an intracellular signaling component is not able to influence TGFB1 promoter activation [134]. In the following the authors were able to show that TGFB1 activation by IL-13Rα2 occurs in a STAT6 independent way, whereas AP-1 seems to play an essential role: IL-13-stimulated MM6 cells expressing IL-13Rα2 showed markedly increased binding of AP-1 family members c-jun and Fra-2 in EMSA supershift analyses, indicating that AP-1 is at least one of the transcription factors involved in IL-13Rα2 signaling leading to activation of the TGFB1 promoter [134].

The above mentioned study is so far the first and only one describing signaling properties of IL-13Rα2, an intriguing fact that must be confirmed in future studies. Also the underlying mechanism determining whether IL-13Rα2 acts as a decoy or signaling receptor, respectively, remains to be further elucidated.

4.3 Role of IL-13Rα2 in fibrotic disease

As mentioned previously, IL-13 has emerged as a central mediator of tissue remodeling processes including idiopathic pulmonary fibrosis, ulcerative colitis, as well as liver cirrhosis [135-138]. A commonly used model to explore type-2 cytokine-dependent inflammation and fibrosis is the murine model of schistosomiasis [130]. In schistosomiasis, a chronic inflammatory disease of the liver and gut, Th2 cytokines are required for granuloma formation and development of hepatic fibrosis [130]. In this disease, eggs laid by adult parasites are trapped in host tissues, a process inducing and promoting granuloma formation, collagen deposition, and ultimately, extensive tissue remodeling and fibrosis [89, 130].

4.3.1 Pulmonary granuloma formation

In the pulmonary model of granuloma formation, live eggs are purified from the livers of *Schistosoma mansoni*-infected mice and then injected intravenously into naïve animals [130]. As a consequence, eggs lodge in the lungs and induce an inflammatory response, leading finally to pulmonary fibrosis. Several studies investigated the underlying mechanism promoting this fibrotic response: Short after intravenous egg injection a rapid induction of both IL-4 and IL-13 is observed in the lungs [128, 139]. Once this Th2 response is established, there is evidence that IL-4 is not required to maintained the polarized cytokine profile, whereas a modest IL-13 response is sufficient and essential to maintain a significant granulomatous response [130, 139].
To investigate a possible influence of IL-13Rα2, mice were treated with soluble IL-13Rα2-Fc fusion protein (sIL-13Rα2-Fc) which blocks IL-13 activity. Administration of sIL-13Rα2-Fc into *Schistosoma mansoni*-infected mice reduced the size of the granulomatous lesions by more than 50%, demonstrating a non-redundant role for IL-13 in pulmonary granuloma formation [139].

4.3.2 Liver fibrosis in schistosomiasis

A second widespread animal model of fibrotic disease is the murine model of schistosomiasis-induced liver fibrosis. Here, eggs are predominantly laid in the portal venous system and subsequently trapped in the liver [130, 140]. As mentioned above, these parasite eggs cause a vigorous Th2-linked inflammatory response in the liver cumulating in a destructive accumulation of collagen and extracellular matrix deposition, and thus the development of liver fibrosis [130, 140].

Also in this model, IL-13 was identified as the dominant mediator of tissue remodeling and fibrosis. Mice treated with the inhibitor sIL-13Rα2-Fc showed a significant decline in liver fibrosis compared to untreated animals [93, 141]. To underline the central role of IL-13, several studies could demonstrate that after infection with *Schistosoma mansoni*, serum and liver tissue level of IL-13 were clearly elevated, egg-specific Th2 lymphocytes produced even almost 100-fold more IL-13 than IL-4. In line with these findings it is not surprising that IL-13 -/- mice failed to develop the severe fibrotic liver tissue pathology observed in this disease [141].

Apart from evident pathologic effect of IL-13, and to a lesser extent IL-4, recent studies focused on the pattern of IL-4/IL-13 receptor expression as a possibly equally important regulatory mechanism. In a first step, mRNA expression of IL-13R isotypes was quantified at various time points following infection with *S. mansoni* [142]. Although the γc and IL-13Rα1 mRNA showed very little evidence of regulation in the cause of infection, IL-4Rα and IL-13Rα2 were highly regulated in the liver, displaying an opposite pattern of expression [141]. In the initial stage of disease IL-4Rα mRNA expression was high and in the following by week 9, mRNA levels decreased markedly and remained low throughout infection [128, 141, 142]. In contrast, IL-13Rα2 was almost undetectable prior to infection but was significantly up-regulated after egg-deposition [128, 130]. Also concerning the histopathological localization of IL-4R and IL-13Rα2 a discrepancy was detected, as IL-4Rα was found at higher levels within the granuloma, whereas the expression of IL-13Rα2 was primarily restricted to the periphery of the granuloma [128, 130]. These findings might lead to the hypothesis that IL-13Rα2 is highly produced and expressed during polarized Th2 responses. Studies conducted with IL-13 deficient mice showed a essential role for the ligand IL-13 on IL-13Rα2 expression as decoy receptor levels were markedly reduced in these knockout animals, a fact that could be rapidly restored after exogenous administration of recombinant IL-13 ligand [76, 128, 141]. In this scenario, IL-13Rα2 seems to act as a negative feedback inhibitor of IL-13, induced by the Th2 immune response itself. In addition, other experiments with several cytokine-deficient mice suggested that also IL-10, IL-12 and IFN-γ might mobilize IL-13Rα2 from intracellular stores to the cell surface and thus can be regarded as important endogenous inducers of IL-13Rα2 activity and function. [131, 143]

To elucidate the functional impact of IL-13Rα2 in the pathogenesis of remodeling diseases, besides the above mentioned up-regulation during development of fibrosis, the generation of knockout mice with a targeted deletion of IL-13Rα2 brought tremendous insight into disease pathology. In the absence of IL-13Rα2 (IL-13Rα2 -/- mice) hepatic fibrosis was significantly increased compared to wild-type mice [76, 142]. When in these knockout animals the decoy receptor activity was reconstituted by administration of sIL-13Rα2-Fc, the fibrotic response was largely prevented, reducing fibrosis in IL-13Rα2-deficient mice by >70%, formally displaying an exacerbated pattern of fibrosis [128, 130, 142]. Also the impaired immune modulation could be completely restored.

Also the histological pattern of hepatic fibrosis in infected IL-13Rα2 -/- mice was intriguing. In these mice collagen deposition seemed to extent beyond the areas surrounding the granulomas, as observed in wild-type animals, spreading throughout the entire liver parenchyma itself [128, 130]. These data suggest that the protective role of IL-13Rα2 might extent to areas not directly affected by parasite eggs. The IL-13Rα2 -/- animals thus failed to suppress their inflammatory response in the chronic phase of infection, displayed by a marked exacerbation in granulomatous inflammation at later time points [128, 130].
Another striking finding in these IL-13Rα2-deficient mice was the fact that Th2-cytokine expression, especially that of IL-13, was markedly reduced in the liver and serum of these animals [128, 130]. Fibrosis expands in IL-13Rα2 knockout animals, despite the significant decline in IL-13 tissue and serum concentration, suggesting that even reduced levels of IL-13 are sufficient to generate fibrosis when IL-13Rα2 expression is absent [128, 130]. These results emphasize the functional importance of IL-13Rα2 in regulation of Th2 immune response as they suggest a strong enhancement of IL-13 bioactivity in the absence of the decoy receptor [130]. Furthermore, the IL-13 receptor system, especially IL-13Rα2, might have a much greater influence on the development of tissue fibrosis than the relative level of IL-13.

4.3.3 Current model of the involvement of the Th1/2 response and IL-13Rα2 in tissue remodeling

Recent studies indicate that several cell types, namely CD4+CD25+ regulatory T-cells (T_{Reg}), macrophages and dendritic cells cooperate via secretion of IL-10 to generate Th2 cell responses [89, 144]. While promoting the development of polarized Th2 immune responses IL-10 furthermore inhibits the production of IFN-γ by Th1 cells [89, 145] (Figure 4.1). In this Th2 dominated setting, IL-13 not only induces ECM and collagen deposition by fibroblasts but also promotes expression of its decoy receptor IL-13Rα2 to regulate and attenuate the fibrotic response [119, 128, 129, 142]. For this reason, both IL-10 and IL-13Rα2 might cooperate to control tissue fibrosis during polarized Th2 responses [89] (Figure 4.1).

Another possibility is a highly polarize Th1 response. In this setting, the secretion of IFN-γ induces a downregulation of collagen production and additionally relative low levels of IL-13 [144]. Consequently, tissue fibrosis is minimal and decoy-receptor expression remains low.

In severe and uncontrollable cases of tissue fibrosis, as for example in idiopathic pulmonary fibrosis, the scenario of a mixed Th1/Th2 response might occur. In this case, moderate amounts of IFN-γ are able to reduce the production of the decoy receptor IL-13Rα2, whereas the simultaneously induced Th2 response augments the concentration of IL-13. Although the relative levels of IL-13 might even not change, for example in the serum of the patients, the concentration of "free" IL-13, which is able to bind signaling receptors, increases substantially as the regulatory functions of the decoy receptor are decreased [146-149]. This scenario could explain the unusual tendency of mixed immune responses to trigger severe tissue pathology.

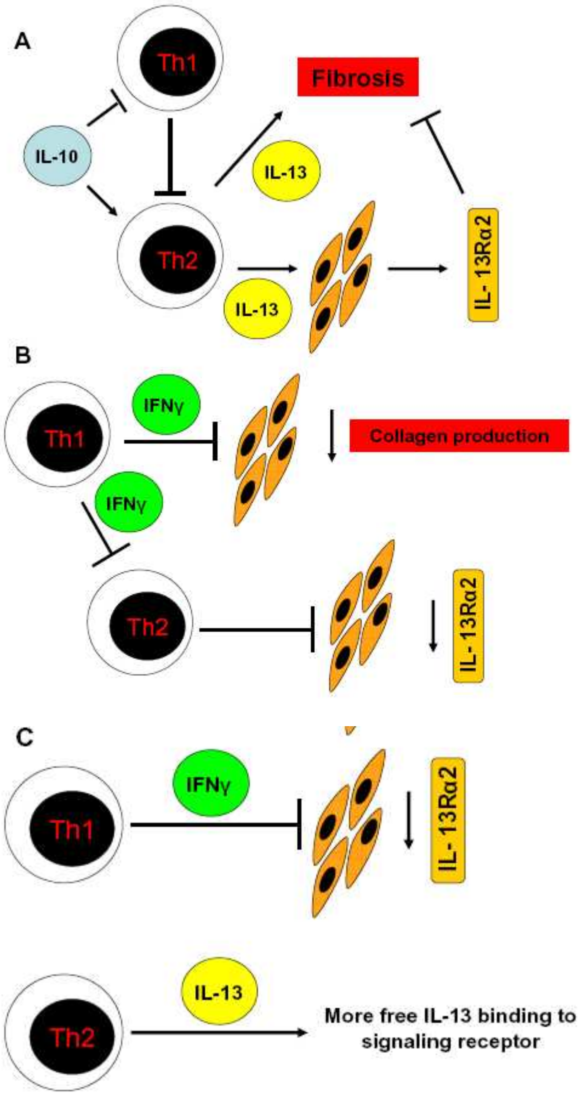

Figure 4.1 Involvement of Th1/Th2 response and IL-13Rα2 in tissue fibrosis (adapted from [89])

4.4 The role of IL-13 and IL-13Rα2 in IPAH

As the role of IL-13 and IL-13Rα2 has been to a large extent investigated in the pathogenesis of tissue remodeling diseases as pulmonary fibrosis, our study for the first time focuses on the role of this cytokine and its receptors on vascular remodeling as shown in PAH. Unexpectedly, we observed an anti-proliferative effect of IL-13 on paSMC while pro-proliferative effects of IL-13 have been described in lung (myo-) fibroblasts and airway epithelial cells. The IL-13 elicited a potent anti-proliferative effect on paSMC which was associated with the activation of STAT3 and STAT6. Phosphorylation of STAT6 is the classical signal transduction pathway activated by IL-13 but in addition to STAT6, STAT3 was also activated by IL-13 in paSMC, indicating a paSMC-specific signal transduction pathway and may thus be amenable to selective pharmacological modulation.

At present, little is known about the expression and localization of IL-13 receptors in the healthy lung. Immunohistochemical analysis of lung biopsies from patients with IPF revealed a predominantly interstitial staining for all three receptor subunits [150]. These authors also observed significant expression of the IL-13Rα1 isoform in the blood vessels, whereas strong staining for IL-13Rα2 was detectable in the lung epithelium of IPF patients [150]. In our study we observed a strong vascular staining of the IL-13Rα2 isoform. In addition, laser-captured microdissection with subsequent quantitative RT-PCR analysis confirmed, as a quantitative approach, enriched expression of IL-13Rα2 on paSMC compared with lung homogenates, and enhanced expression of IL-13Rα2 in small pulmonary arteries from lungs from patients with IPAH, compared with controls. These results were obtained investigating samples from IPAH patients, as well as from two animal models of PAH, the mouse model of chronic hypoxia-induced pulmonary hypertension and the rat model of monocrotaline-induced pulmonary hypertension, indicating that selective up-regulation of IL-13Rα2 is a consistent and conserved feature of PAH that may be closely related to pathogenesis.

Microarray analysis revealed a firm and consistent regulation of a plethora of genes after IL-13 stimulation of paSMC. We finally focused on endothelin-1 which expression was massively down-regulated by IL-13. We could confirm these results on both, mRNA and protein levels. As already published endothelin-1 plays a pivotal role in the pathogenesis of PAH as it might exert pro-proliferative and vasconstrictive effects on paSMC and vessels. The observed anti-proliferative effect of IL-13 on paSMC could be thus explained by the down-regulation of the pro-proliferative endothelin-1.

Bearing these observations in mind one could propose the following involvement of IL-13 and IL-13α2 in the pathogenesis of IPAH disease: In healthy subjects, baseline IL-13 concentrations in the vascular wall may be responsible for maintaining paSMC in a quiescent, non-proliferating state. In the condition of PAH, increased expression of IL-13Rα2 in paSMC leads to an attenuation of the direct anti-proliferative effect of locally secreted IL-13. This shifts the paSMC from a quiescent cell to a pro-proliferative and ECM-secreting cell type, triggering and/or activating pulmonary arterial hypertrophy (Figure 4.2). This study thus highlights the importance of the IL-13 system in PAH, a cytokine that may well be amenable to therapeutic intervention in human disease.

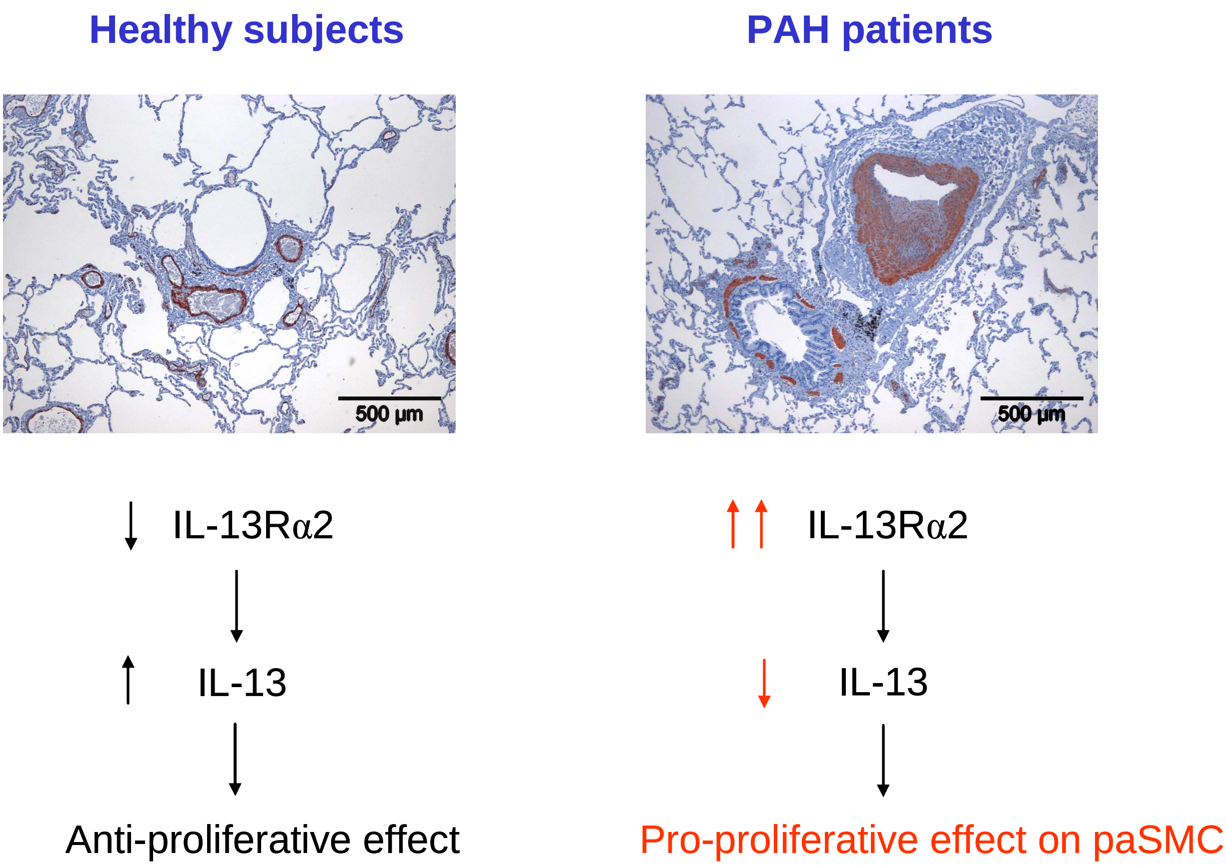

Figure 4.2 Involvement of IL-13Rα2 in the pathogenesis of PAH

4.5 Outlook and future directions

In order to further elucidate the influence of IL-13Rα2 on the pathogenesis of PAH the use of specific knockout animals, as investigated in fibrotic disorders, is of major importance. To mimic PH, IL-13Rα2 -/- and/or IL-13 -/- mice could be subjected to hypoxia and effects like right-ventricular hypertrophy and survival can be studied. According to our data, we hypothesize that IL-13Rα2 -/- animals show less signs of pulmonary hypertension compared to controls as there are augmented levels of “free”, anti-proliferative IL-13 which can interact with the respective signaling receptors.

Furthermore, IL-13 signaling through the IL-13Rα2 isoform has been described to be directly involved in TGF-β1 production and tissue fibrosis via AP-1 transcription factors. In this respect, it would be intriguing to further investigate, whether paSMC would exhibit distinct signaling activities via AP-1 similar to these observations.

By analyzing IL-13 regulated genes in paSMC via microarray a plethora of potential candidates involved in IL-13-induced growth inhibition was generated. In this study we only focused on endothelin-1, but especially the most up-regulated genes, belonging to the CCL-family, require further investigation.

5 Summary

Idiopathic pulmonary arterial hypertension (IPAH) is characterized by medial hypertrophy and pulmonary artery smooth muscle cell (paSMC) proliferation in pulmonary arteries. Interleukin (IL)-13 is a potent regulator of tissue fibrosis and remodeling, and its effects are dependent on the cell-type specific expression of the IL-13 receptor isotypes IL-4Rα, IL-13Rα1, and IL-13Rα2. This study analyzed the expression of the IL-13 receptors in IPAH *in vivo* and paSMC *ex vivo*, and the effects of IL-13 stimulation on paSMC proliferation and apoptosis.

Using quantitative RT-PCR and immunohistochemistry, we detected an increased expression of IL-13Rα2, but not IL-4Rα, or IL-13Rα1, in lungs of IPAH patients compared with controls (transplant donors). Similar results were obtained in lungs of mice subjected to chronic hypoxia-induced pulmonary hypertension or rats exposed to monocrotaline. Immunohistochemistry and laser-captured microdissection analysis further demonstrated a strong localization of IL-13Rα2 to paSMC. Functional analysis using freshly isolated paSMC revealed that IL-13 induced a dose-dependent growth inhibition, without inducing apoptotic effects. This anti-proliferative effect of IL-13 was due to G_0/G_1 cell cycle arrest and phosphorylation of STAT3 and STAT6 in paSMC. Finally, ectopic overexpression of IL-13Rα2 in primary paSMC attenuated the anti-proliferative effect exerted by IL-13, and diminished IL-13-induced STAT3 and 6 phosphorylation. Our studies thus demonstrate that IL-13 is a potent anti-proliferative regulator of paSMC. Up-regulation of the decoy receptor IL-13Rα2 on paSMC in IPAH leads to a loss of this anti-proliferative effect and therefore enhanced paSMC proliferation during the pathogenesis of the disease.

Furthermore, microarray analysis revealed that IL-13 induced a massive downregulation of the pro-proliferative endothelin-1 in paSMC, a finding that was also confirmed on protein level. Thus, the described anti-proliferative effect of IL-13 on paSMC might be mediated by a downregulation of endothelin-1.

6 Zusammenfassung

Idiopathische pulmonale Hypertonie (IPAH) ist charakterisiert durch eine Mediahypertrophie und Proliferation der pulmonalen glatten Gefäßmuskelzellen (paSMC). Interleukin-13 (IL-13) ist ein potenter Regulator von Gewebefibrose mit entsprechenden Umbauprozessen (remodeling) und seine biologischen Effekte sind abhängig vom zelltypspezifischen Expressionsmusters der IL-13 Rezeptor Isotypen IL-4Rα, IL-13Rα1 und IL-13Rα2. In der vorliegenden Studie untersuchten wir die Expression der IL-13 Rezeptoren in Proben von Lungen, entnommen von IPAH Patienten, *in vivo* und paSMC *ex vivo* und ferner die Effekte der IL-13 Stimulation auf die Proliferation und Apoptose von paSMC.

Mittels quantitativer RT-PCR und Immunohistochemie konnten wir eine verstärkte Expression von IL-13Rα2, nicht aber von IL-4Rα und IL-13Rα1, in Lungen von IPAH-Patienten im Vergleich zu Kontrollpatienten detektieren. Ähnliche Resultate konnten in Lungen von Mäusen mit durch chronischer Hypoxie ausgelöster pulmonaler Hypertonie und dem Monokrotalin-Rattenmodell beobachtet werden. Untersuchungen mittels Immunhistochemie und Laser-gestützter Mikrodissektion zeigten weiterhin eine starke Lokalisation von IL-13Rα2 in paSMC. Funktionelle Analysen an frisch isolieren paSMC zeigten, dass IL-13 eine dosis-abhängige Inhibition des Zellwachstums ohne apoptotische Effekte induziert. Dieser anti-proliferative Effekt von IL-13 beruhte auf einem Stopp des Zellzyklus in der G0/G1-Phase und einer Phosphorylierung von STAT3 und STAT6 in paSMC. Überexpression von IL-13Rα2 führte zu einer signifikanten Abnahme der IL-13 induzierten Wachshemmung und verringerte die zuvor beobachtete Phosphorylierung von STAT3 und STAT6. Weiterführende Microarray-Untersuchungen zeigten u.a., dass IL-13 zu einer stark reduzierten Genexpression des pro-proliferativen Endothelin-1 in paSMC führt.

Unsere Studie zeigt, dass IL-13 ein potenter anti-proliferativer Regulator des paSMC-Wachstums ist, was durch eine IL-13-induzierte Minderexpression von Endothelin-1 erklärt werden kann. Verstärkte Expression von IL-13Rα2 auf paSMC von IPAH Patienten führt zu einem Verlust dieses anti-proliferativen Effekts und deshalb einer gesteigerten Proliferation der paSMC im Verlauf der Erkrankung.

7 References

1. Rubin, L.J., *Primary pulmonary hypertension.* N Engl J Med, 1997. **336**(2): p. 111-7.
2. Archer, S. and S. Rich, *Primary pulmonary hypertension: a vascular biology and translational research "Work in progress".* Circulation, 2000. **102**(22): p. 2781-91.
3. Martin, K.B., J.R. Klinger, and S.I. Rounds, *Pulmonary arterial hypertension: new insights and new hope.* Respirology, 2006. **11**(1): p. 6-17.
4. Rich, S., et al., *Primary pulmonary hypertension. A national prospective study.* Ann Intern Med, 1987. **107**(2): p. 216-23.
5. Rubin, L.J., *Pulmonary arterial hypertension.* Proc Am Thorac Soc, 2006. **3**(1): p. 111-5.
6. Loyd, J.E., et al., *The presence of genetic anticipation suggests that the molecular basis of familial primary pulmonary hypertension may be trinucleotide repeat expansion.* Chest, 1997. **111**(6 Suppl): p. 82S-83S.
7. McLaughlin, V.V. and M.D. McGoon, *Pulmonary arterial hypertension.* Circulation, 2006. **114**(13): p. 1417-31.
8. Newman, J.H., et al., *Pulmonary arterial hypertension: future directions: report of a National Heart, Lung and Blood Institute/Office of Rare Diseases workshop.* Circulation, 2004. **109**(24): p. 2947-52.
9. Gaine, S.P. and L.J. Rubin, *Primary pulmonary hypertension.* Lancet, 1998. **352**(9129): p. 719-25.
10. Simonneau, G., et al., *Clinical classification of pulmonary hypertension.* J Am Coll Cardiol, 2004. **43**(12 Suppl S): p. 5S-12S.
11. Chin, K.M. and L.J. Rubin, *Pulmonary arterial hypertension.* J Am Coll Cardiol, 2008. **51**(16): p. 1527-38.
12. Chazova, I., et al., *Pulmonary artery adventitial changes and venous involvement in primary pulmonary hypertension.* Am J Pathol, 1995. **146**(2): p. 389-97.
13. Strange, J.W., et al., *Recent insights into the pathogenesis and therapeutics of pulmonary hypertension.* Clin Sci (Lond), 2002. **102**(3): p. 253-68.
14. Jeffery, T.K. and N.W. Morrell, *Molecular and cellular basis of pulmonary vascular remodeling in pulmonary hypertension.* Prog Cardiovasc Dis, 2002. **45**(3): p. 173-202.
15. Humbert, M., et al., *Cellular and molecular pathobiology of pulmonary arterial hypertension.* J Am Coll Cardiol, 2004. **43**(12 Suppl S): p. 13S-24S.
16. Eickelberg, O. and W. Seeger, *[Pulmonary hypertension: pathophysiology, genetics and functional genomics].* Internist (Berl), 2005. **46**(7): p. 759-68.
17. Cool, C.D., et al., *Three-dimensional reconstruction of pulmonary arteries in plexiform pulmonary hypertension using cell-specific markers. Evidence for a dynamic and heterogeneous process of pulmonary endothelial cell growth.* Am J Pathol, 1999. **155**(2): p. 411-9.
18. Mandegar, M., et al., *Cellular and molecular mechanisms of pulmonary vascular remodeling: role in the development of pulmonary hypertension.* Microvasc Res, 2004. **68**(2): p. 75-103.
19. Tuder, R.M., et al., *Exuberant endothelial cell growth and elements of inflammation are present in plexiform lesions of pulmonary hypertension.* Am J Pathol, 1994. **144**(2): p. 275-85.
20. Giaid, A., et al., *Expression of endothelin-1 in the lungs of patients with pulmonary hypertension.* N Engl J Med, 1993. **328**(24): p. 1732-9.

21. Moncada, S. and J.R. Vane, *Pharmacology and endogenous roles of prostaglandin endoperoxides, thromboxane A2, and prostacyclin.* Pharmacol Rev, 1978. **30**(3): p. 293-331.
22. Gerber, J.G., et al., *Moderation of hypoxic vasoconstriction by infused arachidonic acid: role of PGI2.* J Appl Physiol, 1980. **49**(1): p. 107-12.
23. Woods, M., et al., *Endothelin-1 is induced by cytokines in human vascular smooth muscle cells: evidence for intracellular endothelin-converting enzyme.* Mol Pharmacol, 1999. **55**(5): p. 902-9.
24. Hassoun, P.M., et al., *Endothelin 1: mitogenic activity on pulmonary artery smooth muscle cells and release from hypoxic endothelial cells.* Proc Soc Exp Biol Med, 1992. **199**(2): p. 165-70.
25. Chan, S.Y. and J. Loscalzo, *Pathogenic mechanisms of pulmonary arterial hypertension.* J Mol Cell Cardiol, 2008. **44**(1): p. 14-30.
26. Gabbay, E., J. Fraser, and K. McNeil, *Review of bosentan in the management of pulmonary arterial hypertension.* Vasc Health Risk Manag, 2007. **3**(6): p. 887-900.
27. Clozel, M., et al., *The endothelin ETB receptor mediates both vasodilation and vasoconstriction in vivo.* Biochem Biophys Res Commun, 1992. **186**(2): p. 867-73.
28. Masaki, T., et al., *Endothelin in perinatal pharmacology.* Semin Perinatol, 1991. **15**(1): p. 27-9.
29. Stewart, D.J., et al., *Increased plasma endothelin-1 in pulmonary hypertension: marker or mediator of disease?* Ann Intern Med, 1991. **114**(6): p. 464-9.
30. Yoshibayashi, M., et al., *Plasma endothelin concentrations in patients with pulmonary hypertension associated with congenital heart defects. Evidence for increased production of endothelin in pulmonary circulation.* Circulation, 1991. **84**(6): p. 2280-5.
31. Giaid, A., et al., *Endothelin-1 immunoreactivity and mRNA in the transplanted human heart.* Transplantation, 1995. **59**(9): p. 1308-13.
32. Mason, N.A., et al., *High expression of endothelial nitric oxide synthase in plexiform lesions of pulmonary hypertension.* J Pathol, 1998. **185**(3): p. 313-8.
33. McQuillan, L.P., et al., *Hypoxia inhibits expression of eNOS via transcriptional and posttranscriptional mechanisms.* Am J Physiol, 1994. **267**(5 Pt 2): p. H1921-7.
34. Griffiths, M.J. and T.W. Evans, *Inhaled nitric oxide therapy in adults.* N Engl J Med, 2005. **353**(25): p. 2683-95.
35. Moudgil, R., E.D. Michelakis, and S.L. Archer, *The role of k+ channels in determining pulmonary vascular tone, oxygen sensing, cell proliferation, and apoptosis: implications in hypoxic pulmonary vasoconstriction and pulmonary arterial hypertension.* Microcirculation, 2006. **13**(8): p. 615-32.
36. Archer, S.L., et al., *Molecular identification of the role of voltage-gated K+ channels, Kv1.5 and Kv2.1, in hypoxic pulmonary vasoconstriction and control of resting membrane potential in rat pulmonary artery myocytes.* J Clin Invest, 1998. **101**(11): p. 2319-30.
37. Abenhaim, L., et al., *Appetite-suppressant drugs and the risk of primary pulmonary hypertension. International Primary Pulmonary Hypertension Study Group.* N Engl J Med, 1996. **335**(9): p. 609-16.
38. Patel, A.J., M. Lazdunski, and E. Honore, *Kv2.1/Kv9.3, a novel ATP-dependent delayed-rectifier K+ channel in oxygen-sensitive pulmonary artery myocytes.* Embo J, 1997. **16**(22): p. 6615-25.
39. Michelakis, E.D., et al., *Dichloroacetate, a metabolic modulator, prevents and reverses chronic hypoxic pulmonary hypertension in rats: role of increased expression and activity of voltage-gated potassium channels.* Circulation, 2002. **105**(2): p. 244-50.

40. Celada, P., F. Martin, and F. Artigas, *Effects of chronic treatment with dexfenfluramine on serotonin in rat blood, brain and lung tissue.* Life Sci, 1994. **55**(15): p. 1237-43.
41. Eddahibi, S., et al., *Pathobiology of pulmonary arterial hypertension.* Eur Respir J, 2002. **20**(6): p. 1559-72.
42. Herve, P., et al., *Increased plasma serotonin in primary pulmonary hypertension.* Am J Med, 1995. **99**(3): p. 249-54.
43. Eddahibi, S., et al., *Serotonin transporter overexpression is responsible for pulmonary artery smooth muscle hyperplasia in primary pulmonary hypertension.* J Clin Invest, 2001. **108**(8): p. 1141-50.
44. Wilkins, M.R., D.J. Nunez, and J. Wharton, *The natriuretic peptide family: turning hormones into drugs.* J Endocrinol, 1993. **137**(3): p. 347-59.
45. Silberbach, M. and C.T. Roberts, Jr., *Natriuretic peptide signalling: molecular and cellular pathways to growth regulation.* Cell Signal, 2001. **13**(4): p. 221-31.
46. Guazzi, M. and M. Samaja, *The role of PDE5-inhibitors in cardiopulmonary disorders: from basic evidence to clinical development.* Curr Med Chem, 2007. **14**(20): p. 2181-91.
47. Morse, J.H., et al., *Mapping of familial primary pulmonary hypertension locus (PPH1) to chromosome 2q31-q32.* Circulation, 1997. **95**(12): p. 2603-6.
48. Nichols, W.C., et al., *Localization of the gene for familial primary pulmonary hypertension to chromosome 2q31-32.* Nat Genet, 1997. **15**(3): p. 277-80.
49. Thomson, J.R., et al., *Sporadic primary pulmonary hypertension is associated with germline mutations of the gene encoding BMPR-II, a receptor member of the TGF-beta family.* J Med Genet, 2000. **37**(10): p. 741-5.
50. Newman, J.H., et al., *Genetic basis of pulmonary arterial hypertension: current understanding and future directions.* J Am Coll Cardiol, 2004. **43**(12 Suppl S): p. 33S-39S.
51. Romagnani, S., *Immunologic influences on allergy and the TH1/TH2 balance.* J Allergy Clin Immunol, 2004. **113**(3): p. 395-400.
52. Del Prete, G., *Human Th1 and Th2 lymphocytes: their role in the pathophysiology of atopy.* Allergy, 1992. **47**(5): p. 450-5.
53. Romagnani, S., *Regulation of the T cell response.* Clin Exp Allergy, 2006. **36**(11): p. 1357-66.
54. Mosmann, T.R., et al., *Two types of murine helper T cell clone. I. Definition according to profiles of lymphokine activities and secreted proteins.* J Immunol, 1986. **136**(7): p. 2348-57.
55. Opal, S.M. and V.A. DePalo, *Anti-inflammatory cytokines.* Chest, 2000. **117**(4): p. 1162-72.
56. Colavita, A.M., A.J. Reinach, and S.P. Peters, *Contributing factors to the pathobiology of asthma. The Th1/Th2 paradigm.* Clin Chest Med, 2000. **21**(2): p. 263-77, viii.
57. Spellberg, B. and J.E. Edwards, Jr., *Type 1/Type 2 immunity in infectious diseases.* Clin Infect Dis, 2001. **32**(1): p. 76-102.
58. de Vries, J.E., *The role of IL-13 and its receptor in allergy and inflammatory responses.* J Allergy Clin Immunol, 1998. **102**(2): p. 165-9.
59. McKenzie, A.N., et al., *Structural comparison and chromosomal localization of the human and mouse IL-13 genes.* J Immunol, 1993. **150**(12): p. 5436-44.
60. de Waal Malefyt, R., et al., *Effects of IL-13 on phenotype, cytokine production, and cytotoxic function of human monocytes. Comparison with IL-4 and modulation by IFN-gamma or IL-10.* J Immunol, 1993. **151**(11): p. 6370-81.

61. Jung, T., et al., *Interleukin-13 is produced by activated human CD45RA+ and CD45RO+ T cells: modulation by interleukin-4 and interleukin-12.* Eur J Immunol, 1996. **26**(3): p. 571-7.
62. Sornasse, T., et al., *Differentiation and stability of T helper 1 and 2 cells derived from naive human neonatal CD4+ T cells, analyzed at the single-cell level.* J Exp Med, 1996. **184**(2): p. 473-83.
63. de Vries, J.E., J.M. Carballido, and G. Aversa, *Receptors and cytokines involved in allergic TH2 cell responses.* J Allergy Clin Immunol, 1999. **103**(5 Pt 2): p. S492-6.
64. Brombacher, F., *The role of interleukin-13 in infectious diseases and allergy.* Bioessays, 2000. **22**(7): p. 646-56.
65. Punnonen, J., et al., *Interleukin 13 induces interleukin 4-independent IgG4 and IgE synthesis and CD23 expression by human B cells.* Proc Natl Acad Sci U S A, 1993. **90**(8): p. 3730-4.
66. Punnonen, J., B.G. Cocks, and J.E. de Vries, *IL-4 induces germ-line IgE heavy chain gene transcription in human fetal pre-B cells. Evidence for differential expression of functional IL-4 and IL-13 receptors during B cell ontogeny.* J Immunol, 1995. **155**(9): p. 4248-54.
67. Zurawski, G. and J.E. de Vries, *Interleukin 13, an interleukin 4-like cytokine that acts on monocytes and B cells, but not on T cells.* Immunol Today, 1994. **15**(1): p. 19-26.
68. Yoshimura, A., et al., *Negative regulation of cytokine signaling influences inflammation.* Curr Opin Immunol, 2003. **15**(6): p. 704-8.
69. Galizzi, J.P., et al., *Molecular cloning of a cDNA encoding the human interleukin 4 receptor.* Int Immunol, 1990. **2**(7): p. 669-75.
70. Caput, D., et al., *Cloning and characterization of a specific interleukin (IL)-13 binding protein structurally related to the IL-5 receptor alpha chain.* J Biol Chem, 1996. **271**(28): p. 16921-6.
71. Jiang, H., M.B. Harris, and P. Rothman, *IL-4/IL-13 signaling beyond JAK/STAT.* J Allergy Clin Immunol, 2000. **105**(6 Pt 1): p. 1063-70.
72. Takeda, K., et al., *Impaired IL-13-mediated functions of macrophages in STAT6-deficient mice.* J Immunol, 1996. **157**(8): p. 3220-2.
73. Shirakawa, I., et al., *Atopy and asthma: genetic variants of IL-4 and IL-13 signalling.* Immunol Today, 2000. **21**(2): p. 60-4.
74. Johnston, D.A., et al., *Genomics and the biology of parasites.* Bioessays, 1999. **21**(2): p. 131-47.
75. McKenzie, G.J., et al., *A distinct role for interleukin-13 in Th2-cell-mediated immune responses.* Curr Biol, 1998. **8**(6): p. 339-42.
76. McKenzie, G.J., et al., *Simultaneous disruption of interleukin (IL)-4 and IL-13 defines individual roles in T helper cell type 2-mediated responses.* J Exp Med, 1999. **189**(10): p. 1565-72.
77. Shimoda, K., et al., *Lack of IL-4-induced Th2 response and IgE class switching in mice with disrupted Stat6 gene.* Nature, 1996. **380**(6575): p. 630-3.
78. Bancroft, A.J., A.N. McKenzie, and R.K. Grencis, *A critical role for IL-13 in resistance to intestinal nematode infection.* J Immunol, 1998. **160**(7): p. 3453-61.
79. Urban, J.F., Jr., et al., *IL-13, IL-4Ralpha, and Stat6 are required for the expulsion of the gastrointestinal nematode parasite Nippostrongylus brasiliensis.* Immunity, 1998. **8**(2): p. 255-64.
80. Robinson, D.S., et al., *Predominant TH2-like bronchoalveolar T-lymphocyte population in atopic asthma.* N Engl J Med, 1992. **326**(5): p. 298-304.

81. Walker, C., et al., *Activated T cells and eosinophilia in bronchoalveolar lavages from subjects with asthma correlated with disease severity.* J Allergy Clin Immunol, 1991. **88**(6): p. 935-42.
82. Coyle, A.J., et al., *Interleukin-4 is required for the induction of lung Th2 mucosal immunity.* Am J Respir Cell Mol Biol, 1995. **13**(1): p. 54-9.
83. Gavett, S.H., et al., *Interleukin-4 receptor blockade prevents airway responses induced by antigen challenge in mice.* Am J Physiol, 1997. **272**(2 Pt 1): p. L253-61.
84. Grunewald, S.M., et al., *An antagonistic IL-4 mutant prevents type I allergy in the mouse: inhibition of the IL-4/IL-13 receptor system completely abrogates humoral immune response to allergen and development of allergic symptoms in vivo.* J Immunol, 1998. **160**(8): p. 4004-9.
85. Minty, A., et al., *Interleukin-13 is a new human lymphokine regulating inflammatory and immune responses.* Nature, 1993. **362**(6417): p. 248-50.
86. Wills-Karp, M., et al., *Interleukin-13: central mediator of allergic asthma.* Science, 1998. **282**(5397): p. 2258-61.
87. Grunig, G., et al., *Requirement for IL-13 independently of IL-4 in experimental asthma.* Science, 1998. **282**(5397): p. 2261-3.
88. Wynn, T.A., *Cellular and molecular mechanisms of fibrosis.* J Pathol, 2008. **214**(2): p. 199-210.
89. Wynn, T.A., *Fibrotic disease and the T(H)1/T(H)2 paradigm.* Nat Rev Immunol, 2004. **4**(8): p. 583-94.
90. Cheever, A.W., et al., *Anti-IL-4 treatment of Schistosoma mansoni-infected mice inhibits development of T cells and non-B, non-T cells expressing Th2 cytokines while decreasing egg-induced hepatic fibrosis.* J Immunol, 1994. **153**(2): p. 753-9.
91. Le Moine, A., et al., *Critical roles for IL-4, IL-5, and eosinophils in chronic skin allograft rejection.* J Clin Invest, 1999. **103**(12): p. 1659-67.
92. Ong, C., et al., *Anti-IL-4 treatment prevents dermal collagen deposition in the tight-skin mouse model of scleroderma.* Eur J Immunol, 1998. **28**(9): p. 2619-29.
93. Chiaramonte, M.G., et al., *An IL-13 inhibitor blocks the development of hepatic fibrosis during a T-helper type 2-dominated inflammatory response.* J Clin Invest, 1999. **104**(6): p. 777-85.
94. Oriente, A., et al., *Interleukin-13 modulates collagen homeostasis in human skin and keloid fibroblasts.* J Pharmacol Exp Ther, 2000. **292**(3): p. 988-94.
95. Rankin, J.A., et al., *Phenotypic and physiologic characterization of transgenic mice expressing interleukin 4 in the lung: lymphocytic and eosinophilic inflammation without airway hyperreactivity.* Proc Natl Acad Sci U S A, 1996. **93**(15): p. 7821-5.
96. Zhu, Z., et al., *Pulmonary expression of interleukin-13 causes inflammation, mucus hypersecretion, subepithelial fibrosis, physiologic abnormalities, and eotaxin production.* J Clin Invest, 1999. **103**(6): p. 779-88.
97. Lanone, S., et al., *Overlapping and enzyme-specific contributions of matrix metalloproteinases-9 and -12 in IL-13-induced inflammation and remodeling.* J Clin Invest, 2002. **110**(4): p. 463-74.
98. Lee, C.G., et al., *Interleukin-13 induces tissue fibrosis by selectively stimulating and activating transforming growth factor beta(1).* J Exp Med, 2001. **194**(6): p. 809-21.
99. Murata, T., et al., *Two different IL-13 receptor chains are expressed in normal human skin fibroblasts, and IL-4 and IL-13 mediate signal transduction through a common pathway.* Int Immunol, 1998. **10**(8): p. 1103-10.

100. Saito, A., et al., *Potential action of IL-4 and IL-13 as fibrogenic factors on lung fibroblasts in vitro.* Int Arch Allergy Immunol, 2003. **132**(2): p. 168-76.
101. Hesse, M., et al., *Differential regulation of nitric oxide synthase-2 and arginase-1 by type 1/type 2 cytokines in vivo: granulomatous pathology is shaped by the pattern of L-arginine metabolism.* J Immunol, 2001. **167**(11): p. 6533-44.
102. Sedding, D.G., et al., *Caveolin-1 facilitates mechanosensitive protein kinase B (Akt) signaling in vitro and in vivo.* Circ Res, 2005. **96**(6): p. 635-42.
103. Gentleman, R.C., et al., *Bioconductor: open software development for computational biology and bioinformatics.* Genome Biol, 2004. **5**(10): p. R80.
104. Edwards, D., *Non-linear normalization and background correction in one-channel cDNA microarray studies.* Bioinformatics, 2003. **19**(7): p. 825-33.
105. Smyth, G.K. and T. Speed, *Normalization of cDNA microarray data.* Methods, 2003. **31**(4): p. 265-73.
106. Smyth, G.K., *Linear models and empirical bayes methods for assessing differential expression in microarray experiments.* Stat Appl Genet Mol Biol, 2004. **3**: p. Article3.
107. Draghici, S., et al., *A systems biology approach for pathway level analysis.* Genome Res, 2007. **17**(10): p. 1537-45.
108. Schermuly, R.T., et al., *Chronic sildenafil treatment inhibits monocrotaline-induced pulmonary hypertension in rats.* Am J Respir Crit Care Med, 2004. **169**(1): p. 39-45.
109. Dumitrascu, R., et al., *Activation of soluble guanylate cyclase reverses experimental pulmonary hypertension and vascular remodeling.* Circulation, 2006. **113**(2): p. 286-95.
110. Weissmann, N., et al., *Basic features of hypoxic pulmonary vasoconstriction in mice.* Respir Physiol Neurobiol, 2004. **139**(2): p. 191-202.
111. Kwapiszewska, G., et al., *Identification of proteins in laser-microdissected small cell numbers by SELDI-TOF and Tandem MS.* BMC Biotechnol, 2004. **4**: p. 30.
112. Morrell, N.W., et al., *Altered growth responses of pulmonary artery smooth muscle cells from patients with primary pulmonary hypertension to transforming growth factor-beta(1) and bone morphogenetic proteins.* Circulation, 2001. **104**(7): p. 790-5.
113. Teichert-Kuliszewska, K., et al., *Bone morphogenetic protein receptor-2 signaling promotes pulmonary arterial endothelial cell survival: implications for loss-of-function mutations in the pathogenesis of pulmonary hypertension.* Circ Res, 2006. **98**(2): p. 209-17.
114. Richter, A., et al., *Impaired transforming growth factor-beta signaling in idiopathic pulmonary arterial hypertension.* Am J Respir Crit Care Med, 2004. **170**(12): p. 1340-8.
115. Marcos, E., et al., *Serotonin-induced smooth muscle hyperplasia in various forms of human pulmonary hypertension.* Circ Res, 2004. **94**(9): p. 1263-70.
116. Du, L., et al., *Signaling molecules in nonfamilial pulmonary hypertension.* N Engl J Med, 2003. **348**(6): p. 500-9.
117. Taraseviciene-Stewart, L., et al., *Inhibition of the VEGF receptor 2 combined with chronic hypoxia causes cell death-dependent pulmonary endothelial cell proliferation and severe pulmonary hypertension.* Faseb J, 2001. **15**(2): p. 427-38.
118. Feng, N., et al., *The interleukin-4/interleukin-13 receptor of human synovial fibroblasts: overexpression of the nonsignaling interleukin-13 receptor alpha2.* Lab Invest, 1998. **78**(5): p. 591-602.
119. Zheng, T., et al., *Cytokine regulation of IL-13Ralpha2 and IL-13Ralpha1 in vivo and in vitro.* J Allergy Clin Immunol, 2003. **111**(4): p. 720-8.

120. Andrews, R., et al., *Reconstitution of a functional human type II IL-4/IL-13 receptor in mouse B cells: demonstration of species specificity.* J Immunol, 2001. **166**(3): p. 1716-22.
121. Donaldson, D.D., et al., *The murine IL-13 receptor alpha 2: molecular cloning, characterization, and comparison with murine IL-13 receptor alpha 1.* J Immunol, 1998. **161**(5): p. 2317-24.
122. Guo, J., et al., *Chromosome mapping and expression of the human interleukin-13 receptor.* Genomics, 1997. **42**(1): p. 141-5.
123. Yoshikawa, M., et al., *TNF-alpha and IL-4 regulate expression of IL-13 receptor alpha2 on human fibroblasts.* Biochem Biophys Res Commun, 2003. **312**(4): p. 1248-55.
124. Zhang, J.G., et al., *Identification, purification, and characterization of a soluble interleukin (IL)-13-binding protein. Evidence that it is distinct from the cloned Il-13 receptor and Il-4 receptor alpha-chains.* J Biol Chem, 1997. **272**(14): p. 9474-80.
125. Daines, M.O., et al., *Level of expression of IL-13R alpha 2 impacts receptor distribution and IL-13 signaling.* J Immunol, 2006. **176**(12): p. 7495-501.
126. Akaiwa, M., et al., *Localization of human interleukin 13 receptor in non-haematopoietic cells.* Cytokine, 2001. **13**(2): p. 75-84.
127. Daines, M.O. and G.K. Hershey, *A novel mechanism by which interferon-gamma can regulate interleukin (IL)-13 responses. Evidence for intracellular stores of IL-13 receptor alpha -2 and their rapid mobilization by interferon-gamma.* J Biol Chem, 2002. **277**(12): p. 10387-93.
128. Chiaramonte, M.G., et al., *Regulation and function of the interleukin 13 receptor alpha 2 during a T helper cell type 2-dominant immune response.* J Exp Med, 2003. **197**(6): p. 687-701.
129. Jakubzick, C., et al., *Impact of interleukin-13 responsiveness on the synthetic and proliferative properties of Th1- and Th2-type pulmonary granuloma fibroblasts.* Am J Pathol, 2003. **162**(5): p. 1475-86.
130. Mentink-Kane, M.M. and T.A. Wynn, *Opposing roles for IL-13 and IL-13 receptor alpha 2 in health and disease.* Immunol Rev, 2004. **202**: p. 191-202.
131. Wynn, T.A., *IL-13 effector functions.* Annu Rev Immunol, 2003. **21**: p. 425-56.
132. Wood, N., et al., *Enhanced interleukin (IL)-13 responses in mice lacking IL-13 receptor alpha 2.* J Exp Med, 2003. **197**(6): p. 703-9.
133. Bernard, J., et al., *Expression of interleukin 13 receptor in glioma and renal cell carcinoma: IL13Ralpha2 as a decoy receptor for IL13.* Lab Invest, 2001. **81**(9): p. 1223-31.
134. Fichtner-Feigl, S., et al., *IL-13 signaling through the IL-13alpha2 receptor is involved in induction of TGF-beta1 production and fibrosis.* Nat Med, 2006. **12**(1): p. 99-106.
135. Sugimoto, R., et al., *Effect of IL-4 and IL-13 on collagen production in cultured LI90 human hepatic stellate cells.* Liver Int, 2005. **25**(2): p. 420-8.
136. Reiman, R.M., et al., *Interleukin-5 (IL-5) augments the progression of liver fibrosis by regulating IL-13 activity.* Infect Immun, 2006. **74**(3): p. 1471-9.
137. Fuss, I.J., et al., *Nonclassical CD1d-restricted NK T cells that produce IL-13 characterize an atypical Th2 response in ulcerative colitis.* J Clin Invest, 2004. **113**(10): p. 1490-7.
138. Vainer, B., et al., *Colonic expression and synthesis of interleukin 13 and interleukin 15 in inflammatory bowel disease.* Cytokine, 2000. **12**(10): p. 1531-6.

139. Chiaramonte, M.G., et al., *IL-13 is a key regulatory cytokine for Th2 cell-mediated pulmonary granuloma formation and IgE responses induced by Schistosoma mansoni eggs.* J Immunol, 1999. **162**(2): p. 920-30.

140. Pearce, E.J. and A.S. MacDonald, *The immunobiology of schistosomiasis.* Nat Rev Immunol, 2002. **2**(7): p. 499-511.

141. Chiaramonte, M.G., et al., *Studies of murine schistosomiasis reveal interleukin-13 blockade as a treatment for established and progressive liver fibrosis.* Hepatology, 2001. **34**(2): p. 273-82.

142. Mentink-Kane, M.M., et al., *IL-13 receptor alpha 2 down-modulates granulomatous inflammation and prolongs host survival in schistosomiasis.* Proc Natl Acad Sci U S A, 2004. **101**(2): p. 586-90.

143. Belperio, J.A., et al., *Interaction of IL-13 and C10 in the pathogenesis of bleomycin-induced pulmonary fibrosis.* Am J Respir Cell Mol Biol, 2002. **27**(4): p. 419-27.

144. Hesse, M., et al., *The pathogenesis of schistosomiasis is controlled by cooperating IL-10-producing innate effector and regulatory T cells.* J Immunol, 2004. **172**(5): p. 3157-66.

145. Wynn, T.A., et al., *An IL-12-based vaccination method for preventing fibrosis induced by schistosome infection.* Nature, 1995. **376**(6541): p. 594-6.

146. Castro, M., et al., *Could asthma be worsened by stimulating the T-helper type 1 immune response?* Am J Respir Cell Mol Biol, 2000. **22**(2): p. 143-6.

147. Ford, J.G., et al., *Il-13 and IFN-gamma: interactions in lung inflammation.* J Immunol, 2001. **167**(3): p. 1769-77.

148. Hansen, G., et al., *Allergen-specific Th1 cells fail to counterbalance Th2 cell-induced airway hyperreactivity but cause severe airway inflammation.* J Clin Invest, 1999. **103**(2): p. 175-83.

149. Randolph, D.A., et al., *Cooperation between Th1 and Th2 cells in a murine model of eosinophilic airway inflammation.* J Clin Invest, 1999. **104**(8): p. 1021-9.

150. Jakubzick, C., et al., *Augmented pulmonary IL-4 and IL-13 receptor subunit expression in idiopathic interstitial pneumonia.* J Clin Pathol, 2004. **57**(5): p. 477-86.

8 Appendix

8.1 Primer sequences, amplicon length and PCR conditions:

8.1.1 Human:

Primer sequence (FP: forward primer, RP: reverse primer), amplicon length (product) and annealing temperature (AT):

Gene name	Primer sequence 5’ - 3’ FP/RP	Product (bp)	AT (℃)
Interleukin-4 Receptor (IL-4R)	TCA TGG ATG ACG TGG TCA GT GTG TCG GAG ACA TTG GTG TG	148	58
Interleukin-13 α1 Receptor (IL-13Rα1)	GTC CCT GGT GTT CTT CCT GA AGT GTG GAA TTG CGC TTC TT	137	59
Interleukin-13 α2 Receptor (IL-13Rα2)	GTT CAA AGT TCC TGG GCA GA CCT ATG CCA GGT TTC CAA GA	131	59
Porphobilinogen deaminase (PBGD)	CCC ACG CGA ATC ACT CTC AT TGT CTG GTA ACG GCA ATG CG	117	59
Heat shock cognate 70 (HSC-70)	TTA CCC GTC CCC GAT TTG AAG AA TGT GTC TGC TTG GTA GGA ATG GT	384	58
Endothelin-1 (ET-1)	GCT CGT CCC TGA TGG ATA AA CTG TTG CCT TTG TGG GAA GT	143	59
Endothelin-2 (ET-2)	TGT TCC AGA CTG GCA AGA CA TTC CTC CAC CTG GAA TGT GT	142	59
Endothelin-3 (ET-3)	ATT CAA GGA CGG CAG AAA AA ATG AGC TTT GGA TGG TGG AG	102	59

8.1.2 Mouse:

Primer sequence (FP: forward primer, RP: reverse primer), amplicon length (product) and annealing temperature (AT):

Gene name	Primer sequence 5' - 3' FP/RP	Product (bp)	AT (°C)
Interleukin-4 Receptor (IL-4R)	TGT GCC ACA TGG AAA TGA AT CAT TGG TGT GGA GTG TGA GG	129	58
Interleukin-13 α1 Receptor (IL-13Rα1)	TTC CAG TCT TTG TCG CAG TG TCC AGT GCA GGG TAT CAT CA	144	59
Interleukin-13 α2 Receptor (IL-13Rα2)	AGC GAA TGG AGT GAA GAG GA GCT CAA TGT GGG TTC AGG TT	150	59
Porphobilinogen deaminase (PBGD)	GGT ACA AGG CTT TCA GCA TCG ATG TCC GGT AAC GGC GGC	135	59

8.1.3 Rat:

Primer sequence (FP: forward primer, RP: reverse primer), amplicon length (product) and annealing temperature (AT):

Gene name	Primer sequence 5' - 3' FP/RP	Product (bp)	AT (°C)
Interleukin-4 Receptor (IL-4R)	CCA GAC CCT GAG AGA GCA AC ATG TCC AGC CTG CTT CTG TT	147	59
Interleukin-13 α1 Receptor (IL-13Rα1)	GCC GAA TTC CAC CTT CTA CA CAG GAT CAG GAA TTG GAG GA	128	59
Interleukin-13 α2 Receptor (IL-13Rα2)	GGA ATG CTG GGA AGG TTA CA CAG TGT GGG TTC AGG GTC TT	130	59
Porphobilinogen deaminase (PBGD)	AGG ATG GGC AAC TGT TGG AC AAC TGT GGG TCA TCC TCT GG	130	59

8.1.4 Cloning primer for human IL-13Rα2 (5' – 3') :

Apa I – IL-13Rα2: GGG CCC ATG GCT TTC GTT TGC TT

Hind III – IL-13Rα2: AAG CTT TCA TGT ATC ACA GAA AA

8.1.5 PCR-conditions for qRT-PCR

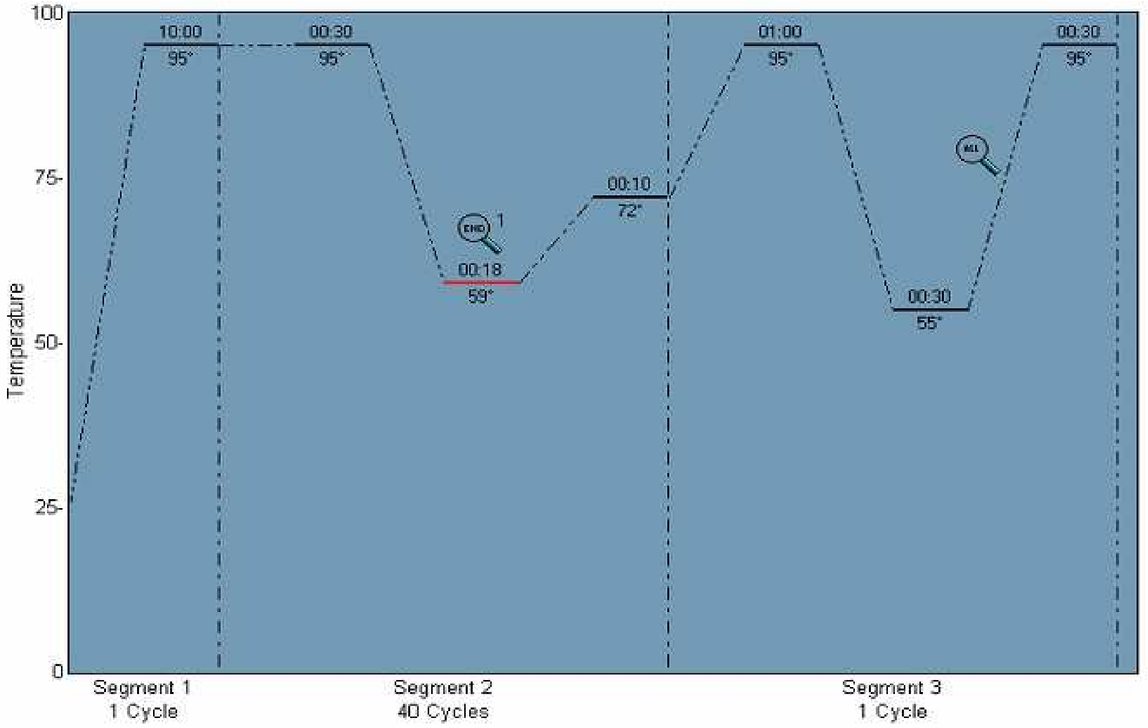

Annotation: The annealing temperature (red line in segment 2) is variable, same as the following extension time. Segment 3 was performed for melting curve analysis

8.2 Microarray data

8.2.1 Genes regulated after 2 h of IL-13 stimulation

Accession	Gene	coeff.	A mean
NM_002982	chemokine (C-C motif) ligand 2 (CCL2)	3.844	10.529
NM_006072	chemokine (C-C motif) ligand 26 (CCL26)	2.643	8.523
NM_002986	chemokine (C-C motif) ligand 11 (CCL11)	1.914	8.503
NM_013324	cytokine inducible SH2-containing protein (CISH)	1.844	7.550
NM_006273	chemokine (C-C motif) ligand 7 (CCL7)	1.624	8.248
NM_005329	hyaluronan synthase 3 (HAS3)	1.491	7.681
NM_001621	aryl hydrocarbon receptor (AHR)	1.467	9.383
NM_001511	chemokine (C-X-C motif) ligand 1 (melanoma growth stimulating activity alpha (CXCL1)	1.420	9.950
NM_000958	prostaglandin E receptor 4 (subtype EP4) (PTGER4)	1.403	8.106
NM_000600	interleukin 6 (interferon beta 2) (IL6)	1.374	9.071
NM_022837	hypothetical protein FLJ22833 (FLJ22833)	1.261	9.767
NM_002089	chemokine (C-X-C motif) ligand 2 (CXCL2)	1.170	9.601
NM_005686	SRY (sex determining region Y)-box 13 (SOX13)	1.046	7.572
NM_005375	v-myb myeloblastosis viral oncogene homolog (avian) (MYB)	1.033	7.690
NM_017651	Abelson helper integration site (AHI1)	1.027	8.315
NM_173475	hypothetical protein MGC48972 (MGC48972)	0.985	7.929
NM_012193	frizzled homolog 4 (Drosophila) (FZD4)	0.982	8.881
NM_007115	tumor necrosis factor alpha-induced protein 6 (TNFAIP6)	0.970	8.409
NM_000958	prostaglandin E receptor 4 (subtype EP4) (PTGER4)	0.912	7.810
NM_014583	LIM and cysteine-rich domains 1 (LMCD1)	0.880	8.159
NM_003670	basic helix-loop-helix domain containing	0.858	9.366
NM_005257	GATA binding protein 6 (GATA6)	0.853	9.312
NM_052901	solute carrier family 25 (mitochondrial carrier phosphate carrier) member 25 (SLC25A25)	0.853	8.315
NM_003211	thymine-DNA glycosylase (TDG)	0.803	8.406
NM_033211	hypothetical gene supported by AF038182	0.780	8.967
NM_000861	histamine receptor H1 (HRH1)	0.763	8.085
AK056836	cDNA FLJ32274 fis	0.737	7.890
NM_002521	natriuretic peptide precursor B (NPPB)	0.706	8.206
NM_004414	Down syndrome critical region gene 1 (DSCR1)	0.676	9.485
NM_002448	msh homeo box homolog 1 (Drosophila) (MSX1)	0.641	7.112
NM_021205	ras homolog gene family member U (RHOU)	0.607	7.020
NM_005944	CD200 antigen (CD200)	0.602	9.467
NM_017651	Abelson helper integration site (AHI1)	0.599	7.941
NM_173490	hypothetical protein LOC134285	0.583	8.771
NM_005982	sine oculis homeobox homolog 1 (Drosophila) (SIX1)	0.574	7.846
AK024263	cDNA FLJ14201 fis	0.568	9.210
NM_006622	polo-like kinase 2 (Drosophila) (PLK2)	0.556	7.882
NM_014795	zinc finger homeobox 1b (ZFHX1B)	0.550	8.114
NM_001717	basonuclin 1 (BNC1)	0.549	7.906
AB040883	mRNA for KIAA1450 protein	0.510	7.605
NM_014992	dishevelled associated activator of morphogenesis 1 (DAAM1)	0.507	7.691
NM_000104	cytochrome P450 family 1, subfamily B	0.479	7.957
NM_003739	aldo-keto reductase family 1" member C3 (3-alpha hydroxysteroid dehydrogenase type II)	0.475	9.832
NM_002089	chemokine (C-X-C motif) ligand 2 (CXCL2)	0.474	10.604
NM_000861	histamine receptor H1 (HRH1)	0.460	7.412
NM_032823	chromosome 9 open reading frame 3 (C9orf3)	0.454	8.431
NM_018664	Jun dimerization protein p21SNFT (SNFT)	0.446	7.139
NM_170677	Meis1 myeloid ecotropic viral integration site 1 homolog 2 (mouse) (MEIS2)	0.440	7.673
NM_003821	receptor-interacting serine-threonine kinase 2 (RIPK2)	0.440	8.975
AK022059	cDNA FLJ11997 fis	0.437	8.254
NM_017761	proline-rich nuclear receptor coactivator 2 (PNRC2)	0.421	9.037
NM_002546	tumor necrosis factor receptor superfamily member 11b (osteoprotegerin) (TNFRSF11B)	0.406	10.203
NM_004932	cadherin 6 K-cadherin (fetal kidney) (CDH6)	0.393	9.105
NM_001957	endothelin receptor type A (EDNRA)	0.391	8.627
NM_002546	tumor necrosis factor receptor superfamily member 11b (osteoprotegerin) (TNFRSF11B)	0.390	10.119
NM_178836	similar to CG12314 gene product (LOC201164)	0.380	7.030

NM_004235	Kruppel-like factor 4 (gut) (KLF4)	0.365	6.815
NM_013352	squamous cell carcinoma antigen recognized by T cells 2 (SART2)	0.359	8.316
NM_032270	factor for adipocyte differentiation 158 (FAD158)	0.328	7.751
NM_005114	heparan sulfate (glucosamine) 3-O-sulfotransferase 1 (HS3ST1)	0.318	6.935
NM_003059	solute carrier family 22 (organic cation transporter)	0.303	7.654
NM_005180	polycomb group ring finger 4 (PCGF4)	0.268	8.464
AF415176	CSGEF (SGEF) mRNA alternatively spliced. [AF415176]	0.248	7.257
NM_020424	hypothetical protein A-211C6.1 (LOC57149)	0.246	7.576
NM_020841	oxysterol binding protein-like 8 (OSBPL8)	0.244	8.365
NM_002061	glutamate-cysteine ligase modifier subunit (GCLM)	0.234	8.920
NM_014016	SAC1 suppressor of actin mutations 1-like (yeast) (SACM1L)	0.225	7.912
NM_001270	chromodomain helicase DNA binding protein 1 (CHD1)	0.219	7.608
NM_018103	leucine rich repeat containing 5 (LRRC5)	0.190	8.455
AK026882	cDNA: FLJ23229 fis	-0.203	8.027
NM_173500	tau tubulin kinase 2 (TTBK2)	-0.219	6.808
NM_173841	interleukin 1 receptor antagonist (IL1RN)	-0.226	7.447
NM_032043	BRCA1 interacting protein C-terminal helicase 1 (BRIP1)	-0.239	7.030
AF086790	aconitase precursor (ACON) mRNA, nuclear gene encoding mitochondrial protein	-0.266	7.553
NM_017556	filamin-binding LIM protein-1 (FBLP-1)	-0.301	7.258
NM_019105	tenascin XB (TNXB)	-0.314	9.528
AF161351	HSPC088 mRNA	-0.316	10.674
NM_005119	thyroid hormone receptor associated protein 3 (THRAP3)	-0.333	7.589
NM_016453	NCK interacting protein with SH3 domain (NCKIPSD)	-0.343	7.236
NM_005598	nescient helix loop helix 1 (NHLH1)	-0.349	7.213
NM_152776	hypothetical protein MGC40579 (MGC40579)	-0.363	7.789
NM_018444	protein phosphatase 2C magnesium-depenent catalytic subunit (PPM2C)	-0.377	8.013
NM_032863	Fraser syndrome 1 (FRAS1)	-0.388	7.417
NM_173622	hypothetical protein FLJ36674 (FLJ36674)	-0.390	7.793
AK091537	cDNA FLJ34218 fis	-0.450	7.573
NM_005653	transcription factor CP2 (TFCP2)	-0.464	7.810
XM_496406	similar to KIAA1693 protein (LOC401967)	-0.501	10.154
NM_183372	hypothetical protein LOC200030	-0.502	10.058
NM_030932	diaphanous homolog 3 (Drosophila) (DIAPH3)	-0.527	7.788
NM_139173	CG10806-like (LOC150159)	-0.535	7.804
NM_002729	hematopoietically expressed homeobox (HHEX)	-0.604	7.685
NM_153437	outer dense fiber of sperm tails 2 (ODF2)	-0.620	9.268
CR620977	cDNA clone CS0CAP004YK15 of Thymus of Homo sapiens (human)	-0.634	8.531
NM_145161	mitogen-activated protein kinase kinase 5 (MAP2K5)	-0.649	8.217
THC2095910	truncated DNA architectural factor HMGA2 (Homo sapiens)	-0.813	7.764
NM_001955	endothelin 1 (EDN1)	-0.854	7.764
NM_019070	DEAD (Asp-Glu-Ala-Asp) box polypeptide 49 (DDX49)	-0.883	8.544

8.2.2 Genes regulated after 6 h of IL-13 stimulation

Accession	Description	coeff.	A mean
NM_002982	chemokine (C-C motif) ligand 2 (CCL2)	4.044	10.529
NM_006072	chemokine (C-C motif) ligand 26 (CCL26)	3.399	8.523
NM_005329	hyaluronan synthase 3 (HAS3) transcript variant 1	2.353	7.681
NM_006273	chemokine (C-C motif) ligand 7 (CCL7)	1.918	8.248
NM_017651	Abelson helper integration site (AHI1)	1.761	8.315
NM_000600	interleukin 6 (interferon beta 2) (IL6)	1.746	9.071
NM_002986	chemokine (C-C motif) ligand 11 (CCL11)	1.639	8.503
AK056836	cDNA FLJ32274 fis	1.636	7.890
NM_022837	hypothetical protein FLJ22833	1.596	9.767
NM_013324	cytokine inducible SH2-containing protein (CISH) transcript variant 1	1.561	7.550
NM_002521	natriuretic peptide precursor B (NPPB)	1.494	8.206
NM_018664	Jun dimerization protein p21SNFT (SNFT)	1.440	7.139
NM_014583	LIM and cysteine-rich domains 1 (LMCD1)	1.412	8.159
NM_175839	spermine oxidase (SMOX)	1.367	9.877
NM_007115	tumor necrosis factor alpha-induced protein 6 (TNFAIP6)	1.266	8.409
AL049227	mRNA cDNA DKFZp564N1116	1.265	9.667
NM_005375	v-myb myeloblastosis viral oncogene homolog (avian) (MYB)	1.245	7.690
NM_012193	Homo sapiens frizzled homolog 4 (Drosophila) (FZD4)	1.206	8.881
NM_001511	chemokine (C-X-C motif) ligand 1 (melanoma growth stimulating activity alpha) (CXCL1)	1.203	9.950
NM_000958	prostaglandin E receptor 4 (subtype EP4) (PTGER4)	1.181	7.810
NM_001621	aryl hydrocarbon receptor (AHR)	1.168	9.383
NM_000958	prostaglandin E receptor 4 (subtype EP4) (PTGER4)	1.158	8.106
NM_017651	Abelson helper integration site (AHI1)	1.123	7.941
NM_005384	nuclear factor interleukin 3 regulated (NFIL3)	1.101	7.668
NM_005686	SRY (sex determining region Y)-box 13 (SOX13)	1.096	7.572
NM_173475	hypothetical protein MGC4897	1.089	7.929
NM_021205	ras homolog gene family member U (RHOU)	1.020	7.020
NM_052901	solute carrier family 25 (mitochondrial carrier phosphate carrier) member 25	1.006	8.315
NM_032603	lysyl oxidase-like 3 (LOXL3)	0.997	8.660
NM_004932	cadherin 6 type 2 K-cadherin (fetal kidney) (CDH6)	0.953	9.105
NM_002448	msh homeo box homolog 1 (Drosophila) (MSX1)	0.949	7.112
NM_013437	low density lipoprotein-related protein 12 (LRP12)	0.945	8.730
BC045778	clone IMAGE:4791553	0.935	8.173
NM_018469	uncharacterized hypothalamus protein HT008 (HT008)	0.925	8.615
NM_003504	CDC45 cell division cycle 45-like (S. cerevisiae) (CDC45L)	0.920	8.003
NM_030674	solute carrier family 38 member 1 (SLC38A1)	0.912	9.303
NM_001444	fatty acid binding protein 5 (psoriasis-associated) (FABP5)	0.893	10.124
NM_005257	GATA binding protein 6 (GATA6)	0.891	9.312
NM_173490	hypothetical protein LOC134285	0.887	8.771
NM_005944	CD200 antigen (CD200) transcript variant 1	0.853	9.467
NM_000861	histamine receptor H1 (HRH1)	0.843	8.085
NM_003211	thymine-DNA glycosylase (TDG)	0.825	8.371
NM_001444	fatty acid binding protein 5 (psoriasis-associated) (FABP5)	0.801	10.674
NM_006169	nicotinamide N-methyltransferase (NNMT)	0.801	10.950
NM_003211	thymine-DNA glycosylase (TDG)	0.798	8.406
NM_002201	interferon stimulated gene 20kDa (ISG20)	0.793	7.982
NM_000104	cytochrome P450 family 1 subfamily B polypeptide 1 (CYP1B1)	0.777	7.957
NM_000165	gap junction protein alpha 1 43kDa (connexin 43) (GJA1)	0.759	10.998
NM_002089	chemokine (C-X-C motif) ligand 2 (CXCL2)	0.747	9.601
NM_019593	hypothetical protein KIAA1434 (KIAA1434)	0.739	8.639
NM_012449	six transmembrane epithelial antigen of the prostate (STEAP)	0.737	8.798
NM_014795	zinc finger homeobox 1b (ZFHX1B)	0.726	8.114
NM_001078	vascular cell adhesion molecule 1 (VCAM1)	0.725	7.296
NM_170677	Meis1 myeloid ecotropic viral integration site 1 homolog 2 (mouse) (MEIS2) variant a	0.724	7.673
NM_003243	transforming growth factor beta receptor III (betaglycan 300kDa) (TGFBR3)	0.710	7.208
NM_002402	mesoderm specific transcript homolog (mouse) (MEST) transcript variant 1	0.708	8.327
NM_005738	ADP-ribosylation factor-like 4A (ARL4A) transcript variant 1	0.705	7.555
AK024263	cDNA FLJ14201 fis	0.684	9.210
NM_002089	chemokine (C-X-C motif) ligand 2 (CXCL2)	0.677	10.604
NM_001353	aldo-keto reductase family 1 member C1 (AKR1C1)	0.661	10.241
NM_001206	basic transcription element binding protein 1 (BTEB1)	0.647	7.936
NM_147156	transmembrane protein 23 (TMEM23)	0.647	8.128

NM_002160	tenascin C (hexabrachion) (TNC)	0.619	10.754
NM_005114	heparan sulfate (glucosamine) 3-O-sulfotransferase 1 (HS3ST1)	0.615	6.935
NM_001717	basonuclin 1 (BNC1)	0.611	7.906
NM_013281	fibronectin leucine rich transmembrane protein 3 (FLRT3) transcript variant 1	0.606	7.149
NM_013448	bromodomain adjacent to zinc finger domain 1A (BAZ1A)	0.605	7.720
NM_012302	latrophilin 2 (LPHN2)	0.598	8.827
NM_183013	cAMP responsive element modulator (CREM) transcript variant 19	0.593	7.892
NM_014339	interleukin 17 receptor (IL17R)	0.583	7.729
NM_002546	tumor necrosis factor receptor superfamily member 11b (TNFRSF11B)	0.580	10.133
NM_014992	dishevelled associated activator of morphogenesis 1 (DAAM1)	0.574	7.691
NM_032823	chromosome 9 open reading frame 3 (C9orf3)	0.564	8.431
NM_183013	cAMP responsive element modulator (CREM) transcript variant 19	0.552	7.714
NM_153332	3' exoribonuclease (3'HEXO)	0.532	7.906
NM_021102	serine protease inhibitor Kunitz type 2 (SPINT2)	0.514	7.213
NM_002546	tumor necrosis factor receptor superfamily member 11b (TNFRSF11B)	0.513	10.203
NM_003739	aldo-keto reductase family 1 member C3 (AKR1C3)	0.511	9.832
NM_015928	androgen-induced proliferation inhibitor (APRIN)	0.505	7.220
AB040883	mRNA for KIAA1450 protein	0.504	7.605
NM_001218	carbonic anhydrase XII (CA12) transcript variant 1	0.495	9.435
NM_017850	hypothetical protein FLJ20508	0.488	7.655
NM_019886	carbohydrate (N-acetylglucosamine 6-O) sulfotransferase 7 (CHST7)	0.473	8.338
NM_016210	chromosome 3 open reading frame 18 (C3orf18)	0.471	7.200
NM_022733	hypothetical protein AL133206	0.466	8.093
NM_000861	histamine receptor H1 (HRH1)	0.464	7.412
NM_006070	TRK-fused gene (TFG)	0.460	10.320
NM_006868	RAB31 member RAS oncogene family (RAB31)	0.459	8.456
NM_178836	similar to CG12314 gene product (LOC201164)	0.456	7.030
NM_020841	oxysterol binding protein-like 8 (OSBPL8) transcript variant 1	0.456	8.365
NM_002546	tumor necrosis factor receptor superfamily member 11b (TNFRSF11B)	0.452	10.124
AK024229	cDNA FLJ14167 fis	0.449	6.698
NM_017761	proline-rich nuclear receptor coactivator 2 (PNRC2)	0.445	9.037
BC022398	clone IMAGE:4689481	0.444	6.810
NM_003059	olute carrier family 22 (organic cation transporter) member 4 (SLC22A4)	0.428	7.654
AF415176	CSGEF (SGEF) mRNA	0.428	7.257
THC2049923	Sulfated surface glycoprotein 185 precursor (SSG 185)	0.426	6.933
NM_032270	factor for adipocyte differentiation 158 (FAD158)	0.418	7.751
NM_002546	tumor necrosis factor receptor superfamily member 11b (TNFRSF11B)	0.417	10.119
NM_003312	thiosulfate sulfurtransferase (TST) nuclear gene encoding mitochondrial protein	0.416	9.341
NM_203301	F-box protein 33 (FBXO33)	0.415	7.881
NM_152464	chromosome 17 open reading frame 32 (C17orf32)	0.398	7.072
NM_020424	hypothetical protein A-211C6.1 (LOC57149)	0.394	7.576
NM_014016	SAC1 suppressor of actin mutations 1-like (yeast) (SACM1L)	0.375	7.912
NM_033407	dedicator of cytokinesis 7 (DOCK7)	0.364	8.780
NM_012175	F-box protein 3 (FBXO3 transcript variant 1)	0.363	8.075
U83115	non-lens beta gamma-crystallin like protein (AIM1) mRNA	0.361	7.013
NM_015226	KIAA0350 protein (KIAA0350)	0.357	7.050
NM_013352	squamous cell carcinoma antigen recognized by T cells 2 (SART2)	0.353	8.316
NM_002816	proteasome (prosome macropain) 26S subunit non-ATPase 12 (PSMD12)	0.350	8.834
NM_000826	glutamate receptor ionotropic AMPA 2 (GRIA2)	0.348	6.682
NM_003104	sorbitol dehydrogenase (SORD)	0.345	7.413
NM_032457	BH-protocadherin (brain-heart) (PCDH7) transcript variant c	0.337	6.622
NM_178562	hypothetical protein MGC50844 (MGC50844)	0.333	6.571
NM_005180	polycomb group ring finger 4 (PCGF4)	0.320	8.464
NM_015385	sorbin and SH3 domain containing 1 (SORBS1)	0.317	6.903
AK022059	cDNA FLJ11997 fis	0.314	8.254
NM_013257	serum/glucocorticoid regulated kinase-like (SGKL) transcript variant 1	0.312	6.972
NM_016018	PHD finger protein 20-like 1 (PHF20L1) transcript variant 1	0.306	7.946
NM_002061	glutamate-cysteine ligase modifier subunit (GCLM)	0.304	8.920
AF086558	full length insert cDNA clone ZE15C06	0.288	6.679
NM_003477	pyruvate dehydrogenase complex component X (PDHX)	0.280	7.852
AK095841	cDNA FLJ38522 fis	0.230	7.068
NM_018103	leucine rich repeat containing 5 (LRRC5)	0.221	8.455
NM_001270	chromodomain helicase DNA binding protein 1 (CHD1)	0.215	7.608
AK026882	cDNA: FLJ23229 fis	-0.234	8.027
NM_019105	tenascin XB (TNXB) transcript variant XB	-0.236	9.528
NM_032043	BRCA1 interacting protein C-terminal helicase 1 (BRIP1)	-0.236	7.030
NM_000537	renin (REN)	-0.272	6.725
M27126	lymphocyte antigen (DRw8) mRNA	-0.285	7.646

AF161351	HSPC088 mRNA	-0.291	10.674
NM_144699	ATPase Na+/K+ transporting alpha 4 polypeptide (ATP1A4)	-0.292	7.600
NM_012099	CD3-epsilon-associated protein antisense to ERCC-1 (ASE-1)	-0.296	6.966
NM_018344	solute carrier family 29 (nucleoside transporters)	-0.302	6.659
BC008580	clone IMAGE:4179986	-0.323	7.481
AF174606	F-box protein Fbw3 (FBW3) mRNA	-0.324	7.774
NM_030932	diaphanous homolog 3 (Drosophila) (DIAPH3)	-0.357	7.788
NM_024316	leukocyte receptor cluster (LRC) member 1 (LENG1)	-0.361	7.720
NM_199040	nudix (nucleoside diphosphate linked moiety X)-type motif 4 (NUDT4) variant 2	-0.366	8.912
AF140675	zinc metalloprotease ADAMTS7 (ADAMTS7) mRNA	-0.386	6.832
AY007211	folylpolyglutamate synthetase (FPGS) mRNA	-0.394	6.924
AJ007211	cell division cycle 2-like 1 (PITSLRE proteins) (CDC2L1)	-0.408	7.284
NM_031299	cell division cycle associated 3 (CDCA3)	-0.411	8.434
NM_000226	keratin 9 (epidermolytic palmoplantar keratoderma) (KRT9)	-0.415	7.653
NM_017556	filamin-binding LIM protein-1 (FBLP-1)	-0.422	7.258
AK095727	cDNA FLJ38408 fis	-0.424	8.702
NM_007034	DnaJ (Hsp40) homolog subfamily B member 4 (DNAJB4)	-0.430	8.515
THC2096438	Probable G protein-coupled receptor GPR20	-0.433	6.987
AK056556	cDNA FLJ31994 fis	-0.439	7.262
AK074570	cDNA FLJ90089 fis	-0.450	8.719
NM_018382	hypothetical protein FLJ11292 (FLJ11292)	-0.464	9.854
AY358725	clone DNA105680 ENLS2543 (UNQ2543) mRNA	-0.480	7.235
NM_015898	zinc finger and BTB domain containing 7 (ZBTB7)	-0.493	11.351
NM_152236	growth arrest-specific 2 like 1 (GAS2L1)	-0.493	7.054
NM_014972	KIAA1049 protein (KIAA1049)	-0.494	8.043
XM_372864	similar to Soggy-1 protein precursor (SGY-1) (UNQ735/PRO1429)	-0.503	7.980
T12588	Chromosome 9 exon II Homo sapiens cDNA clone P94_53 5' and 3	-0.530	7.676
NM_145244	DNA-damage-inducible transcript 4-like (DDIT4L)	-0.537	7.177
NM_005598	nescient helix loop helix 1 (NHLH1)	-0.541	7.213
BC081532	chromosome X open reading frame 17 mRNA	-0.563	8.362
NM_005879	TRAF interacting protein (TRIP)	-0.577	8.306
NM_024893	chromosome 20 open reading frame 39 (C20orf39)	-0.583	7.561
NM_020414	DEAD (Asp-Glu-Ala-Asp) box polypeptide 24 (DDX24)	-0.601	8.801
NM_014938	Mlx interactor (MONDOA)	-0.607	8.256
BC031698	clone IMAGE:5167446	-0.611	9.431
NM_001010914	protein immuno-reactive with anti-PTH polyclonal antibodies	-0.631	9.035
NM_001606	ATP-binding cassette sub-family A (ABC1) member 2 (ABCA2)	-0.638	9.467
NM_033257	DiGeorge syndrome critical region gene 6-like (DGCR6L)	-0.652	9.910
NM_002729	hematopoietically expressed homeobox (HHEX)	-0.660	7.685
NM_001682	ATPase Ca++ transporting plasma membrane 1 (ATP2B1)	-0.670	7.651
NM_173841	interleukin 1 receptor antagonist (IL1RN) transcript variant 2	-0.670	7.447
NM_024512	leucine rich repeat containing 2 (LRRC2)	-0.677	8.898
NM_019070	DEAD (Asp-Glu-Ala-Asp) box polypeptide 49 (DDX49)	-0.684	8.544
NM_004815	PTPL1-associated RhoGAP 1 (PARG1)	-0.691	8.376
NM_032935	metallothionein IV (MT4)	-0.731	9.521
NM_032016	STARD3 N-terminal like (STARD3NL)	-0.733	9.881
ENST0032925	Urea transporter erythrocyte	-0.749	8.284
M94173	N-type calcium channel alpha-1 subunit mRNA	-0.773	12.700
AK002019	cDNA FLJ11157 fis	-0.784	8.213
AK056991	cDNA FLJ32429 fis	-0.796	7.877
NM_018003	uveal autoantigen with coiled-coil domains and ankyrin repeats	-0.810	9.527
NM_005723	transmembrane 4 superfamily member 9 (TM4SF9)	-0.830	8.026
NM_018444	phosphatase 2C magnesium-dependent catalytic subunit (PPM2C)	-0.835	8.013
AK091537	cDNA FLJ34218 fis	-0.846	7.573
NM_005653	transcription factor CP2 (TFCP2)	-0.847	7.810
NM_024896	KIAA1815 (KIAA1815)	-0.861	8.614
NM_152776	hypothetical protein MGC40579 (MGC40579)	-0.864	7.789
NM_032564	diacylglycerol O-acyltransferase homolog 2 (mouse) (DGAT2)	-0.868	9.296
NM_002203	integrin alpha 2 (CD49B alpha 2 subunit of VLA-2 receptor) (ITGA2)	-0.875	9.871
NM_001010914	protein immuno-reactive with anti-PTH polyclonal antibodies	-0.877	8.853
NM_032863	Fraser syndrome 1 (FRAS1)	-0.877	7.417
NM_145019	hypothetical protein FLJ30707	-0.879	10.493
NM_005119	thyroid hormone receptor associated protein 3 (THRAP3)	-0.906	7.589
NM_145161	mitogen-activated protein kinase kinase 5 (MAP2K5) transcript variant C	-0.912	8.217
NM_198943	CXYorf1-related protein (MGC52000)	-0.918	9.328
NM_144573	nexilin (F actin binding protein) (NEXN)	-0.925	8.501

XM_496406	similar to KIAA1693 protein (LOC401967)	-0.926	10.154
NM_007036	endothelial cell-specific molecule 1 (ESM1)	-0.934	9.655
NM_183372	hypothetical protein LOC200030	-0.934	10.058
NM_001554	cysteine-rich angiogenic inducer 61 (CYR61)	-0.939	11.368
NM_003544	histone 1 H4b (HIST1H4B)	-0.940	7.901
CR620977	full-length cDNA clone CS0CAP004YK15 of Thymus of Homo sapiens	-0.943	8.531
NM_005933	myeloid/lymphoid or mixed-lineage leukemia (trithorax homolog Drosophila)	-0.973	7.462
BC071729	HSPC063 protein	-0.982	8.034
NM_178229	IQ motif containing GTPase activating protein 3 (IQGAP3)	-1.017	9.793
NM_173622	hypothetical protein FLJ36674 (FLJ36674)	-1.036	7.793
AF001540	clone alpha1 mRNA sequence	-1.060	8.118
NM_138373	myeloid-associated differentiation marker (MYADM)	-1.066	9.617
NM_183372	hypothetical protein LOC200030	-1.137	9.647
AK095459	cDNA FLJ38140 fis	-1.146	9.825
NM_000361	thrombomodulin (THBD)	-1.150	9.243
NM_153437	outer dense fiber of sperm tails 2 (ODF2) variant 2	-1.156	9.268
NM_139173	CG10806-like (LOC150159)	-1.201	7.804
AK095678	cDNA FLJ38359 fis	-1.235	11.474
NM_001901	connective tissue growth factor (CTGF)	-1.238	12.069
NM_020457	THAP domain containing 11 (THAP11)	-1.245	8.692
NM_001955	endothelin 1 (EDN1)	-1.247	7.764
NM_032264	hypothetical protein AE2 (AE2)	-1.247	9.513
BC061638	cDNA clone IMAGE:5547707	-1.315	8.751
NM_181690	v-akt murine thymoma viral oncogene homolog 3 (AKT3)	-1.390	8.415
AK092668	cDNA FLJ35349 fis	-1.475	7.994

Der Lebenslauf wurde aus der elektronischen Version der Arbeit entfernt.

The curriculum vitae was removed from the electronic version of the paper.

Publications:

1. **Hecker M**, Zakrzewicz A, Kwapiszewska G, Marsh LM, Sedding D, Klepetko W, Seeger W, Weissmann N, Schermuly RT, Eickelberg O. The Interleukin 13 receptor system: A novel pathomechanism involved in pulmonary arterial hypertension. **submitted**

2. Jayachandran A, Königshoff M, Yu H, Rupniewska E, **Hecker M**, Klepetko W, Seeger W, Eickelberg O. SNAI transcription factors are key mediators of epithelial-to-mesenchymal transition in lung fibrosis. **submitted**

3. Mayer K, Kiessling A, Ott J, Schäfer MB, **Hecker M**, Schulz R, Günther A, Wang J, Roth J, Seeger W, Kang JX. Fat-1 mice are protected from acute lung injury. i**n revision**

4. Bi MH, Ott J, Fischer T, **Hecker M**, Dietrich H, Schäfer MB, Markat P, Wang EB, Seeger W, Mayer K. Induction of lymphocyte apoptosis in a murine model of acute lung injury – modulation by lipid emulsions. **in revision**

5. Schäfer MB, Pose A, Ott J, **Hecker M**, Behnk A, Schulz R, Weissmann N, Günther A, Seeger W, Mayer K. Peroxisome proliferator-activated receptor-a reduces inflammation and vascular leakage in a murine model of acute lung injury. ***Eur Respir J* - in press**

6. Hecker A, Kaufmann A, **Hecker M**, Padberg W, Grau V. Expression of Interleukin-21, Interleukin-21 receptor and related type-1 cytokines by intravascular graft leukocytes during renal allograft rejection. ***Immunobiology* - in press**

7. **Hecker M**, Walmrath HD, Seeger W, Mayer K. Clinical aspects of acute lung insufficiency (ALI/TRALI). ***Transfusion Med Hemother*** 35:80-88, 2008

8. Zakrzewicz A, **Hecker M**, Marsh LM, Kwapiszewska G, Nejman B, Long L, Seeger W, Schermuly RT, Morrell NW, Morty RE, Eickelberg O. Receptor for activated C-kinase 1, a novel interaction partner of type II bone morphogenetic protein receptor, regulates smooth muscle cell proliferation in pulmonary arterial hypertension. ***Circulation*** 115:2957-68, 2007

9. Zakrzewicz A, Kouri FM, Nejman B, Kwapiszewska G, **Hecker M**, Sandu R, Dony E, Seeger W, Schermuly RT, Eickelberg O, Morty RE. The TGF-β/Smad2,3 signalling axis is impaired in experimental pulmonary hypertension. ***Eur Respir J*** 29:1094-104, 2007

10. Morty RE, Nejman B, Kwapiszewska G, **Hecker M**, Zakrzewicz A, FM Kouri, Peters DM, Dumitrascu R, Seeger W, Knaus P, Schermuly RT, Eickelberg O. Dysregulated bone morphogenetic protein signaling in monocrotaline-induced pulmonary arterial hypertension. ***Arterioscler Thromb Vasc Biol*** 27:1072-8, 2007

11. Seay U, Sedding D, Krick S, **Hecker M**, Seeger W, Eickelberg O. Transforming growth factor-β-dependent growth inhibition in primary vascular smooth muscle cells is p38-dependent. ***J Pharmacol Exp Ther*** 315:1005-12, 2005

12. Eickelberg O and **Hecker M**. TGF-β signalling: The known and the unknown. ***Zellbiologie aktuell*** 30:20-23, 2004

13. **Hecker M**, Qiu D, Marquardt K, Bein G, Hackstein H. Continuous CMV seroconversion in a large group of healthy blood donors. ***Vox Sang*** 86:41-44, 2004

14. **Hecker M**, Bohnert A, Koenig IR, Bein G, Hackstein H. Novel genetic variation of human interleukin-21 receptor is associated with elevated IgE levels in females. ***Genes Immun*** 4:228-233, 2003

15. Hackstein H*, **Hecker M***, Kruse S, Bohnert A, Ober C, Deichmann K, Bein G. A novel polymorphism in the 5' promotor region of human interleukin-4 receptor α-chain gene is associated with decreased soluble interleukin-4 protein levels. ***Immunogenetics*** 53:264-269, 2001 * co-first authors

Oral presentations

102nd International Conference of the American Thoracic Society (2007). Title: Functional Relevance of the Interleukin 13 Receptor System in Idiopathic Pulmonary Arterial Hypertension

European Respiratory Society Annual Congress (2006). Title: Functional Relevance of the Interleukin 13 Receptor System in Idiopathic Pulmonary Arterial Hypertension

33td Annual Meeting of the German Society of Immunology (2002). Title: Novel genetic variation of human interleukin-21 receptor is associated with elevated IgE levels in females

15th European Histocompartibility Conference in Granada/Spain (2001). Title: A novel polymorphism in the 5' promotor region of human interleukin-4 receptor α-chain gene is associated with decreased soluble interleukin-4 protein levels

32nd Annual Meeting of the German Society of Immunology (2001). Title: A novel polymorphism in the 5' promotor region of human interleukin-4 receptor α-chain gene is associated with decreased soluble interleukin-4 protein levels

Abstracts and Posters:

101st International Conference of the American Thoracic Society (2006) Title: Increased expression and functional relevance of the Interleukin 13 system in Idiopathic Pulmonary Fibrosis (IPF)

112th Annual Meeting of the German Society of Internal Medicine (2006). Title: Increased expression and functional relevance of the Interleukin 13 system in Idiopathic Pulmonary Fibrosis (IPF)

European Respiratory Society Annual Congress (2005). Title: Increased expression and functional relevance of the Interleukin 13 system in Idiopathic Pulmonary Fibrosis (IPF)

European Respiratory Society Annual Congress (2004). Title: Live cell imaging of Smad2 and Smad3 signal transduction in response to TGF-β.

10 Acknowledgements

I would like to gratefully acknowledge my supervisor, Dr. Oliver Eickelberg, for great guidance and support during the experimental work in the lab, inspiring and fruitful discussions and excellent training in molecular biology in the Graduate Program "Molecular Biology and Medicine of the Lung" and numerous journal clubs.

I would like to thank Prof. Werner Seeger, Director of the Department of Internal Medicine II and Chairman of the University of Giessen Lung Center (UGLC), for providing an encouraging and motivating atmosphere, fruitful discussions and excellent conditions for scientific work.

Many thanks I would like to express to Anka Zakrzewicz for an excellent and funny time in the lab, a perfect teaching of the Polish language and a nice friendship since many years: Dziekuje bardzo za wszystko, krolik !!!

Next, I wish to acknowledge Grazyna Kwapiszewska, Leigh Marsh, and Jochen Wilhelm for great help and support, the groups of Prof. Weissmann, Prof. Schermuly and Prof. Grau for excellent collaboration. Thanks a lot to Dr. Rory Morty for the inspiring discussions and the great help with the correction of this thesis and the publication. Furthermore, I really would like to say "thank you" to Ulrike Seay for excellent technical assistance and support. Many thanks to my good friends from the lab/MBML (Aparna, Anka, Bozena, Darek, Ewa, Grazyna, Katja, Kamila, Leigh, Maciej) for sharing good and bad moments, great company during the past years, the fun we had and the tons of coffee we were enjoying together.

Above all, deepest thanks to my parents, my brothers and sisters, for their great and constant support in every respect which helped and encouraged me a lot in the last years!!!